

بِسْمِ اللَّهِ الرَّحْمَنِ الرَّحِيمِ

A Computational Approach for the Thermal Aspects in Boundary Layer Flows



By

Usman Ali

**Department of Mathematics
Quaid-I-Azam University
Islamabad, Pakistan
2021**

A Computational Approach for the Thermal Aspects in Boundary Layer Flows



By

Usman Ali

Supervised By

Prof. Dr. Muhammad Yousaf Malik

**Department of Mathematics
Quaid-I-Azam University
Islamabad, Pakistan
2021**

A Computational Approach for the Thermal Aspects in Boundary Layer Flows



By

Usman Ali

A THESIS SUBMITTED IN THE PARTIAL FULFILLMENT OF THE REQUIREMENT FOR

THE DEGREE OF

DOCTOR OF PHILOSOPHY

IN

MATHEMATICS

Supervised By

Prof. Dr. Muhammad Yousaf Malik

This thesis is dedicated to my *Baji*

Mrs. Farhat Munir

And my dearest and beloved uncle

Mr. Kamran Manzoor

Thanks to all of you for their support, love and encouragement. You are the personalities whom act like road to reach me at my destination.

Acknowledgement

I start my acknowledgement with the name of Almighty Allah (S.W.T) for his everlasting blessings, love and care. Bundle of thanks to Almighty Allah (S.W.T) for giving me the strength, wisdom and confidence to complete this work. After Almighty Allah (S.A.W), I pay my sincere gratitude to Holy Prophet Muhammad (PBUH) for his gaudiness towards the seeking of knowledge. I also thanks to Holy Prophet Muhammad (PBUH) family members (Hazrat Ali (R.A), Hazrat Fatima (R.A), Hazrat Imam Hassan (R.A), Hazrat Imam Hussain (R.A)).

I say thanks from core of my heart to my kind supervisor Pof. Muhammad Yousaf Malik for his believing and caring attitude and providing me the excellent atmosphere to accomplish this work His exert gaudiness, constructive criticism and continuous encouragement helped me in all time during my research and writing this thesis. I would also like to thank my teachers who taught me able to overcome all the challenges, particularly Prof. Tasawar Hayat, Prof. Muhammad Ayub, Prof. Sohail Nadeem, Prof. Masood Khan, Prof. Babar Majeed Mirza, Prof. Khalid Saifullah, Dr. Amir Nadeem, Dr. Tahir Mahmood, Dr. Zahid Mehmood.

I would not imagine completing my acknowledgement without saying thanks to my baji **Mrs. Farhat Munir** who showed me the way of wisdom and success and always encouraged me in my hard times. I would like to thank the personalities without whom my life is incomplete and colorless, my parents, brothers, sisters, cousins, mamu g. I could not achieve any goal of my life without their support, love and prayers. Especially thanks to Abu Jan, Ammi Jan and sister who encouraged me at every moment when I was struggling. I found me the luckiest person on the planet having such loving and caring family.

Last, but not least, I would like to say thanks to my dearest friend Dr. Zubair Ali Moughal, Mr. Muhammad Rizwan, Dr. Arifullah Khan, Mr. Arshad Hussain, Mr. Zeeshan for his friendship and love during M. Sc to Ph. D studies. I am pleased to acknowledge my senior lab fellows Dr. Arif Hussain, Mr. Awais, Dr. Khalil, Dr. Mair, Dr. Imad. This is injustice to completing this portion without saying thanks to my good and bad times partner Dr. Muhammad Irfan.

Usman Ali

Author's Declaration

I Usman Ali hereby state that my PhD thesis titled A Computational Approach for the Thermal Aspects in Boundary Layer Flows is my own work and has not been submitted previously by me for taking any degree from the Quaid-i-Azam University Islamabad, Pakistan or anywhere else in the country/world. At any time if my statement is found to be incorrect even after my graduate the university has the right to withdraw my PhD degree.

Name of Student: Usman Ali

Date: 12/04/2021

(Usman Ali)

Plagiarism Undertaking

I solemnly declare that research work presented in the thesis titled "A Computational Approach for the Thermal Aspects in Boundary Layer Flows" is solely my research work with no significant contribution from any other person. Small contribution/help wherever taken has been duly acknowledged and that complete thesis has been written by me. I understand the zero tolerance policy of the HEC and Quaid-i-Azam University towards plagiarism. Therefore, I as an Author of the above titled thesis declare that no portion of my thesis has been plagiarized and any material used as reference is properly referred/cited.

I undertake that if I am found guilty of any formal plagiarism in the above titled thesis even afterward of PhD degree, the University reserves the rights to withdraw/revoke my PhD degree and that HEC and the University has the right to publish my name on the HEC/University Website on which names of students are placed who submitted plagiarized thesis.



Student/Author Signature:

Name: Usman Ali

Certificate of Approval


This is to certify that the research work presented in this thesis entitled A Computational Approach for the Thermal Aspects in Boundary Layer Flows was conducted by Mr. Usman Ali under the kind supervision of Prof. Dr. Muhammad Yousaf Malik. No part of this thesis has been submitted anywhere else for any other degree. This thesis is submitted to the Department of Mathematics, Quaid-i-Azam University, Islamabad in partial fulfillment of the requirements for the degree of Doctor of Philosophy in field of Mathematics from Department of Mathematics, Quaid-i-Azam University Islamabad, Pakistan.

Student Name: Usman Ali

Signature: 

External committee:

a) External Examiner 1:

Signature: 

Name: Dr. Muhammad Mushtaq

Office Address: Department of Mathematics COMSATS University, Park Road Chak Shahzad, Islamabad.

b) External Examiner 2:

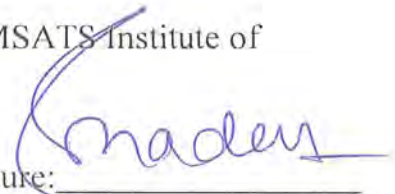
Signature: 

Name: Dr. Muhammad Awais

Designation: Assistant Professor

Office Address: Department of Mathematics, COMSATS Institute of Information Technology, Attock

c) Internal Examiner

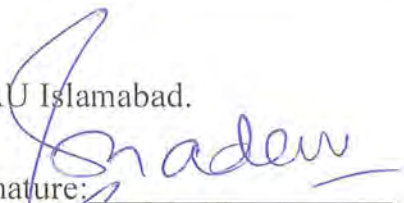
Signature: 

Name: Prof. Dr. Muhammad Yousaf Malik

Designation: Professor

Office Address: Department of Mathematics, QAU Islamabad.

Supervisor Name:

Signature: 

Prof. Dr. Muhammad Yousaf Malik

Name of Dean/ HOD

Signature: 

Prof. Dr. Sohail Nadeem

A Computational Approach for the Thermal Aspects in Boundary Layer Flows


By

Usman Ali

CERTIFICATE

A DISSERTATION SUBMITTED IN THE PARTIAL FULFILLMENT OF THE REQUIREMENTS FOR THE DEGREE OF THE DOCTOR OF PHILOSOPHY

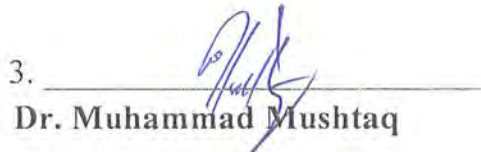
We accept this dissertation as conforming to the required standard.

1. 

Prof. Dr. Sohail Nadeem
(Chairman)

2. 

Prof. Dr. Muhammad Yousaf Malik
(Supervisor)

3. 

Dr. Muhammad Mushtaq
Assistant Professor

Department of Mathematics COMSATS
University, Park Road, Chak Shahzad,
Islamabad.

(External Examiner)

4. 

Dr. Muhammad Awais
Assistant Professor

Department of Mathematics
COMSATS Institute of Information
Technology, Attock.

(External Examiner)

Department of Mathematics
Quaid-I-Azam University
Islamabad, Pakistan
2021

Preface

The main theme of this dissertation is about the computational approach for the flows at boundary layer in concern with heat transfer rate by invoking various effects to the energy equation which includes heat absorption/generation, Joule heating, thermal radiation and nano-fluids etc. The nano particles are the major source to enhance heat transfer rate in fluid flows. Nano-fluid is the advance type of fluid which shows the combination of base fluid and nano sized particles. These nano particles include metals like silicon, copper and aluminum etc.

Beside this, three main sources of heat transfer are the conduction, convection and radiation. The researchers of recent times have been examining the heat transfer rate in different perspectives. As in this dissertation, the heat transfer phenomena is observed by using Cattaneo-Christov heat flux model. This type of heat flux is the generalized shape of Fourier's law which helps to transform heat equation into hyperbolic form. This law is used to determine the thermo-elastic and concentration elastic effects in Newtonian as well as non-Newtonian fluid models. The study of behavior of concentration of fluid is an important feature to be discussed in fluid dynamics. For this purpose, the concentration equation is debated through Homogeneous-Heterogeneous chemical reactions.

The mathematical model for the problem is designed by considering the laws of conservation. The equations of motion are presented as Navier-Stokes equation which reflects as a Partial Differential Equations (PDE's). The equipment which is used to alter these equations into Ordinary Differential Equations (ODE's) is a well know similarity transformation technique. This technique helps to reduce independent variables that appears in PDE's and provides a system of ODE's. The obtained set of equations are then converted to system of first order ODE's as it is simpler to deal with or we convert them into initial value problem by using suitable substitutions. The missing initial conditions are supposed to take as some particular values. These supposed values against the missing initial conditions are taken on a hit and trial

bases which is known as shooting technique. The numerical solutions are calculated by using Runge-Kutta Fehlberg method in shooting scheme. The impacts of numerous physical quantities upon velocity of fluid, temperature of fluid and concentration of fluid are portrayed through graphs by using MATLAB. The main purpose of representing the graphs is to determine how the base fluids are affected by considering certain effects in the momentum energy and concentration equation. The heat transfer rate or Nusselt number and mass transfer rate that is Sherwood number are examined. Moreover, their numerical values are computed and compared with the previous results. The comparison shows an excellent match with the existing literature which provides the consistency and accuracy of the computational approach. The transfer of heat and mass phenomena by way of Carreau steady two-dimensional infinite shear rate viscosity model over moving wedge is analysed in chapter 1. The results for dilatant and pseudoplastic fluids are reported. The independent variables are reduced from partial differential equations in order to get ordinary differential equations by applying admissible similarity transformation technique. This system is sorted out in a numerically by means of Runge-Kutta methodology associated by shooting algorithm. The reduction in the temperature of Carreau fluid is captured due to greater values of viscosity ratio parameter in case of shear thickening and reverse trend is examined for the shear thinning case. Further, the concentration in Carreau fluid declines against wedge angle parameter for shear thickening and thinning. The headnotes of this chapter are published in “**Case Studies in Thermal Engineering, 12(2018): 126-136**”. <https://doi.org/10.1016/j.csite.2018.04.007>

The Carreau viscosity model with heat absorption /generation and chemical reaction, a steady flow at a boundary layer for moving wedge is studied in chapter 2. The mathematical shape is designed in coupled partial differential equations and then sorted out in a numerical way by implementing shooting scheme charted with Runge-Kutta Fehlberg technique. The graphs depict the consequence of physical parameters upon fluid concentration, velocity and

temperature. The temperature readings are observed for positive and negative values of parameter of heat generation. Further, the Carreau fluid concentration is inspected for parameter of chemical reaction. The executive summary of the chapter is presented in “**Case Studies in Thermal Engineering, 12 (2018): 462–469**”.
<https://doi.org/10.1016/j.csite.2018.06.006>

The chapter 3 includes the results for Jeffery fluid with thermal stratification effects at a stagnation point. The thermal energy characteristics are studied through the generalized Fourier’s law of heat flux. The flow is magnified by the stretching cylinder. The homogeneous-heterogeneous chemically reactive species are considered. The steady state flow of a boundary layer is examined when the reactants and auto-catalyst have equal diffusion coefficient. The concerned mathematical problem is developed by laws of conservation of momentum, mass and energy which provides coupled partial differential equation. The order of these equations is reduced by way of similarity transformation. Later, the set of reduced coupled equations are computed numerically by implementing Runge-Kutta Fehlberg technique with shooting algorithm. The curves for temperature and velocity of fluid are plotted for different engineering parameters. The coefficient of skin friction is examined, and the obtained outcomes are comparison with existing literature. This pagination is delineated in “**Physica A: Statistical Mechanics and its Applications, 542 (2020): 123428**”.
<https://doi.org/10.1016/j.physa.2019.123428>

The Jeffery fluid past a point of stagnation towards a cylindrical surface with the homogenous-heterogeneous reactions, magnetic field and heat generation effects are elaborated in chapter 4. The heat transport process is debated by Cataneo-Christov heat flux concerned to thermal stratification. The consequential PDE’s descend to ODE’s by carrying out the set of similarity transformation. These equations are sorted out in a numerical procedure named as Runge-Kutta Fehlberg method with shooting approach. The consequences of involved parameters are

analysed by means of graphs. The obtain outcomes are validated with an existing published work. The table of contents for this chapter are published in “**Canadian Journal of Physics, 97(7) (2019): 735-741**”. <https://doi.org/10.1139/cjp-2018-0491>

The chapter 5 emphasizes on magneto-hydrodynamics, heat generation/absorption and slip effects over a Newtonian flow field with homogeneous-heterogeneous chemical reactions induced by the rotating disk. The concerned steady state flow is examined in case when reactants and auto-catalyst possess equality in coefficients of diffusion. The Cattaneo-Christov approach is proposed to derive the energy equation and heat transfer phenomena. The consequential PDE's (Partial Differential Equations) descend to ODE's (Ordinary Differential Equations) by insinuating similarity transform. Further, these equations are sorted out by way of numerical scheme called Runge-Kutta Fehlberg method with shooting scheme. The influence of arising parameters towards fluid velocity, temperature and concentration is observed through graphs. Further, the computational results for the friction coefficient and the rate of heat transfer are examined. The main results of this paper is published in “**Physica Scripta, 94 (2019): 085217 (9pp)**”, <https://doi.org/10.1088/1402-4896/ab11ff>

A Newtonian nanofluid flow field is demonstrated in chapter 6 with thermal radiation and heat generation/absorption. Further, in this study mixed convection, magnetic field, stagnation point, temperature stratification, Joule heating, concentration stratification and chemical reaction are included. The flow field is caused by the inclined stretching cylinder. The mathematical shape is developed in coupled partial differential framework and is descended to coupled ordinary differential framework by means of admissible transformation. The numerical findings are presented by Runge-Kutta Fehlberg method along with shooting scheme. The temperature trend towards higher values of heat absorption/generation and thermal radiation is studied and analysed in detail. Further, the guesstimates for local Nusselt

number as well as the skin friction coefficient are presented. The detailed summary is published in “**Physica A, 553 (2020): 124026**”. <https://doi.org/10.1016/j.physa.2019.124026>

Nomenclature

$\tilde{\Omega}$	Angular velocity
k^*	Absorption coefficient ($1/m$)
D_B	Brownian diffusion coefficient (m^2/s)
N_b	Brownian motion parameter
N	Buoyancy force parameter
\bar{i}	Characteristic length
A, B	Chemical species
\tilde{a}, \tilde{b}	Concentration of chemical species
$\tilde{l}_1, \tilde{l}_s, b, c, m$	Constants
\tilde{K}	Curvature parameter
C	Concentration of fluid
Gr^*	Concentration Grashoff number
\tilde{D}_A, \tilde{D}_B	Diffusion coefficients
\tilde{c}, \tilde{d}	Dimensionless constant
Ec	Eckert number
u_e	Free stream velocity (m/s)
\bar{A}_1	First Rivlin Ericksen tensor
g	Gravitational acceleration (m/s^2)
\bar{I}	Identity tensor
Re_x	Local Reynolds number
Le	Lewis number
Γ	Material time constant
D_M	Mass diffusivity
B_o	Magnetic field coefficient
M	Magnetic field parameter
P	Pressure (N/m^2)
n	Power law index

Pr	Prandtl number
K_0	Reaction rate constant
\tilde{R}	Radius of cylinder
q_r	Roseland radiative heat flux (W / s^2)
T_w	Surface temperature
C_w	Surface concentration
c_p	Specific heat (J / kgK)
Sc	Schmidt number
q_w	Surface heat flux (W / s^2)
j_w	Surface mass flux
L_s	Strength of heterogeneous reaction parameter
L	Strength of homogeneous reaction parameter
a^*	Stretching constant
T	Temperature (K)
k	Thermal conductivity (W / mK)
\tilde{S}	Thermal stratification
D_T	Thermophoresis diffusion coefficient (m^2 / s)
R_T	Thermal radiation parameter
N_t	Thermophoresis parameter
Gr	Thermal Grashoff number
\bar{V}	Velocity vector
(u, v, w)	Velocity components (m / s)
Ω	Wedge angle

Greek letters

$\tilde{\alpha}$	Angel of inclination
μ	Apparent viscosity (kg / ms)
$\bar{\tau}$	Cauchy stress tensor
δ_2	Concentration stratification
γ	Chemical reaction parameter

β_T	Coefficient of thermal expansion
β_c	Coefficient of concentration expansion
θ	Dimensionless temperature
ϕ	Dimensionless concentration
$\tilde{\beta}$	Deborah number
ρ	Density of fluid (kg / m^3)
σ	Electrical conductivity (S / m)
δ	Heat generation/absorption parameter
μ_∞	Infinite shear rate viscosity (kg / ms)
ν^*	Kinematic viscosity (m^2 / s)
λ_m	Mixed convection parameter
τ	Ratio of nanoparticles
$\tilde{\lambda}_1$	Ratio of relaxation time to retardation
$\tilde{\lambda}_2$	Retardation time
η	Similarity variable
τ_w	Surface shear stress
Ψ	Stream function
σ^*	Stefan-Boltzman constant
$\dot{\gamma}$	Second invariant strain tensor
$\tilde{\gamma}$	Thermal relaxation parameter
$\tilde{\lambda}^*$	Thermal relaxation time
α	Thermal diffusivity (m^2 / s)
β^*	Viscosity ratio parameter
α^*	Velocity slip parameter
λ	Velocity ratio parameter
β	Wedge angle parameter
μ_0	Zero shear rate viscosity (kg / ms)

Contents

0.	Introduction	3
1.	Thermal aspects in a Carreau viscosity model through wedge	11
1.1	Mathematical formulation.....	11
1.2	Computational algorithm.....	15
1.3	Results and discussion.....	17
1.4	Graphical representation.....	20
1.5	Concluding remarks.....	24
2.	On heat generation/absorption and chemical reaction in a non-Newtonian fluid flow	26
2.1	Mathematical formulation.....	26
2.2	Computational algorithm.....	29
2.3	Results and discussion.....	31
2.4	Graphical representation.....	33
2.5	Concluding remarks.....	37
3.	Thermal energy in a Jeffery fluid flow regime: A generalized Fourier's law outcomes	39
3.1	Mathematical formulation.....	39
3.2	Computational algorithm.....	44
3.3	Results and discussion.....	46
3.4	Graphical representation.....	49
3.5	Concluding remarks.....	55

4.	MHD effects in a non-Newtonian flow model with homogeneous-heterogeneous reactions	57
4.1	Mathematical formulation.....	57
4.2	Computational algorithm.....	62
4.3	Results and discussion.....	64
4.4	Graphical representation.....	67
4.5	Concluding remarks.....	73
5.	On Cattaneo-Christov heat flux in a Newtonian flow field with MHD and velocity slip	74
5.1	Mathematical formulation.....	74
5.2	Computational algorithm.....	78
5.3	Results and discussion.....	80
5.4	Graphical representation.....	84
5.5	Concluding remarks.....	91
6.	On thermal radiation and joule heating in a mixed convective nanofluid flow	92
6.1	Mathematical formulation.....	92
6.2	Computational algorithm.....	96
6.3	Results and discussion.....	98
6.4	Graphical representation.....	102
6.5	Concluding remarks.....	111
	References	112

Chapter 0

Introduction

From the past few decades, the researchers have been paying attention to unveil the features of the non-Newtonian type of fluid phenomena that admits the non-linear relation between shear rate and shear stress. The diversity of flow of non-Newtonian fluid model leads to uncertainty regarding rheological aspects. Thus, we cannot explain the complete picture by means of single constitutive equation which relates shear stress and deformation rate. The most frequently used non-Newtonian fluid involves paints, custard, ketchup, toothpaste, honey and various salt solutions.

The major concern of the researchers working in this field is the development/enhancement in the use of non-Newtonian fluid phenomena. This flow phenomena towards wedge arises in certain chemical engineering systems. Furthermore, an analysis subject to boundary layer flow is more fascinating in recent years in view of its applications at an industrial scale such as polymer extrusion, aerodynamics, condensation of metallic plates in a cooling bath, glass as well as polymer industries. The recent developments subject to non-Newtonian fluid models can be assessed in the Refs. [1-3].

The Carreau fluid model is from non-Newtonian class and is assumed to be a good approximation for numerous shear thinning fluids to meet the rheological conduct at extreme low and high shear rates whereas many other models are valid merely in specific conditions. The comprehensive study on Carreau fluid model can be assessed in Refs. [4-6].

Presently the observations concerning chemical reactions and heat generation/absorption became centre of attraction for researchers. Analysis regarding chemically reactive species that generates diffusion through a stretching sheet is made by Andersson et al. [7]. Apart from other

fields, detailed computational study of hypersonic flow in a physical manner involving chemical reactions is done by Argyris et al. [8]. Motulevich [9] focused on impact of chemical reactions with heat transfer. The comprehensive study for computational fluid dynamics for the purpose of chemical reaction engineering was done by Kuipers and Swaaij [10]. The mathematical model is considered for the dispersion of chemically reactive species by Pal [11]. The comprehensive study about chemically reactive species in porous media is done by the Samson et al. [12]. Hjertager et al. [13] emphasized on turbulent flow modelling, emerged with chemical reactions. A detailed study regarding chemically reacting systems is made by Bisio et al. [14]. Kandasamy et al. [15] visualized the problems related to chemical reactions in the flow along wedge and presented useful results. The analysis for chemically reactive species through electrically conducting fluid induced by the stretching sheet is done by Raptis and Perdikis [16]. The viscous fluid blended with chemical reaction through application of Lie group analysis is deliberated by Bhuvaneswari et al. [17].

Owning the importance of heat absorption/ generation in a fluid flow phenomenon, various researchers reported their findings. Chen [18] designates the effect of power-law fluid along heat generation/absorption through stretched surface. The process of heat generation for chemical and engineering aspects has been considered in Refs. [19-24]. Mahmoud [25] considered the power-law fluids. He analyzed the slip effects associated with heat generation over a moving surface. The numerical approximations for the problem related to nanofluid with heat generation effects are discussed by Rajarathinam and Nithyadevi [26].

The difference that occurs in fluid layers due to a variation in densities of various fluids or modification in temperature and concentration is termed as stratification. The thermal stratification phenomena play a crucial role in an engineering and industrial aspects as its application involves thermally stratified water reservoirs and lakes, heterogeneous reactions or mixtures in atmosphere. The disadvantage includes prevention of mixing of oxygen from upper

to lower layer of water so that the lack of oxygen in water occur through some biological treatments. The heat transfer in a medium with stratification is studied by Angirasa and Peterson [27]. They deduced that thermally stratified phenomena greatly influenced the flow as well as temperature fields. An electrically conducting fluid through a thermally stratified field embedded with magnetic effects has been discussed by Chamkha [28]. Devi and Kandasamy [29] presented the results on a wedge flow concerned by the thermal stratification as the temperature fluctuates at each layer in the space in addition with boundary layer theory. Such kind of flows are useful at industrial and agricultural scale. As the stratification is used to improve the efficiency of thermodynamic system. Transient mixed convection flow is used to elaborate this phenomenon and is presented by Bouhdjar and Harhad [30]. Fabiano et al. [31] gave analysis about the volatile boiling of fluid when it comes to collide with hot surfaces and the fluid is induced by thermal stratification. They concluded that evaporation does not occur when superheating the cold phase as its limits were not determined.

The amended shape of Fourier law has been used frequently to identify the characteristics of transfer of heat phenomena. Thus, thermal convection in a Newtonian flow field induced by the porous surface and the heat equation is equipped by using Cattaneo model which is examined by Straughan [32]. Furthermore, this is shown by Straughan [33] that thermal waves are to be propagate with acoustic waves whereas the model of heat waves is proposed by Christov's model which is the generalization of Cattaneo's classical model. The speed and amplitude of waves are observed in this study. The main results for the stress field and temperature in a solid surface are found analytically and Laplace transformation scheme is applied in order to get the thermally stressed equations and Cattaneo's closed form solutions in Al-Qahtani and Yilbas. [34]. As, the Cattaneo gave the idea in the context of heat conduction, Christov tried to modify this formula by adding the term involving time derivative into it. This model is applied to an incompressible fluid and the uniqueness of the solution is observed by

Tibullo and Zampoli [35]. The impacts of transfer of heat in a Maxwell fluid flow regime past a stretched surface with slip velocity is observed whereas the heat transfer phenomena are proposed by the Christov modified model which is debated by Han et al. [36]. The instable thermal phenomena in a fluid inertia past a porous medium is studied and the equation for heat flux is modelled in view of the Cattaneo's theory by Haddad [37]. The study related to thermally convective materials in a Brinkman porosity media considering the fluid inertia and the flux phase through Cattaneo theory is carried out by Shivakumara et al. [38]. A brief note on a Jeffery fluid in a squeezing flow regime where the whole system is placed in a rotating frame, is done by Hayat et al. [39]. The theory of transfer heat is debated by modified classical Fourier's law that is in addition with thermal relaxation time and found that temperature profile decays by maximizing the parameter of thermal relaxation time. The flow at a stagnation point in addition with modified shape of classical Fourier's law is a matter of discussion in Hayat et al. [40].

The magneto hydrodynamic (MHD) is the study related to correlation of fluids with electric conduction and magnetic features. Such type of fluids is of great interest for industrial and technological aspects such as MHD power generation, MHD flow meters etc. Also, MHD effects arise in plasma sources, like MHD generators and inductively heated plasma generators. The remarkable conclusions regarding specifications of MHD turbulence dominated by the ideal invariants were given by Biskamp [41]. The magnetic field is implanted in an astrophysical aspects and the numerical findings for the studied problem were carried out by Hawley and Stone [42]. Ishikawa et al. [43] focused on MHD disk generators employed to the fusion reactors. Evtushenko et al. [44] explored the results for MHD flow through conducting walls or in a slotted channel. A conceptual study for the MHD disk generators was formulated by Inui et al. [45]. The impacts of insulation upon heat flux was observed by Ying and Gaizer [46] and they found that this flux declines due to insulating overlay. A brief discussion on

MHD equations corresponding to their symmetric properties is reported by Goedbloed and Lifschitz [47]. Hua and Walker [48] analysed the MHD flow induced by rectangular duct assisted by the thin conducting walls and transverse magnetic resonance. Somewhere in boundary layer MHD flows, electro-thermal instabilities occur and causes dissection of the electrostatic sheath that transits the current from diffusion to an arc mode channel. This observation was carried out by Kumar et al. [49]. A conducting Oldroyd-B fluid with MHD effects induced by the insulating rotating disk was observed and the exact solutions were found by Ersoy [50]. The MHD convection with heterogeneous effects embedded with magnetic field and micro-disk electrodes were observed by Sugiyama et al. [51]. MHD flow in an astrophysical aspects was observed by Gómez et al. [52]. The electromotive force was employed for the process of MHD power production that arises on the cross section of seawater and magnetic field such investigation was performed by Liu et al. [53]. The MHD generators and inductive heating plasma generators that ascends from plasma genesis were investigated by Herdrich et al. [54]. The characteristics of radiation with MHD effects in astrophysics were observed by Stone and Gardiner [55].

Newtonian fluids are those which satisfies the Newton's viscosity law which reveals that the stress shear is proportional directly to rate of deformation. Thus Newton's law for viscosity

can be expressed in mathematical form as $\tau_{yx} = \mu \frac{du}{dy}$, where τ_{yx} is shear stress, μ is termed

as absolute or dynamic viscosity and $\frac{du}{dy}$ is the rate of deformation. For Newtonian type fluids,

μ as viscosity is independent of rate of deformation. A study of the Newtonian fluid flow in a pipe for the pressure drop through granular bed is considered where the flow problem around the beds of spherical and non-spherical particles is observed experimentally by Dolejs and Machac [56]. The study of interest by Bell and Surana [57] is about the transfer of heat in a fluid flow and the numerical results are found through finite element method. The Navier-

Stokes equation for three-dimensional Newtonian fluid flow with isothermal effects are considered and the finite element formulation is executed for the solution of incompressible Newtonian flows by Musson and Surana [58]. The Newtonian flow field is triggered through two stretching-rotating disks manifested by the surface tension is debated and the useful results for the elongation viscosity measurements by employing stretching liquid bridges are concluded by Kroger and Rath [59]. The Newtonian flow field motion through a cylindrical surface filled by the elastic liquid is considered. As the drag force decreases due to enhancement in the Weissenberg number (We). Here, it is explored that the smaller values of Weissenberg number causes decrease in drag force and the drag force increases by uplifting Weissenberg number (Degand and Walters [60]). The axisymmetric flow of a viscous fluid enclosed in a concentric ring where the high temperature is given to the outer spherical ring as compared to the inner one. The inner and outer spheres are rotated with different angular velocities. A Galerkin finite element approach is executed to find numerical results of the problem influenced by the shear thickening and shear thinning properties studied by Bar-Yoseph and Kryzhanovski [61]. The comparison between the results of Newtonian and non-Newtonian fluids in a rotating regime at extremely high values of Reynolds number and the same inner rotatory cylinder and found it like those of non-rotatory flow observed (see Nouri and Whitelaw [62]). The simulation of the creeping flow of Newtonian fluid and the formulation of boundary element for the dual phase incompressible fluid is presented. The method is elaborated by the formation of a drop as it is impelled by the ambient fluid lying within the convergent channel was observed by Khayat et al. [63]. A theoretical approach to determine the drag and fall velocities of a sphere-shaped particles in Newtonian fluid was proposed by Dolejs et al. [64]. The specifications of a Newtonian flow field with a Bingham fluid are taken and the steady state solutions are deduced for the concerned problem by Comparini and Mannucci [65].

The pioneering work on nano-fluid is done by Choi in 1995. The nanofluid is defined as a mixture of solid-liquid particles. Various industrial processes for example cooling, heating, power generation, electromagnetic and chemical processes use heat transfer fluids as base fluids. Such fluids include oil, water, ethylene glycol etc. These fluids have poor performance for transfer of heat as compared to those solids which enforce the compulsion on enhancing the effectiveness of heat exchanger. To deal with this problem, solid particles are added to the fluids that helps in increasing thermal conductivity several hundred times. In this regard, the characteristics of heat transfer with nano fluids are observed by Xuan and Roetzel [66]. The work related to nanofluids was further extended by Xuan and Li [67] in which they examined the thermal conductivity and heat transfer phenomena for the nanofluids in a duct merged with the dispersal of rigid particles. This study investigates that the nanoparticle (Al_2O_3) has a substantial influence on the boiling process that causes decline for the boiling properties of the fluid. Its results tell us that such fluids are used in thermal or heating process where the specific surface temperature is needed without altering the fluid temperature. Further, they extended the same problem to the narrow tube by Das et al. [68-69]. The previous literature shows experimental work on nanofluids with convective heat transfer that passes through the laminar copper tube and that disturbance in boundary layer is the main reason of nanoparticles to be moved freely discovered by Wen and Yulong [70]. The study emphasizing on a ferromagnetic nanoparticle in the magnetic fluid and the particle size of the primary clusters are evaluated with the aid of Einstein's equation for Brownian motion analysed by Kikura et al. [71]. Further, the use of nano-fluids and nanoparticles are considered in Refs. [72-75].

The mixed convective boundary layer flow has many engineering applications such as nuclear reactors, food processing, solidification process etc. Mixing also plays a vital role to maintain the manufacturing process like drugs, cosmetics etc. The mixed convective flow boundary layer towards an inclined wavy plate merged with transverse magnetic field is examined. It is

observed that magnetic field yields acceleration in a flow close to the leading edge of the wavy surface and retardation in a flow far from the leading edge is noticed by Wang and Chi-Chang [76]. The results deduced by Vinuesa and de Arellano [77] for the mixed convection boundary layer are improved particularly by employing effective reaction rates through the operation of parameterisation. This study is extended to a chemical apparatus that helps in the formation of ozone and deficiency of convective boundary layer. The remarkable conclusions regarding the impacts of Lewis number in a mixed convective flow inside a straight fitted tube are given. The numerical results related to the influence of Lewis number on the Sherwood number close to the tube inlet are found by Orfi and Galanis [78]. The numerical and analytical results for the mixed convection flow through vertical porous surface are presented by Magyari and Emad [79]. Further, the literature concerned to the mixed convective boundary layer flows are presented in Refs. [80-86].

Chapter 1

Thermal aspects in a Carreau viscosity model through wedge

The transfer of heat and mass phenomena by way of steady two-dimensional Carreau viscosity model over moving wedge with infinite shear rate viscosity is analysed in this chapter. The results for the shear thinning as well as shear thickening are reported. The independent variables are reduced from partial differential equations in order to get ordinary differential equations by applying admissible similarity transformation technique. This system is sorted out in a numerical way by means of Runge-Kutta methodology along shooting algorithm. The reduction in the temperature of Carreau fluid is captured due to greater values of viscosity ratio parameter in case of shear thickening and reverse trend is observed for shear thinning case. Further, the concentration in Carreau fluid declines against wedge angle parameter for shear thickening and thinning.

1.1 Mathematical formulation

Consider the steady, incompressible, two dimensional Carreau fluid model past a moving wedge persuading transfer of heat and mass. The flow field occur across the stretched wedge whose velocity is $u_w(x) = bx^m$ and the free stream velocity as $u_e(x) = cx^m$, here b, c and m are the positive constants. It is important to note that $u_w(x) > 0$ indicates the stretched wedge surface velocity whereas $u_w(x) < 0$ relates to shrinking wedge velocity. Thus, wedge angle is taken as $\Omega = \beta\pi$ where $\beta = \frac{2m}{m+1}$ refers to pressure gradient. The surface temperature $T_w(x)$

is supposed to exceeds the ambient fluid temperature $T_\infty (T_w > T_\infty)$. Similar assumption is taken

in case of surface concentration $C_w(x)$ at surface, C_∞ the ambient fluid concentration that is ($C_w > C_\infty$). The governing equations for model of Carreau viscosity fluid are depicted as,

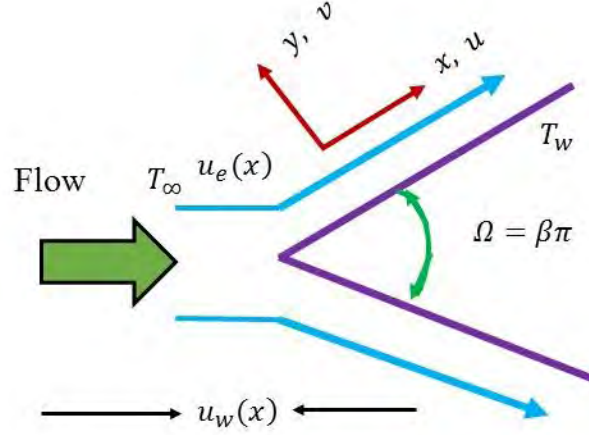


Fig. 1.1: Geometry of the problem.

$$\bar{\tau} = -p\bar{I} + \mu(\dot{\gamma})\bar{A}_1, \quad \mu = \mu_\infty + (\mu_0 - \mu_\infty)[1 + (\Gamma\dot{\gamma})^2]^{\frac{n-1}{2}}, \quad (1.1)$$

$$\dot{\gamma} = \sqrt{\frac{1}{2}\Pi} = \sqrt{\frac{1}{2}\text{trace}(\bar{A}_1^2)}, \quad (1.2)$$

the apparent viscosity μ of a Carreau model can be written as:

$$\mu = \mu_0[\beta^* + (1 - \beta^*)\{1 + (\Gamma\dot{\gamma})^2\}^{\frac{n-1}{2}}]. \quad (1.3)$$

In the above expression, $\bar{\tau}$ is the Cauchy's tensor for stress, the pressure p , \bar{I} be the tensor identity, $\bar{A}_1 = \text{grad}\bar{V} + (\text{grad}\bar{V})^T$ is the first Rivlin Erickson tensor, $\dot{\gamma}$ is the second invariant rate of strain tensor, Γ is the material time constant and n is the power law index respectively.

Also, $\beta^* = \frac{\mu_\infty}{\mu_0}$ is the ratio parameter of viscosity with μ_0 and μ_∞ as zero shear rate and infinite

shear rate of viscosity. For the steady two-dimensional flow, the velocity, temperature and concentration fields are considered,

$$\bar{V} = (u(x, y), v(x, y), 0), \quad T = T(x, y), \quad C = C(x, y) \quad (1.4)$$

where u and v represents the components of velocity in the x and y directions, respectively.

Thus, ultimate mathematical equations for the flow problem are given as:

$$\frac{\partial u}{\partial x} + \frac{\partial v}{\partial y} = 0, \quad (1.5)$$

$$u \frac{\partial u}{\partial x} + v \frac{\partial u}{\partial y} = u_e \frac{du_e}{dx} + \nu^* \left(\frac{\partial^2 u}{\partial y^2} \right) [\beta^* + (1 - \beta^*) \{1 + \Gamma^2 \left(\frac{\partial u}{\partial y} \right)^2\}^{\frac{n-1}{2}}] \\ + \nu^* \Gamma^2 (1 - \beta^*) (n-1) \left(\frac{\partial u}{\partial y} \right)^2 \left(\frac{\partial^2 u}{\partial y^2} \right) \{1 + \Gamma^2 \left(\frac{\partial u}{\partial y} \right)^2\}^{\frac{n-3}{2}}, \quad (1.6)$$

$$u \frac{\partial T}{\partial x} + v \frac{\partial T}{\partial y} = \alpha \frac{\partial^2 T}{\partial y^2}, \quad (1.7)$$

$$u \frac{\partial C}{\partial x} + v \frac{\partial C}{\partial y} = D_M \frac{\partial^2 C}{\partial y^2}, \quad (1.8)$$

where ν^* is the kinematic viscosity, $\alpha = \frac{k}{\rho c_p}$ as thermal diffusivity and D_M as mass

diffusivity. The related end point conditions against the moving wedge are formulated as follows.

$$u = u_w(x) = bx^m, \quad v = 0, \quad T = T_w, \quad C = C_w \quad \text{at } y = 0 \quad (1.9)$$

$$u = u_e(x) = cx^m, \quad T \rightarrow T_\infty, \quad C \rightarrow C_\infty \quad \text{as } y \rightarrow \infty \quad (1.10)$$

for solution purpose one can use the set of transformation.

$$\eta = y \sqrt{\frac{c(m+1)}{2\nu^*}} x^{\frac{m-1}{2}}, \quad \psi(x, y) = f(\eta) \sqrt{\frac{2\nu^* c}{m+1}} x^{\frac{m+1}{2}}, \quad \theta(\eta) = \frac{T - T_\infty}{T_w - T_\infty}, \quad \phi(\eta) = \frac{C - C_\infty}{C_w - C_\infty}, \quad (1.11)$$

where η as the similarity variable, $f(\eta), \theta(\eta), \phi(\eta)$ are the non-dimensional fluid velocity, temperature and concentration, ψ implies the stream function which meets continuity equation

with $u = \frac{\partial \psi}{\partial y}$ and $v = -\frac{\partial \psi}{\partial x}$. By utilizing these relations one can obtain the equations written

as:

$$[\beta^* + (1 - \beta^*)\{1 + (f''(\eta))^2 We^2\}^{\frac{n-3}{2}} \{1 + n(f''(\eta))^2 We^2\}]f'''(\eta) + f(\eta)f''(\eta) + \beta[1 - f'(\eta)^2] = 0, \quad (1.12)$$

$$\theta''(\eta) + \text{Pr} f(\eta)\theta'(\eta) = 0, \quad (1.13)$$

$$\phi''(\eta) + \text{Sc}f(\eta)\phi'(\eta) = 0 \quad (1.14)$$

The corresponding end point conditions,

$$f'(0) = \lambda, f(0) = 0, \theta(0) = 1, \phi(0) = 1, \quad (1.15)$$

$$f'(\infty) \rightarrow 1, \theta(\infty) \rightarrow 0, \phi(\infty) \rightarrow 0, \quad (1.16)$$

The involved physical quantities are defined as:

$$We^2 = \left(\frac{c^3 \Gamma^2 x^{3m-1}}{2\nu^*}\right), \text{Pr} = \frac{\mu c_p}{k}, \lambda = \frac{b}{c}, \text{Sc} = \frac{\nu^*}{D_M}. \quad (1.17)$$

where We the Weissenberg number, Pr as Prandtl number, λ the velocity ratio parameter and Sc the Schmidt number. Also, the local coefficient of skin friction C_{fx} , the local Nusselt number Nu_x and local Sherwood number Shu_x can be defined as

$$C_{fx} = \frac{\tau_w}{u_w^2(x) \rho}, Nu_x = \frac{q_w x}{(T_w - T_\infty)k}, Shu_x = \frac{xj_w}{D_M(C_w - C_\infty)}, \quad (1.18)$$

where τ_w is termed as shear stress on surface, q_w the heat flux on surface and j_w the mass flux on surface is given as:

$$\tau_w = \mu_0 \left(\frac{\partial u}{\partial x}\right) [\beta^* + (1 - \beta^*)\{1 + \Gamma^2 \left(\frac{\partial u}{\partial x}\right)^2\}^{\frac{n-1}{2}}], \quad q_w = -k \left(\frac{\partial T}{\partial y}\right), \quad j_w = -D_M \frac{\partial C}{\partial y}, \quad (1.19)$$

one can obtain the dimensionless forms:

$$\sqrt{\text{Re}_x} C_{fx} = \frac{2}{\sqrt{2 - \beta}} [(1 - \beta^*)\{1 + (f''(0))^2 We^2\}^{\frac{n-1}{2}} + \beta^*] f''(0), \quad (1.20)$$

$$\frac{Nu_x}{\sqrt{\text{Re}_x}} = -\frac{2}{\sqrt{2 - \beta}} \theta'(0), \quad \frac{Shu_x}{\sqrt{\text{Re}_x}} = -2 \frac{1}{\sqrt{2 - \beta}} \phi'(0).$$

where $\text{Re}_x = \frac{xu_e}{\nu^*}$ is the local Reynolds number.

1.2 Computational algorithm

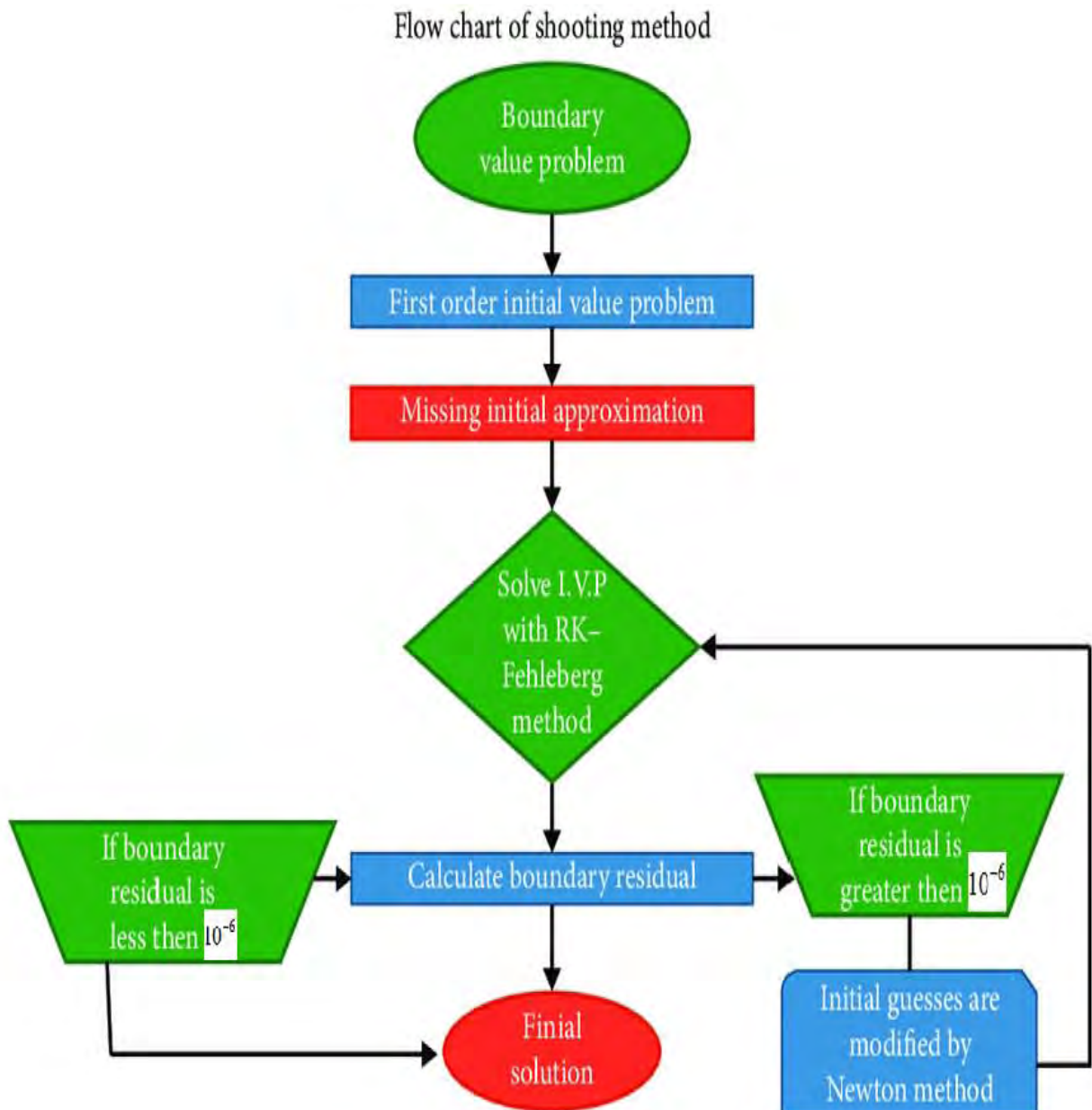


Fig. 1.2: Algorithm of shooting method.

The system (see *Eqs. (1.12)-(1.14)*) is nonlinear therefore we focus on numerical solution. For this purpose, the shooting scheme along Runge-Kutta integration process is utilized. To seek first order differential equation system (from *Eq. (1.12) - (1.14)*), follow the procedure given below:

$$f'''(\eta) = \frac{-\{1 - (f'(\eta))^2\}\beta - f(\eta)f''(\eta)}{[\beta^* + (1 - \beta^*)\{1 + n(f''(\eta))^2 We^2\}\{1 + (f''(\eta))^2 We^2\}^{\frac{n-3}{2}}]}, \quad (1.21)$$

$$\theta''(\eta) = -Pr f(\eta)\theta'(\eta), \quad (1.22)$$

$$\phi''(\eta) = -Scf(\eta)\phi'(\eta), \quad (1.23)$$

Introduce the dummy variables as

$$\begin{aligned} y_1 &= f(\eta), \quad y_2 = f'(\eta), \quad y_3 = f''(\eta), \quad y_3' = f'''(\eta), \\ y_4 &= \theta(\eta), \quad y_5 = \theta'(\eta), \quad y_5' = \theta''(\eta), \\ y_6 &= \phi(\eta), \quad y_7 = \phi'(\eta), \quad y_7' = \phi''(\eta), \end{aligned} \quad (1.24)$$

Now by incorporating *Eq. (1.24)* into *Eqs. (1.21) - (1.23)*, we obtain.

$$\begin{aligned} y_1' &= y_2 \\ y_2' &= y_3 \\ y_3' &= \frac{[-\beta(1 - y_2^2) - y_1 y_3]}{\beta^* + (1 - \beta^*)[1 + nWe^2 y_3^2][1 + We^2 y_3^2]^{\frac{n-3}{2}}} \\ y_4' &= y_5 \\ y_5' &= -Pr y_1 y_5 \\ y_6' &= y_7 \\ y_7' &= -Scy_1 y_7 \end{aligned} \quad (1.25)$$

Along with transformed boundary conditions as

$$\begin{pmatrix} 0 \\ \lambda \\ u_1 \\ 1 \\ u_2 \\ 1 \\ u_3 \end{pmatrix} = \begin{pmatrix} y_1 \\ y_2 \\ y_3 \\ y_4 \\ y_5 \\ y_6 \\ y_7 \end{pmatrix} \quad (1.26)$$

where, u_1, u_2 and u_3 are assumed as initial guesses for the values of $f''(0)$, $\theta'(0)$ and $\phi'(0)$.

We have done with the following procedure.

- Choose the value of η_∞ that lies between 5 and 10.
- Initial guesses for $y_3(0), y_5(0)$ and $y_7(0)$. Initially, $y_3(0) = y_5(0) = y_7(0) = 1$ are selected.
- Obtain the solution of Odes with the help of R-K four-fifth order methodology.
- Find absolute difference between provided and the calculated values of $y_3(\infty) = y_5(\infty)$ and $y_7(\infty)$ that is residuals at the boundary are acquired. The solution converges if its absolute difference is less than tolerance value, which is supposed to be 10^{-5} in this case.

1.3 Results and discussion

It is worth noticing that $\beta > 0$ show the favourable pressure gradient and $\beta < 0$ termed as an opposed pressure. Further, $m = 0 (\beta = 0)$ insinuates the flow through flat plate and $m = 1 (\beta = 1)$ reveals the flow at a stagnation point. The constant ratio parameter of velocity $\lambda > 0$ classify the moving wedge in the same direction and $\lambda < 0$ in the reverse direction to the free stream while $\lambda = 0$ relates to a static wedge. The two-dimensional steady Carreau fluid towards a moving wedge is investigated numerically. *Figs. 1.3 - 1.8* presents the influence of wedge angle parameter (β), ratio parameter for viscosity (β^*), ratio parameter for velocity (λ), Pr and Sc for shearing thinning ($n < 1$) and shear thickening

($n > 1$). In particular, the impacts of parameters of velocity ratio on Carreau velocity for both $\beta = 0$, and $\beta = 1$ is examined and given by way of *Fig. 1.3* where shearing thinning aspects are under consideration while similar impact in shear thickening case is testified in *Fig. 1.4*. *Figs. 1.5 - 1.6* depict the influence of enhancement in ratio parameter of viscosity on temperature of Carreau fluid for shearing thickening as well as shear thinning case when Prandtl number is altered as $Pr = 0.4$ and $Pr = 0.7$. Moreover, the effect of wedge angle parameter on concentration profile is tested for shearing thinning as well as shear thickening case when Schmidt number is altered by $Sc = 0.22$ and $Sc = 0.54$. In detail, from *Figs. 1.3 - 1.4*, we observe that the fluid velocity rises by enlarging parameter of velocity ratio λ for shear thickening and thinning. Further, it is examined that the velocity profiles are nearer to each other when the flow passes close to the point of stagnation. These figures show that the momentum boundary layer thickness for shear thickening case exceeds as compared to shear thinning case. *Figs. 1.5 - 1.6* portray the impacts of viscosity ratio parameter β^* upon temperature boundary layer. We observe that temperature is enhancing function towards ratio parameter of viscosity for shear thinning fluid and it diminishes upon viscosity ratio parameter in shear thickening case. From *Figs. 1.5-1.6*, it is also clear that for the large values of Prandtl number the Carreau fluid temperature shows significant declined values.

Figs. 1.7 - 1.8 indicate the graphical variation in the concentration for varying values of wedge angle parameter β along with distinct values of Schmidt number for shear thickening as well as shear thinning fluid. One can see that the Carreau fluid concentration is a decreasing function towards wedge angle parameter for shear thickening and thinning. Further, it is examined that concentration profile reflects large amount of decline towards variation in Schmidt number.

The system of *Eq. (1.5) - (1.8)* narrates Carreau fluid flow towards moving wedge in the presence of characteristics of transfer of heat and mass. If we ignore the involvement of mass transfer towards two dimensional Carreau fluid flow by way of moving wedge. Such case

resembles with Khan and Sardar [86]. Therefore, **Table 1.1** and **Table 1.2** are constructed in this direction. It is witnessed from both tables that we have an excellent match for both local coefficient of skin friction and local Nusselt number via ratio parameter of viscosity, ratio parameter of velocity and parameter of wedge angle. This comparison within a limiting sense yields the confirmation of execution of the computational algorithm.

1.4 Graphical representation

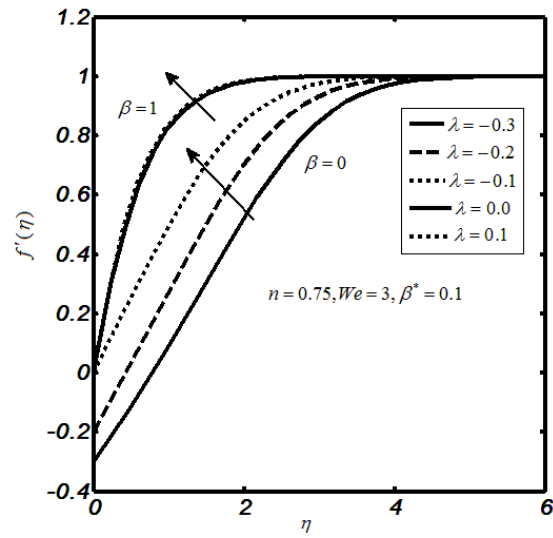


Fig. 1.3: Impacts of λ on $f'(\eta)$ for $n < 1$.

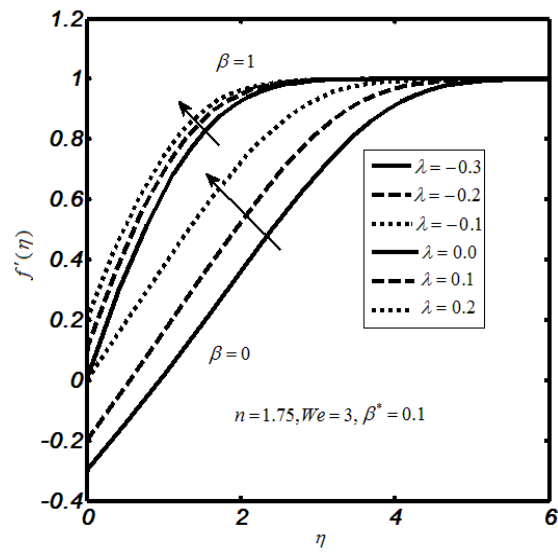


Fig. 1.4: Impacts of λ on $f'(\eta)$ for $n > 1$.

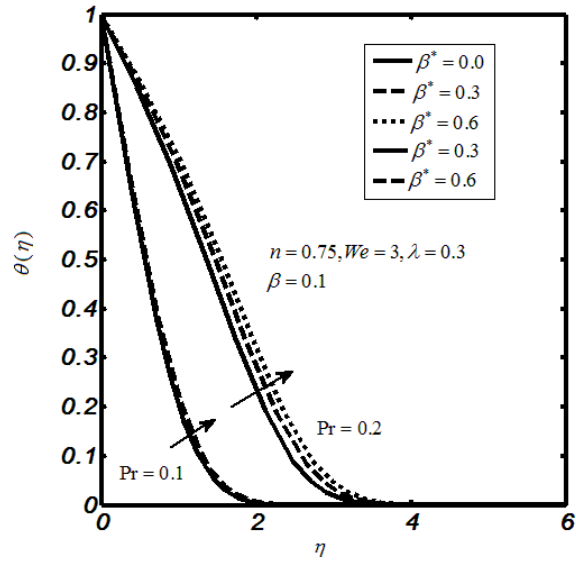


Fig. 1.5: Impact of β^* on $\theta(\eta)$ for $n < 1$.

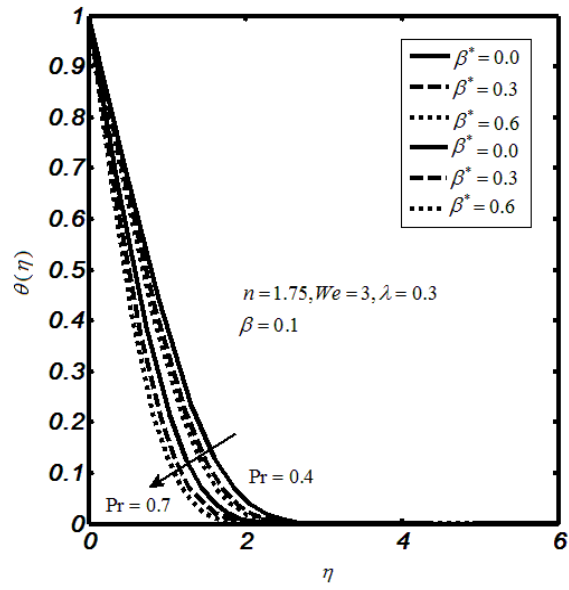


Fig. 1.6: Impact of β^* on $\theta(\eta)$ for $n > 1$.

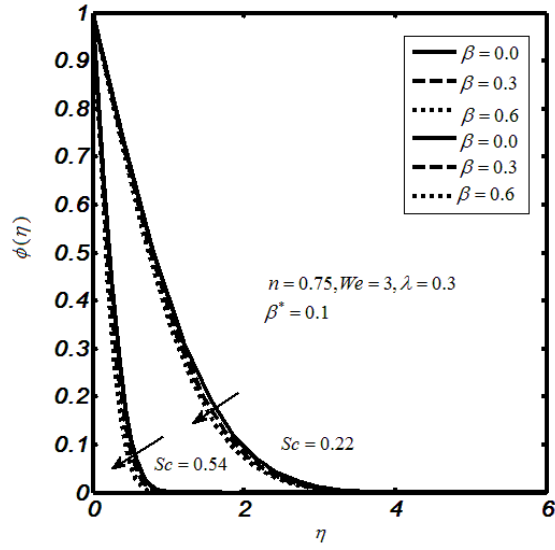


Fig. 1.7: Influence for β on $\phi(\eta)$ for $n < 1$.

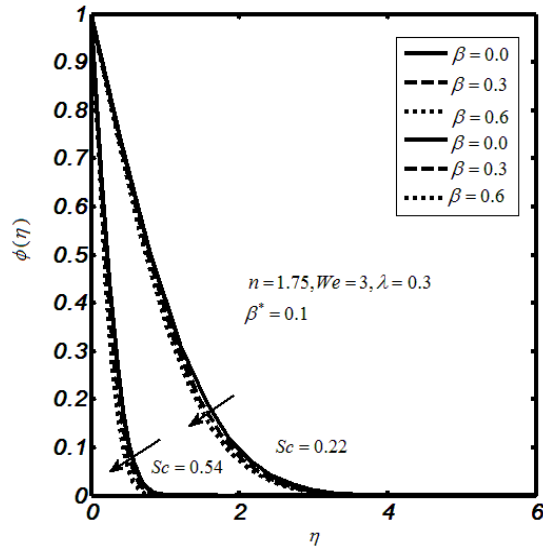


Fig. 1.8: Influence for β on $\phi(\eta)$ for $n > 1$.

Table 1.1: Numerical approximations for local coefficient of skin friction $\sqrt{\text{Re}C_{fx}}$.

β^*	β	λ	Khan and Sardar [86]		Current results	
			$\sqrt{\text{Re}C_{fx}}$		$\sqrt{\text{Re}C_{fx}}$	
			n = 0.75	n = 1.75	n = 0.7	n = 1.75
0.0	0.3	0.2	0.961012	1.22977	0.961012	1.22977
0.2	0.3	0.2	0.979203	1.20104	0.979203	1.20104
0.4	0.3	0.2	0.996203	1.16925	0.996203	1.16925
0.8	0.3	0.2	1.026900	1.09174	1.026900	1.09174
0.001	0.0	0.2	0.594385	0.706434	0.594385	0.706434
0.001	0.3	0.2	0.961107	1.22963	0.961107	1.22963
0.001	0.6	0.2	1.310680	1.77143	1.310680	1.77143
0.001	1.2	0.2	2.23300	3.26384	2.23300	3.26384
0.001	0.3	-0.3	1.170530	1.56324	1.170530	1.56324
0.001	0.3	-0.2	1.157030	1.54768	1.157030	1.54768
0.001	0.3	0.0	1.084620	1.43226	1.084620	1.43226
0.001	0.3	0.2	0.961107	1.22963	0.961107	1.22963

Table 1.2: Numerical approximations for local Nusselt number $\sqrt{\text{Re}}Nu_x$.

β^*	β	λ	Khan and Sardar [86]		Current results	
			$\sqrt{\text{Re}}Nu_x$		$\sqrt{\text{Re}}Nu_x$	
			n = 0.75	n = 1.75	n = 0.75	n = 1.75
0.0	0.3	0.2	0.916605	0.860677	0.916605	0.860677
0.2	0.3	0.2	0.912067	0.865626	0.912067	0.865626
0.4	0.3	0.2	0.90800	0.871354	0.90800	0.871354
0.8	0.3	0.2	0.900932	0.886604	0.900932	0.886604
0.001	0	0.2	0.795146	0.758852	0.795146	0.758852
0.001	0.3	0.2	0.916581	0.860700	0.916581	0.860700
0.001	0.6	0.2	1.04584	0.973570	1.04584	0.973570
0.001	1.2	0.2	1.44201	1.33020	1.44201	1.33020
0.001	0.3	-0.3	0.664451	0.529774	0.664451	0.529774
0.001	0.3	-0.2	0.722834	0.605179	0.722834	0.605179
0.001	0.3	0.0	0.825856	0.740896	0.825856	0.740896
0.001	0.3	0.2	0.916581	0.860700	0.916581	0.860700

1.5 Concluding Remarks.

The present communication contains concise analysis on two dimensional Carreau fluid steady flow over moving wedge when the characteristics of transfer of heat and mass are to be carried out. The observations in this regard are itemized as follows:

- The velocity portrait for Carreau fluid towards wedge increases upon velocity ratio parameter for thinning and thickening of shear rate.
- The velocity variations for wedge ($\beta \neq 0$) is enriched as compared to flat surface ($\beta = 0$).
- The Carreau fluid temperature is increasing function in response to ratio parameter of viscosity for thinning of shear case but inverse trend is noticed for thickening of shear case.

- The decline trend in Carreau temperature is significant for $Pr = 0.7$ than that of $Pr = 0.4$ which supports the inverse relation of Prandtl number with thermal diffusivity.
- The Carreau concentration reflects decline nature for higher values of wedge angle for both shear thickening and thinning cases.
- Higher values of Schmidt number show decrease in Carreau fluid concentration.
- The obtained outcomes are resembled with existing work which confirms the execution of computational algorithm.

Chapter 2

On heat generation/absorption and chemical reaction in a non-Newtonian fluid flow

The Carreau viscosity model with heat absorption /generation and chemical reaction, a steady flow at a boundary layer for moving wedge is studied in this chapter. The mathematical shape is designed in coupled partial differential equations and then solved numerically by Runge-Kutta Fehlberg technique chartered with shooting scheme. To investigate the impacts of physical parameter upon temperature and concentration, graphs are plotted. The temperature readings are observed for different values of parameter of heat generation. Further, the Carreau fluid concentration is inspected for parameter of chemical reaction.

2.1 Mathematical formulation

Let us consider the Carreau fluid model with both heat absorption/generation and chemical reaction. The flow field is generated by the moving wedge having velocity $u_w(x) = bx^m$ and the velocity of free stream is $u_e(x) = cx^m$. Note that $u_w(x) > 0$ indicates the surface velocity of a stretchable wedge and $u_w(x) < 0$ refers to surface velocity of contracting wedge. The wedge angle is taken to be $\Omega = \beta\pi$ where $\beta = \frac{2m}{m+1}$ is concerned with the pressure gradient. The governing equations for the model of Carreau viscosity are defined as,

$$\begin{aligned}\bar{\tau} &= -p\bar{I} + \mu(\dot{\gamma})\bar{A}_1, \\ \mu &= \mu_\infty + (\mu_0 - \mu_\infty)[1 + (\Gamma\dot{\gamma})^2]^{\frac{n-1}{2}},\end{aligned}\tag{2.1}$$

$$\dot{\gamma} = \sqrt{\frac{1}{2} \pi} = \sqrt{\frac{1}{2} \text{trace}(\bar{A}_1^2)}, \quad (2.2)$$

the apparent viscosity μ concerned with the Carreau fluid model is shown as:

$$\mu = \mu_0 [\beta^* + (1 + \beta^*) \{1 + (\Gamma \dot{\gamma})^2\}^{\frac{n-1}{2}}], \quad (2.3)$$

for two-dimensional steady flow, the velocity, temperature, and concentration fields are,

$$\bar{V} = [u(x, y), v(x, y), 0], T = T(x, y), C = C(x, y), \quad (2.4)$$

where u and v indicate the velocity components in x and y -directions, respectively.

Now, the equations of mass, momentum, energy, and concentration are as follows:

$$\frac{\partial v}{\partial y} + \frac{\partial u}{\partial x} = 0, \quad (2.5)$$

$$\begin{aligned} u \frac{\partial u}{\partial x} + v \frac{\partial u}{\partial y} = & u_e \frac{du_e}{dx} + v^* \left(\frac{\partial^2 u}{\partial y^2} \right) [\beta^* + (1 - \beta^*) \{1 + \left(\frac{\partial u}{\partial y} \right)^2 \Gamma^2\}^{\frac{n-1}{2}}] \\ & + v^* (1 - \beta^*) \Gamma^2 \left(\frac{\partial u}{\partial y} \right)^2 \left(\frac{\partial^2 u}{\partial y^2} \right) (n-1) \{1 + \left(\frac{\partial u}{\partial y} \right)^2 \Gamma^2\}^{\frac{n-1}{2}}, \end{aligned} \quad (2.6)$$

$$u \frac{\partial T}{\partial x} + v \frac{\partial T}{\partial y} = \alpha \frac{\partial^2 T}{\partial y^2} + \frac{Q_\infty}{\rho C_p} (T - T_\infty), \quad (2.7)$$

$$v \frac{\partial C}{\partial y} + u \frac{\partial C}{\partial x} = D_M \frac{\partial^2 C}{\partial y^2} - K_0 (C - C_\infty), \quad (2.8)$$

the corresponding end point conditions for moving wedge are identified as:

$$u = u_w(x) = bx^m, \quad v = 0, \quad C = C_w, \quad T = T_w \quad \text{at } y = 0 \quad (2.9)$$

$$u = u_e(x) = cx^m, \quad C \rightarrow C_\infty, \quad T \rightarrow T_\infty \quad \text{as } y \rightarrow \infty \quad (2.10)$$

Introduce the following transformations:

$$\psi(x, y) = f(\eta) \sqrt{\frac{2cv^*}{m+1}} x^{\frac{1+m}{2}}, \quad \eta = y \sqrt{\frac{c(1+m)}{2v^*}} x^{\frac{m-1}{2}}, \quad \phi(\eta) = \frac{C - C_\infty}{C_w - C_\infty}, \quad \theta(\eta) = \frac{T - T_\infty}{T_w - T_\infty}, \quad (2.11)$$

where ψ meets continuity equation as $u = \frac{\partial \psi}{\partial y}$ and $v = -\frac{\partial \psi}{\partial x}$. Hence, the reformed system

of equations is stated as:

$$[\beta^* + (1 - \beta^*)\{1 + (f'')^2 We^2\}^{\frac{n-3}{2}} \{1 + n(f'')^2 We^2\}]f''' + f f'' + [1 - (f')^2]\beta = 0, \quad (2.12)$$

$$\theta'' + Pr f \theta' + 2 Pr \delta \theta = 0, \quad (2.13)$$

$$\phi'' + Sc f \phi' - 2 Sc \gamma \phi = 0, \quad (2.14)$$

with end point conditions

$$f(0) = 0, f'(0) = \lambda, \theta(0) = 1, \phi(0) = 1, \quad (2.15)$$

$$f'(\infty) \rightarrow 1, \theta(\infty) \rightarrow 0, \phi(\infty) \rightarrow 0, \quad (2.16)$$

these quantities are defined as follows:

$$We^2 = \left(\frac{c^3 \Gamma^2 x^{3m-1}}{2\nu^*}\right), \quad Pr = \frac{\mu c_p}{k}, \quad \lambda = \frac{b}{c}, \quad \delta = \frac{Q_\infty}{\rho c_p} \frac{1}{c(m+1)x^{m-1}}, \quad (2.17)$$

$$Sc = \frac{\nu^*}{D_M}, \quad \gamma = \frac{K_1}{c}, \quad K_1 = \frac{K_0}{(m+1)x^{m-1}},$$

Engineers take keen interest in parameters that are used in the flow as well as heat transfer

problem which include Nu_x , C_{fx} and Shu_x written as:

$$Nu_x = \frac{xq_w}{k(T_w - T_\infty)}, \quad C_{fx} = \frac{\tau_w}{\rho u_w^2(x)/2}, \quad Shu_x = \frac{x j_w}{D_M(C_w - C_\infty)}, \quad (2.18)$$

where q_w , τ_w and j_w are given as

$$\tau_w = \mu_0 \left(\frac{\partial u}{\partial x}\right) [\beta^* + (1 - \beta^*)\{1 + \Gamma^2 \left(\frac{\partial u}{\partial x}\right)^2\}^{\frac{n-1}{2}}], \quad q_w = -k\left(\frac{\partial T}{\partial y}\right), \quad j_w = -D_M \frac{\partial C}{\partial y}, \quad (2.19)$$

by using Eq. (2.11), $\sqrt{Re}C_{fx}$, $\frac{Nu_x}{\sqrt{Re}}$ and $\frac{Shu_x}{\sqrt{Re}}$ take the non-dimensional form,

$$\sqrt{\text{Re}} C_{fx} = \frac{2}{\sqrt{2-\beta}} [\beta^* + (1-\beta^*) \{1 + (f''(0))^2 We^2\}^{\frac{n-1}{2}}] f''(0), \quad (2.20)$$

$$\frac{Nu_x}{\sqrt{\text{Re}}} = -\frac{2}{\sqrt{2-\beta}} \theta'(0), \quad \frac{Shu_x}{\sqrt{\text{Re}}} = -\frac{2}{\sqrt{2-\beta}} \phi'(0),$$

where $\text{Re}_x = \frac{xu_e}{\nu^*}$ is the Reynolds number.

2.2 Computational algorithm

The system of ordinary differential equations *Eq.* (2.12) - (2.14) is extremely nonlinear coupled system. The algorithm for shooting method is designed to get the solution along with boundary conditions given in *Eq.* (2.15) - (2.16). Therefore, this system is assembled into Odes as the initial value problems can be handled by using Runge-Kutta Fehlberg technique. Thus, we may write *Eq.* (2.12) – (2.14) as:

$$f''' = \frac{-\beta(1-(f')^2) - ff''}{[(1-\beta^*) \{1 + n(f'')^2 We^2 + \beta^*\} \{1 + (f'')^2 We^2\}^{\frac{n-3}{2}}]} \quad (2.21)$$

$$\theta'' = -\text{Pr} f \theta' - 2 \text{Pr} \delta \theta, \quad (2.22)$$

$$\phi'' = -\text{Sc} f \phi' + \frac{2}{m+1} \text{Sc} \gamma \phi, \quad (2.23)$$

to reduce the above set of higher order differential equations into first order system, we

introduced new variables as:

$$f = y_1, f' = y_2, f'' = y_3, f''' = y_3', \theta = y_4, \theta' = y_5, \theta'' = y_5' \quad (2.24)$$

$$\phi = y_6, y_7 = \phi', y_7' = \phi'',$$

by incorporating *Eq.* (2.24) into *Eq.* (2.21) - (2.23), we get.

$$\begin{aligned}
y_1' &= y_2 \\
y_2' &= y_3 \\
y_3' &= \frac{[-\beta(1-y_2^2) - y_1 y_3]}{\beta^* + (1-\beta^*)[1+nWe^2 y_3^2][1+We^2 y_3^2]^{\frac{n-3}{2}}} \\
y_4' &= y_5 \\
y_5' &= -Pr y_1 y_5 - 2Pr \delta y_4 \\
y_6' &= y_7 \\
y_7' &= -Sc y_1 y_7 + \frac{2}{m+1} Sc \gamma y_6,
\end{aligned} \tag{2.25}$$

together with the transformed boundary conditions provided by Eq. (2.15) - (2.16) as:

$$\begin{pmatrix} y_1 \\ y_2 \\ y_3 \\ y_4 \\ y_5 \\ y_6 \\ y_7 \end{pmatrix} = \begin{pmatrix} 0 \\ \lambda \\ u_1 \\ 1 \\ u_2 \\ 1 \\ u_3 \end{pmatrix} \tag{2.26}$$

here, u_1, u_2 and u_3 are the initial guesses for the values of $f''(0), \theta'(0)$ and $\phi'(0)$.

The following steps are carried out for shooting methodology.

- Suggesting the values of η_∞ that lies in between 5 and 10.
- The initial guesses for $y_3(0), y_5(0)$ and $y_7(0)$. Initially, $y_3(0) = y_5(0) = y_7(0) = 1$ are selected.
- Then we get the solution of Odes with the help of four-fifth order R-K methodology.
- Lastly, the absolute difference between provided and computed values that is residuals at boundary are acquired. The solution converges if its boundary residual values are less than tolerance error (10^{-5}).

2.3 Results and discussion

A numerical computation is done to explore the obtained results for the Carreau model along reactions of chemical and heat absorption/generation. The partially coupled set of Eq. (2.12) - (2.14) with end point conditions Eq. (2.15) - (2.16) are sorted out by employing Runge-Kutta four-fifth order method associated by shooting scheme to extract numerical results. The consequences of various parameters are determined and witnessed with the help of graphs.

Note that $\beta > 0$ shows the favourable pressure gradient and $\beta < 0$ indicates pressure gradient in opposite direction. Further, $m = 0 (\beta = 0)$ termed as the flow through a flat plate and $m = 1 (\beta = 1)$ indicates the flow at a stagnation point. The parameter of constant velocity ratio $\lambda > 0$ specify a moving wedge in the same direction, $\lambda < 0$ shows the opposite direction to the free stream velocity. Also, $\lambda = 0$ is concerned with the static wedge. Here, the two-dimensional steady flow of Carreau fluid towards moving wedge is examined through numerical approach.

Figs. 2.1 - 2.2 are the impacts of positive values of δ upon $\theta(\eta)$ for both $n < 1$ and $n > 1$ when $\beta = 0$ and $\beta = 1$. *Figs. 2.3 - 2.4* indicates the influences of negative values of δ upon $\theta(\eta)$ when $\beta = 0$ and $\beta = 1$. *Fig. 2.5-2.6* depicts the graphical variation for the concentration corresponding to alternating values of γ when $\beta = 0$ and $\beta = 1$.

Now in detail, from *Figs. 2.1-2.2*, it is witnessed that the fluid temperature $\theta(\eta)$ enlarges for positive values of δ for both $n < 1$ and $n > 1$ cases. Due to higher values of heat generation parameter, bulk energy is produced which consequently enhances the temperature field. The temperature profiles are nearer to each other when the flow approaches to the point of stagnation. However, *Figs. 2.1-2.2* shows that the magnitude of the temperature is higher for $\beta = 0$ as compared to $\beta = 1$.

Figs. 2.3-2.4 describe the impacts of the negative values of δ upon temperature profile. The fluid temperature diminishes for negative values of δ . Due to lowest values of heat absorption parameter the lesser heat is produced which consequently declines the temperature field. However, *Figs. 2.3-2.4* shows that the magnitude of the temperature is higher for $\beta = 0$ as compared to $\beta = 1$. Further, the flow over a flat plate $\beta = 0$ is termed as a plate with maximum temperature of the fluid. Apparently, it is because of motion of the fluid i.e., zero pressure gradient and temperature seem to be enhancing at the wedge surface due to fluid.

Figs. 2.5-2.6 indicates graphical variation in the concentration for distinct values of γ for both $n < 1$ and $n > 1$. It is noticed that the behaviour of concentration declines by uplifting the values of γ for both $n < 1$ and $n > 1$.

Table 2.1 exhibits the impacts of β^* , λ and Pr upon $\sqrt{\text{Re}}C_{fx}$ for $n < 1$. This is testified that the coefficient of local skin friction magnifies for growing values of β^* , λ and Pr when $n = 0.75$. **Table 2.2** exhibits the influence of β^* , Pr and δ on $\frac{Nu_x}{\sqrt{\text{Re}}}$. It is explored that values

of $\frac{Nu_x}{\sqrt{\text{Re}}}$ enhances when uplifting β^* and Pr but opposite trend is observed for δ when

$n = 0.75$. **Table 2.3** indicates the impact of β^* , Pr and γ on $\frac{Shu_x}{\sqrt{\text{Re}}}$. It is examined that $\frac{Shu_x}{\sqrt{\text{Re}}}$

is uplifted when enlarging the values of β^* , Pr and γ for $n = 0.75$.

2.4 Graphical representation

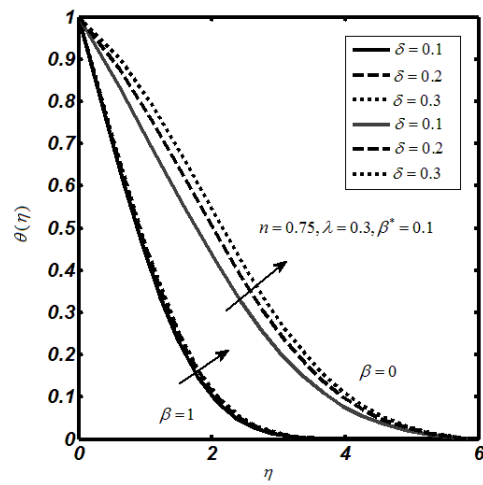


Fig. 2.1: Influence of positive values of δ on $\theta(\eta)$ for $n < 1$.

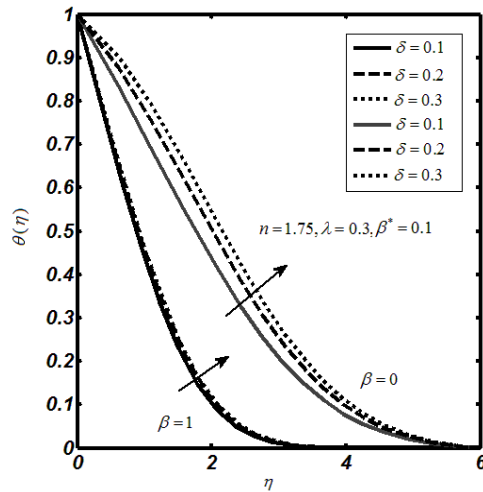


Fig. 2.2: Influence of positive values of δ on $\theta(\eta)$ for $n > 1$.

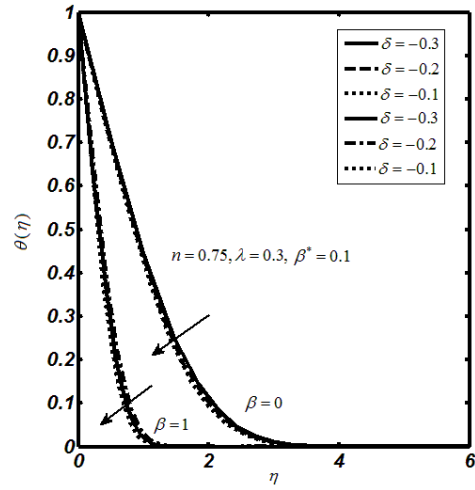


Fig. 2.3: Influence of negative values of δ on $\theta(\eta)$ for $n < 1$.

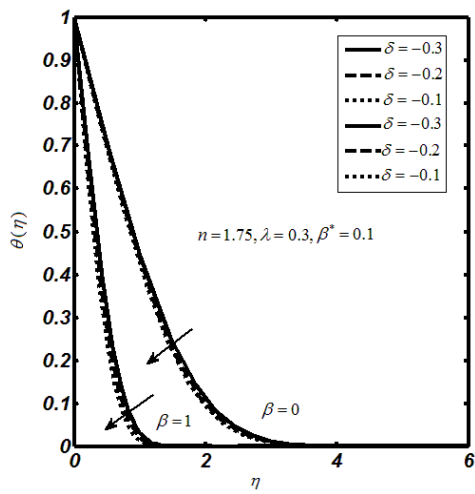


Fig. 2.4: Influence of negative values of δ on $\theta(\eta)$ for $n > 1$.

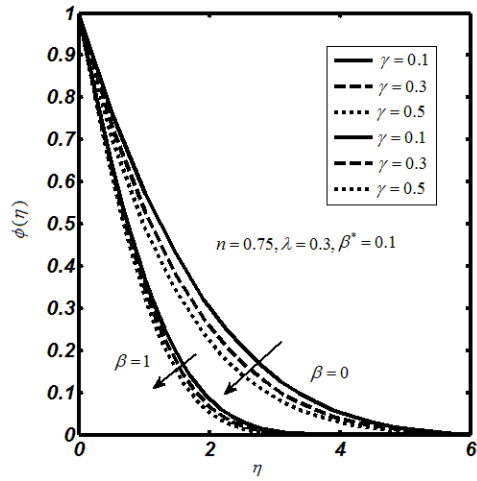


Fig. (2.5): Impacts for γ on $\phi(\eta)$ for $n < 1$.

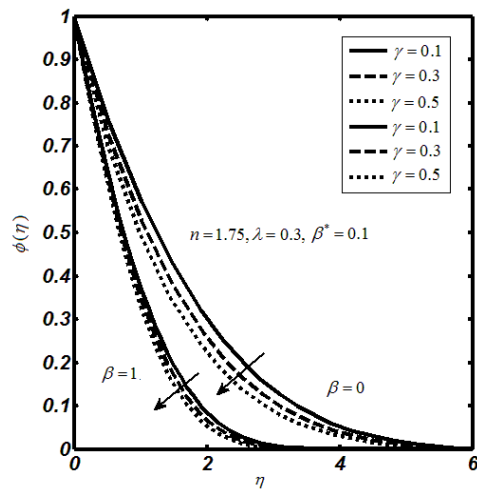


Fig. (2.6): Impacts for γ on $\phi(\eta)$ for $n > 1$.

Table 2.1: Numerical values of $\sqrt{\text{Re}C_{fx}}$ for $We = 3$ and $n = 0.75$.

β^*	β	λ	$\sqrt{\text{Re}C_{fx}}$ $n = 0.75$
0	0.3	0.2	0.2419
0.3	0.3	0.2	0.3984
0.5	0.3	0.2	0.4083
0.7	0.3	0.2	0.4453
0.001	0	0.2	0.4276
0.001	0.3	0.2	0.5139
0.001	0.6	0.2	0.5759
0.001	0.9	0.2	0.9374
0.001	0.3	-0.3	0.1849
0.001	0.3	-0.2	0.2329
0.001	0.3	0	0.3434
0.001	0.3	0.2	0.4309

Table 2.2: Numerical approximations for $\frac{Nu_x}{\sqrt{\text{Re}}}$ for $\lambda = 0.3, W = 3$ and $n = 0.75$.

β^*	β	δ	$\frac{Nu_x}{\sqrt{\text{Re}}}$ $n = 0.75$
0	0.3	0.2	0.2575
0.3	0.3	0.2	0.2889
0.5	0.3	0.2	0.3016
0.7	0.3	0.2	0.3112
0.001	0	0.2	0.2419
0.001	0.3	0.2	0.4930
0.001	0.6	0.2	0.6532
0.001	0.9	0.2	0.7693
0.001	0.3	-0.3	0.7556
0.001	0.3	-0.2	0.6763
0.001	0.3	0	0.4930

0.001	0.3	0.2	0.2575
-------	-----	-----	--------

Table 2.3: Numerical approximations of $\frac{Shu_x}{\sqrt{Re}}$ for $\lambda = 0.3, W = 3, n = 0.75$.

β^*	Pr	γ	$\frac{Shu_x}{\sqrt{Re}}$ $n = 0.75$
0	0.3	0.2	0.2419
0.3	0.3	0.2	0.4084
0.5	0.3	0.2	0.4403
0.7	0.3	0.2	0.5533
0.001	0	0.2	0.4276
0.001	0.3	0.2	0.5739
0.001	0.6	0.2	0.6359
0.001	0.9	0.2	0.9374
0.001	0.3	-0.3	0.1849
0.001	0.3	-0.2	0.2329
0.001	0.3	0	0.3434
0.001	0.3	0.2	0.4309

2.5 Concluding remarks

Here we deduced useful results for Carreau model past through moving wedge. The analysis regarding transfer of heat and mass is done that involves of chemical reactions too. We invoked R-K Fehlberg fourth-fifth order technique along shooting approach in order to get numerical results. The observations are itemized as follows:

- The temperature of Carreau fluid is growing function for positive values of \mathcal{D} for the shear thickening and thinning.

- The decline nature for Carreau temperature is observed for negative values of δ for shear thinning and thickening.
- The Carreau concentration illustrates decaying nature for positive values of γ for thinning and thickening of shear rate.
- It is witnessed that coefficient of skin friction, local Nusselt number and Sherwood number increases for higher values of β^* , Pr , λ and γ when $n = 0.75$.

Chapter 3

Thermal energy in a Jeffery fluid flow regime: A generalized Fourier's law outcomes

This chapter includes the results for Jeffery fluid with thermal stratification effects at a stagnation point. The thermal energy characteristics are studied through Cattaneo-Christov heat flux model. The flow is magnified by the stretching cylinder. The homogeneous-heterogeneous chemically reactive species are considered. The concerned mathematical problem is developed by laws of conservation of momentum, mass and energy which provides coupled partial differential equation. The order of these equations is reduced by way of similarity transformation. Later, the set of reduced coupled equations are computed numerically via Runge-Kutta Fehlberg technique with shooting algorithm. The curves for temperature and velocity of fluid are plotted for different engineering parameters. The coefficient of skin friction is examined, and the obtained outcomes are comparison with existing literature.

3.1 Mathematical formulation

The generalized shape of Fourier's law model that describes heat transfer is given as

$$q + \tilde{\lambda}^* [\bar{V} \cdot \nabla q - q \cdot \nabla \bar{V} + (\nabla \cdot \bar{V})q + \frac{\partial q}{\partial t}] = -k \nabla T, \quad (3.1)$$

where q is the flux of heat, $\tilde{\lambda}^*$ is the relaxation time of flux of heat, k is thermal conductivity. Eq. (3.1) is simply the Fourier's law when $\tilde{\lambda}^* = 0$. For an incompressible fluid, the above equation reduces to the following form.

$$q + \tilde{\lambda}^* [\bar{V} \cdot \nabla q - q \cdot \nabla \bar{V}] = -k \nabla T, \quad (3.2)$$

Later, the energy equation is carried out by way of Eq. (3.2). Consider a two-dimensional Jeffery model flow on a boundary layer through a stretched cylinder. The thermal stratification with Cattaneo-Christov heat flux model is considered and coordinates in cylindrical form are x and r assumed along the axial and normal to surface. The stretching occurs with the velocity $u_w(x) = \frac{bx}{\tilde{l}}$ and free stream velocity is considered as $u_e(x) = \frac{cx}{\tilde{l}}$, \tilde{l} is the characteristic length and the flow is taken at a stagnation point. Taking homogeneous-heterogeneous reaction where isothermal cubic autocatalytic reaction (homogeneous) but a single first order reaction (heterogeneous) on a catalyst surface which is indicated as:



whereas \tilde{a} and \tilde{b} are the concentration for chemical species A and B , \tilde{l}_1, \tilde{l}_s are constants.

Now, by implementing the approximations for the boundary layer, the conservation laws become,

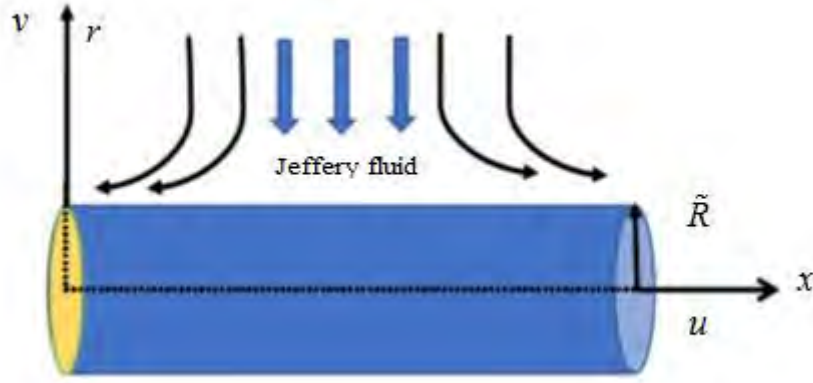


Fig 3.1: Geometry of the problem.

$$\frac{\partial}{\partial x}(ru) + \frac{\partial}{\partial r}(rv) = 0, \quad (3.5)$$

$$\begin{aligned} \frac{\partial u}{\partial x}u + \frac{\partial u}{\partial r}v = u_e(x) \frac{d}{dx}u_e(x) + \frac{\mu}{\rho(\tilde{\lambda}_1 + 1)} \left[\frac{\partial^2 u}{\partial r^2} + \frac{\partial u}{\partial r} \frac{1}{r} + \tilde{\lambda}_2 \left(\frac{v}{r} \frac{\partial^2 u}{\partial r^2} + \frac{\partial^2 u}{\partial r^2} \frac{\partial v}{\partial r} + \frac{\partial^3 u}{\partial r^3} v \right. \right. \\ \left. \left. + \frac{\partial^2 u}{\partial x \partial r} \frac{u}{r} + \frac{\partial^2 u}{\partial x \partial r} \frac{\partial u}{\partial r} + \frac{\partial^3 u}{\partial r^2 \partial x} u \right) \right], \quad (3.6) \end{aligned}$$

$$\begin{aligned} u \frac{\partial T}{\partial x} + v \frac{\partial T}{\partial r} + \tilde{\lambda}^* (v^2 \frac{\partial^2 T}{\partial r^2} + u^2 \frac{\partial^2 T}{\partial x^2} + 2uv \frac{\partial^2 T}{\partial x \partial r} + u \frac{\partial u}{\partial x} \frac{\partial T}{\partial x} + u \frac{\partial v}{\partial x} \frac{\partial T}{\partial r} + v \frac{\partial u}{\partial r} \frac{\partial T}{\partial x} \\ + \frac{\partial u}{\partial r} \frac{\partial T}{\partial r} v) = \alpha \left(\frac{\partial T}{\partial r} \frac{1}{r} + \frac{\partial^2 T}{\partial r^2} \right), \quad (3.7) \end{aligned}$$

$$\frac{\partial \tilde{a}}{\partial x}u + \frac{\partial \tilde{a}}{\partial r}v = \left(\frac{\partial^2 \tilde{a}}{\partial r^2} + \frac{1}{r} \frac{\partial \tilde{a}}{\partial r} \right) \tilde{D}_A - \tilde{l}_1 \tilde{a} \tilde{b}^2, \quad (3.8)$$

$$u \frac{\partial \tilde{b}}{\partial x} + v \frac{\partial \tilde{b}}{\partial r} = \tilde{D}_B \left(\frac{\partial^2 \tilde{b}}{\partial r^2} + \frac{1}{r} \frac{\partial \tilde{b}}{\partial r} \right) + \tilde{l}_1 \tilde{a} \tilde{b}^2, \quad (3.9)$$

where (u, v) are the components of velocity, $u_e(x)$ the velocity of free stream, ρ the fluid density, μ as viscosity of fluid, T as fluid temperature, α as thermal diffusivity, c_p as specific heat capacity, T_∞ the ambient temperature, $\tilde{\lambda}_1$ the ratio of relaxation-retardation times,

$\tilde{\lambda}_2$ the time of retardation, A and B are the chemical species with coefficients of diffusion as \tilde{D}_A and \tilde{D}_B . The associated end point conditions are.

$$u = u_w(x) = \frac{bx}{\tilde{l}}, v = 0 \text{ at } r = \tilde{R}, u = u_e(x) = \frac{cx}{\tilde{l}} \text{ as } r \rightarrow \infty, \quad (3.10)$$

$$T = T_w(x) = T_o + \tilde{c}\left(\frac{x}{\tilde{l}}\right) \text{ at } r = \tilde{R}, T = T_\infty(x) = T_o + \tilde{d}\left(\frac{x}{\tilde{l}}\right) \text{ as } r \rightarrow \infty, \quad (3.11)$$

$$\tilde{D}_A \frac{\partial \tilde{a}}{\partial r} = \tilde{l}_s \tilde{a}, \tilde{D}_B \frac{\partial \tilde{b}}{\partial r} = -\tilde{l}_s \tilde{a} \text{ at } r = \tilde{R}, \tilde{a} \rightarrow \tilde{a}_o, \tilde{b} \rightarrow 0 \text{ as } r \rightarrow \infty, \quad (3.12)$$

where T_w indicates surface and T_∞ as ambient temperature, \tilde{c} and \tilde{d} are dimensionless constants, \tilde{R} is the radius of cylinder. We use the following similarity transformations as:

$$\eta = \sqrt{\frac{b}{v^* \tilde{l}}} \left(\frac{r^2 - \tilde{R}^2}{2\tilde{R}} \right), u = \frac{bx}{\tilde{l}} f'(\eta), \tilde{v} = -\frac{\tilde{R}}{r} \sqrt{\frac{bv^*}{\tilde{l}}} f(\eta), \quad (3.13)$$

$$\theta(\eta) = \frac{T_\infty - T}{T_\infty - T_w}, \tilde{m}(\eta) = \frac{\tilde{a}}{\tilde{a}_o}, \tilde{n}(\eta) = \frac{\tilde{b}}{\tilde{b}_o},$$

Now by invoking Eq. (3.13) into Eq. (3.6) - (3.9), we get.

$$(1 + 2\tilde{K}\eta)f''' + (1 + \tilde{\lambda}_1)(ff'' - f'^2) + 2\tilde{K}f'' + \tilde{K}\tilde{\beta}(ff'' - 3ff') + \tilde{\beta}(1 + 2\tilde{K}\eta)(f''^2 - ff^{(4)}) + (1 + \tilde{\lambda}_1)\lambda^2 = 0, \quad (3.14)$$

$$(1 + 2\tilde{K}\eta)\theta'' + 2\tilde{K}\theta' + \text{Pr} f\theta' - \text{Pr}(\tilde{S} + \theta)f' + \text{Pr} \tilde{\gamma}[ff''(\tilde{S} + \theta) - ff'\theta' - f'^2(\tilde{S} + \theta) - f^2\theta''] = 0, \quad (3.15)$$

$$\frac{1}{Sc} [\tilde{m}''(1 + 2\tilde{K}\eta) + 2\tilde{m}'\tilde{K}] + f\tilde{m}' - m\tilde{m}^2 L = 0, \quad (3.16)$$

$$\frac{\tilde{\delta}^*}{Sc} [\tilde{n}''(1 + 2\tilde{K}\eta) + 2\tilde{n}'\tilde{K}] + f\tilde{n}' + m\tilde{n}^2 L = 0, \quad (3.17)$$

the transformed boundary conditions are.

$$\begin{aligned} f(0) = 0, f'(0) = 1, \theta(0) = 1 - \tilde{S}, \tilde{m}'(0) = \tilde{m}(0)L_s, \tilde{\delta}^* \tilde{n}'(0) = -\tilde{n}(0)L_s, \\ f'(\infty) = \lambda, \theta(\infty) = 0, \tilde{m}(\infty) \rightarrow 1, \tilde{n}(\infty) \rightarrow 0, \end{aligned} \quad (3.18)$$

where $\tilde{K} = \sqrt{\frac{v^* \tilde{l}}{b \tilde{R}^2}}, \tilde{\beta} = \frac{b \tilde{\lambda}_2}{\tilde{l}}, \text{Pr} = \frac{\mu c_p}{k}, \tilde{\gamma} = \frac{b \tilde{\lambda}^*}{\tilde{l}}, \text{Sc} = \frac{v^*}{\tilde{D}_A}, L = \frac{\tilde{l}_1 \tilde{a}_o^2 \tilde{l}}{u_w}, L_s = \frac{\tilde{l}_s}{\tilde{D}_A} \sqrt{\frac{v^* \tilde{l}}{b}}, \lambda = \frac{c}{b},$

$\tilde{S} = \frac{\tilde{d}}{\tilde{c}}, \tilde{\delta}^* = \frac{\tilde{D}_A}{\tilde{D}_B}$ are named as curvature parameter, Deborah number, Prandtl number, thermal

relaxation parameter, Schmidt number, homogeneous reaction parameter, heterogeneous reaction parameter, velocity ratio parameter, thermal stratification parameter and mass diffusion coefficient. By assuming \tilde{D}_A and \tilde{D}_B (diffusion coefficient constants) equal that is

$\tilde{\delta}^* = 1$. This implies $\tilde{m}(\eta) + \tilde{n}(\eta) = 1$. From Eq. (3.16) - (3.17), we get:

$$\frac{1}{\text{Sc}} [(1 + 2\tilde{K}\eta)\tilde{m}'' + 2\tilde{K}\tilde{m}'] + \tilde{m}'f - L(1 - \tilde{m})^2 \tilde{m} = 0, \quad (3.19)$$

with to the end point conditions

$$\tilde{m}'(0) = \tilde{m}(0)L_s, \tilde{m}(\infty) \rightarrow 1, \quad (3.20)$$

the involved engineering parameters are.

$$C_f = \frac{2\tau_w}{\rho u_w^2}, Nu_x = \frac{-xq_w}{k(T_w - T_c)}, \quad (3.21)$$

$$\tau_w = \left[\frac{\mu}{1 + \tilde{\lambda}_1} \left(\frac{\partial u}{\partial r} \right) + \frac{\mu \tilde{\lambda}_2}{1 + \tilde{\lambda}_1} \left(v \frac{\partial^2 u}{\partial r^2} + u \frac{\partial^2 u}{\partial r \partial x} \right) \right]_{r=\tilde{R}}, q_w = - \left(\frac{\partial T}{\partial r} \right)_{r=\tilde{R}} k,$$

Where C_f and Nu_x are the coefficient of skin friction local Nusselt number with τ_w and q_w as relation of wall stress shear and surface flux at $r = \tilde{R}$. Thus, above expressions in dimensionless form are:

$$\begin{aligned} \frac{1}{2}\sqrt{\text{Re}_x}C_f &= \frac{1}{(\tilde{\lambda}_1+1)}[f''(0)-f'''(0)f(0)\tilde{\beta}-f(0)f''(0)\tilde{\beta}\tilde{K}+f'(0)f''(0)\tilde{\beta}], \\ \frac{Nu_x}{\sqrt{\text{Re}_x}} &= -\theta'(0), \end{aligned} \quad (3.22)$$

Since, $\text{Re}_x = \frac{u_w \tilde{l}}{\nu}$ is termed as local Reynold's number.

3.2 Computational algorithm

As the Eq. (3.14) - (3.20) is extremely nonlinear coupled system. The shooting algorithm is designed in view of Runge-Kutta four-fifth order integration methodology in order to sort out this system. This system is assembled into set of first order ODE's and that can be handled by using Runge-Kutta Fehlberg methodology. Thus Eq. (3.14) -(3.15) and Eq. (3.19) may be written as:

$$\begin{aligned} &f'''(1+2\tilde{K}\eta)+(1+\tilde{\lambda}_1)(f f''-f'^2)+2\tilde{K} f''+\tilde{K} \tilde{\beta}(f'' f'-3f'' f) \\ \tilde{f}^{(4)} &= \frac{+\tilde{\beta}(1+2\tilde{K}\eta) f''^2+(1+\tilde{\lambda}_1)\lambda^2}{\tilde{\beta}(1+2\tilde{K}\eta)}, \end{aligned} \quad (3.23)$$

$$\theta'' = \frac{\text{Pr}(\tilde{S}+\theta) f'-2\tilde{K} \theta'-f \text{Pr} \theta'-\tilde{\gamma} \text{Pr} [f'' f(\tilde{S}+\theta)-\theta' f f'-(\tilde{S}+\theta) f'^2]}{(1+2\tilde{K} \eta)-f^2 \text{Pr} \tilde{\gamma}}, \quad (3.24)$$

$$\tilde{m}'' = \frac{\text{Sc}[L\tilde{m}(1-\tilde{m})^2-f \tilde{m}']-2\tilde{K} \tilde{m}'}{(1+2\tilde{K} \eta)}, \quad (3.25)$$

To get the reduced number of independent variables, we introduce new variables as:

$$\begin{aligned} y_1 &= f, y_2 = f', y_3 = f'', y_4 = f''', y_4' = f^{(4)}, \\ y_5 &= \theta, y_6 = \theta', y_6' = \theta'', y_7 = \tilde{m}, y_8 = \tilde{m}', y_8' = \tilde{m}'', \end{aligned} \quad (3.26)$$

by inserting Eq. (3.26) into Eq. (3.23) - (3.25), the set of first order ODE's is obtained as:

$$\begin{aligned}
y_1' &= y_2 \\
y_2' &= y_3 \\
y_3' &= y_4 \\
y_4' = f^{(4)} &= \frac{(1+2\tilde{K}\eta)y_4 + (1+\tilde{\lambda}_1)(y_1y_3 - y_2^2) + 2\tilde{K}y_3 + \tilde{K}\tilde{\beta}(y_2y_3 - 3y_1y_3) + \tilde{\beta}(1+2\tilde{K}\tilde{\eta})y_3^2 + (1+\tilde{\lambda}_1)\lambda^2}{\tilde{\beta}(1+2\tilde{K}\eta)} \\
y_5' &= y_6 \\
y_6' &= \frac{\Pr(\tilde{S} + y_5)y_2 - 2\tilde{K}y_6 - \Pr y_1y_6 - \Pr\tilde{\gamma}[(\tilde{S} + y_5)y_1y_3 - y_1y_2y_6 - (\tilde{S} + y_5)(y_2^2)]}{(1+2\tilde{K}\eta) - \Pr\tilde{\gamma}y_1^2} \\
y_7' &= y_8 \\
y_8' &= \frac{Sc[Ly_7(1-y_7)^2 - y_1y_8] - 2\tilde{K}y_8}{(1+2\tilde{K}\eta)},
\end{aligned} \tag{3.27}$$

the transformed end point conditions are.

$$y_1(0) = 0, y_2(0) = 1, y_5(0) = 1 - \tilde{S}, y_8(0) = L_s y_7(0), \tag{3.28}$$

$$y_2(\infty) \rightarrow \lambda, y_5(\infty) \rightarrow 0, y_7(\infty) \rightarrow 1,$$

here, $y_3(0) = u_1, y_4(0) = u_2, y_6(0) = u_3, y_7(0) = u_4$, are the initial guesses for the values of $f''(0), f'''(0), \theta'(0)$ and $\tilde{m}(0)$.

We have done with the following procedure in view of shooting methodology.

- Firstly, choose the values of η_∞ .
- Then we take initial guesses for $y_3(0), y_4(0), y_6(0)$ and $y_7(0)$. Initially, $y_3(0) = y_4(0) = y_6(0) = y_7(0) = 1$ are assumed.
- Then we get the solution of Odes with the help of four-fifth order R-K methodology.

- Lastly, the absolute variation in provided and computed values of $y_3(\infty)$, $y_4(\infty)$, $y_6(\infty)$ and $\tilde{y}_7(\infty)$ that is residuals at boundary are computed. The solution converges if it is less than tolerance error 10^{-5} .

3.3 Results and discussion

Focus of this chapter is on Jeffery fluid model with stagnation point and the flow field occur by the cylinder that stretches. The thermal boundary layer is executed by means of Christov-Cattaneo heat flux theory. The heterogeneous- homogeneous chemical reactions are measured. The mathematical equations describing the fluid flow are presented by laws of conservation of mass, energy and momentum. These equations are offered in the form of coupled partial differential framework that can be transformed into coupled ordinary differential framework through appropriate transformation. The numerical results are uncovered by way of Runge-Kutta Fehlberg methodology adjacent to shooting scheme. The obtained physical parameters are $\tilde{\beta}$ (Deborah number), $\tilde{\gamma}$ (thermal relaxation parameter), \tilde{K} , Pr , \tilde{S} , Sc (Schmidt number), L (Homogenous reaction parameter), L_s (Heterogeneous reaction parameter).

Fig. 3.2 shows the decline trend for velocity of Jeffery fluid against various values of $\tilde{\beta}$ i.e., $\tilde{\beta}(=0.2,0.3,0.4,0.5)$. It is observed that the Jeffery fluid velocity has uplifts behavior for \tilde{K} shown in *Fig. 3.3*. This is because the radius of curvature depending upon cylindrical surface decreases when we iterate $\tilde{K}(=0.1,0.2,0.3,0.4)$. As the contact surface area between cylinder and the Jeffery fluid particles reduces. Therefore, the Jeffery fluid faces less resistance and as a result its velocity enhances. The effects of Jeffery fluid temperature upon $\tilde{\gamma}$, \tilde{S} , Pr , and \tilde{K} are presented. *Fig. 3.4* indicates the fluctuation of Jeffery fluid temperature towards $\tilde{\gamma}$. The impacts on Jeffery fluid temperature θ due to iterative values of $\tilde{\gamma}(=0.1,0.2,0.3,0.4)$ are depicted by means of *Fig. 3.4*. The fluid temperature declines towards $\tilde{\gamma}$. To interpret the effects of

temperature stratification upon temperature profile, we introduce the stratification parameter \tilde{S} . The influence of temperature stratification parameter is observed and is presented in *Fig. 3.5*. This indicates that the fluid temperature declines when we iterate the values of \tilde{S} i.e., $\tilde{S}(=0.0,0.1,0.2,0.3)$. Physically, this is since the variation in temperature steadily decays between ambient temperature and the cylindrical surface. The variations in Jeffery fluid temperature towards Pr is delineated in *Fig. 3.6*. This shows that the temperature of fluid descends for the iterative values of Pr that is $Pr(=0.1,0.2,0.3,0.4)$. Physically, Prandtl number demonstrates the ratio of thermal diffusivity to momentum diffusivity. The decrease in thickness of thermal boundary layer is examined due to higher values of Pr as it yields small amount of thermal diffusivity. Hence, decline in heat transfer rate occurs. Also, the inverse relation between Pr and thermal conductivity declines the thermal layer thickness because large values of Pr provides less energy diffusion. Therefore, fluid temperature decreases. Thus, the large values of Pr can be used to decline the thermal boundary layer thickness in flow conduction. It is examined in *Fig. 3.7* that the curvature of the cylinder affects the temperature of the fluid. That is when we iterate the curvature parameter $\tilde{K}(=0.1,0.2,0.3,0.4)$, the Jeffery fluid temperature enhances. This is since higher values of local Nusselt number enhances by increasing curvature parameter \tilde{K} and hence the transfer rate of heat is affected. The impacts of curvature parameter upon fluid temperature are witnessed in *Fig. 3.7*. This figure discloses the fact that fluid velocity declines close to cylindrical surface whereas it enlarges while passing apart from the surface against the extended values of curvature parameter and reverse trend occurs in concentration profile. As, the radius of the cylinder reduces by uplifting the curvature parameter and provides a reason to minimize the area of contact between the fluid and the cylinder. Therefore, the velocity enhances and same is the case with temperature profile. Further, it is worthy to notice that the problem is converted into flow past a flat plate for $\tilde{K} = 0$ upon which the thermal and momentum boundary layer are lesser as compared to the flow

through stretched cylinder $\tilde{K} \neq 0$. The correlation between Jeffery fluid concentration and Schmidt number is presented in *Fig. 3.8*. It is worth noticing that the Jeffery fluid concentration inclines when we iterate $Sc (= 0.1, 0.3, 0.5, 0.7)$. Physically, the ratio of viscous diffusion to molecular diffusion is termed as Schmidt number. The enhancement in Schmidt number exhibits small molecular diffusivity. Thus, the inclination in momentum diffusivity rate causes enhancement in concentration.

The impacts of L on Jeffery fluid concentration is examined in *Fig. 3.9*. It is shown that the higher values of L i.e., $L (= 0.1, 0.2, 0.3)$ decreases the concentration curves. The enhancement in homogeneous reaction parameter causes reduction in fluid concentration profile because of consumption of reactions. Also, it yields fluid viscosity that provides a reason for uplifting in fluid concentration trend. The impacts of L_s on fluid concentration trend is depicted in *Fig. 3.10*. The diffusion rate reduces due to higher values of L_s i.e., $L_s (= 0.1, 0.2, 0.3)$ which declines the concentration because diffusion rate decreases as the reaction rate increase. Therefore, the concentration profile of Jeffery fluid towards L_s decreases. The approximations for the coefficient of skin friction towards values of $\tilde{\lambda}_1$ and $\tilde{\beta}$ are delineated in **Table 3.1** and **Table 3.2**. Thus, the coefficient of skin friction declines towards higher values of $\tilde{\lambda}_1$ whereas inverse trend is examined for larger $\tilde{\beta}$ in **Table 3.1**. Also, variation in $\tilde{\lambda}_1$ causes decline in the coefficient of skin friction in **Table 3.2**.

3.4 Graphical representation

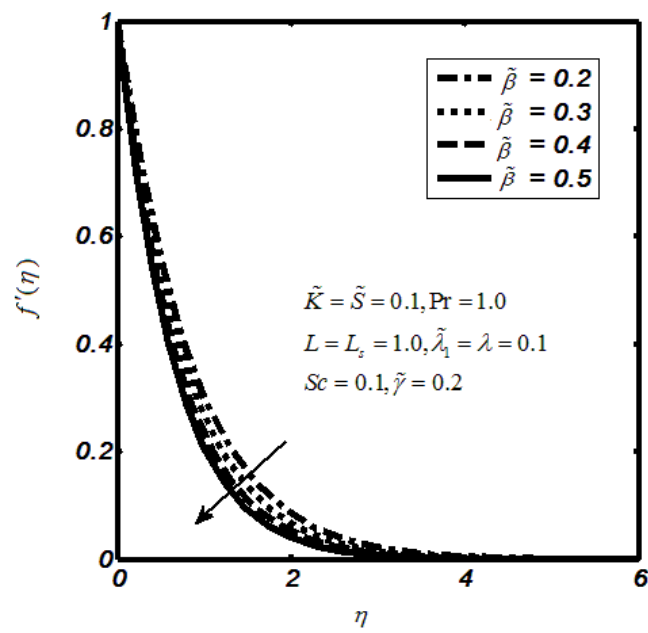


Fig. 3.2: Impacts of $\tilde{\beta}$ upon $f'(\eta)$.

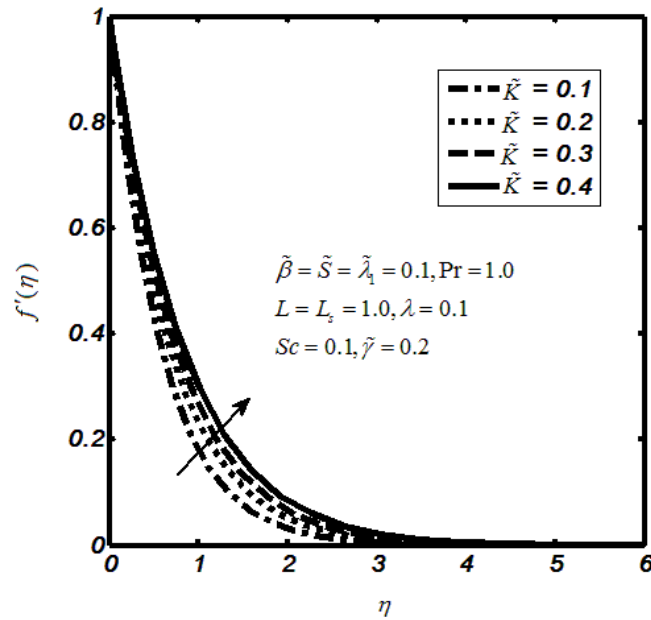


Fig. 3.3: Impacts of \tilde{K} on $f'(\eta)$

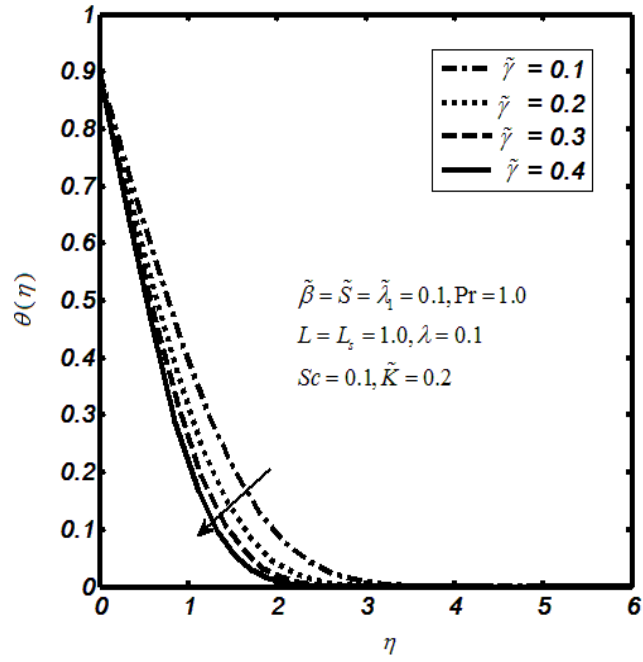


Fig. 3.4: Impacts of $\tilde{\gamma}$ on $\theta(\eta)$.

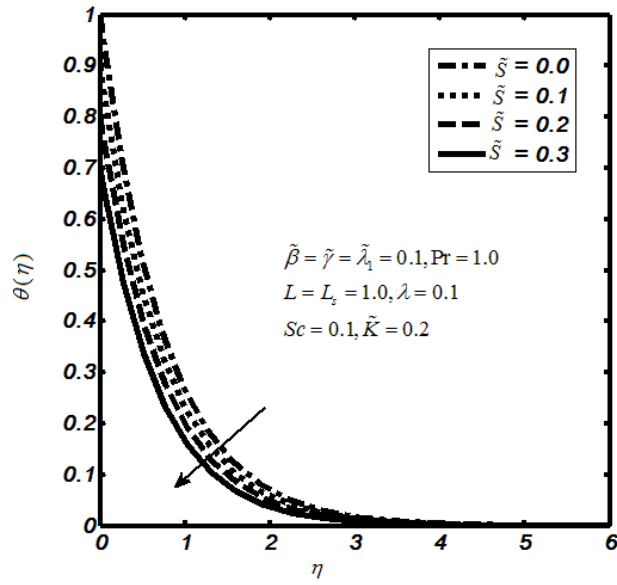


Fig. 3.5: Influence of \tilde{S} on $\theta(\eta)$.

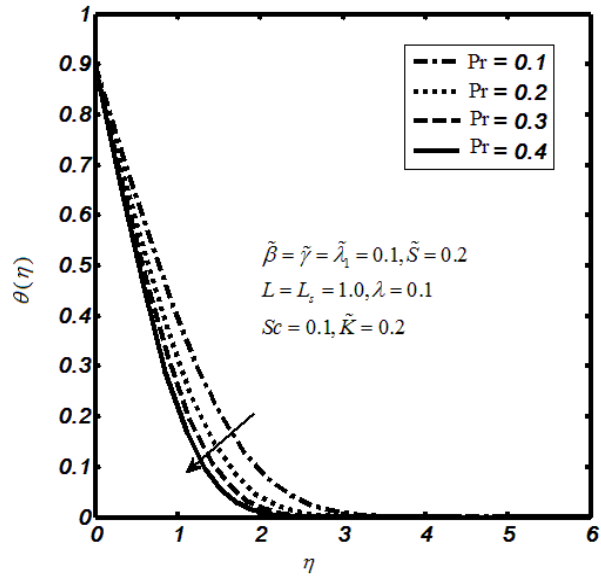


Fig. 3.6: Impacts of Pr on $\theta(\eta)$.

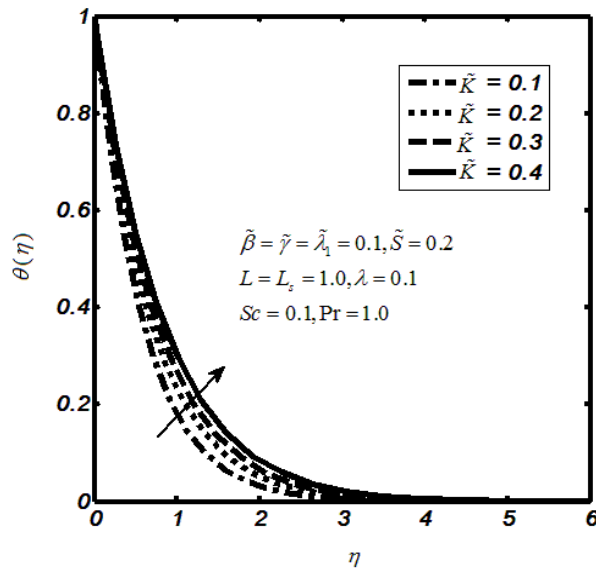


Fig. 3.7: Impacts of \tilde{K} on $\theta(\eta)$.

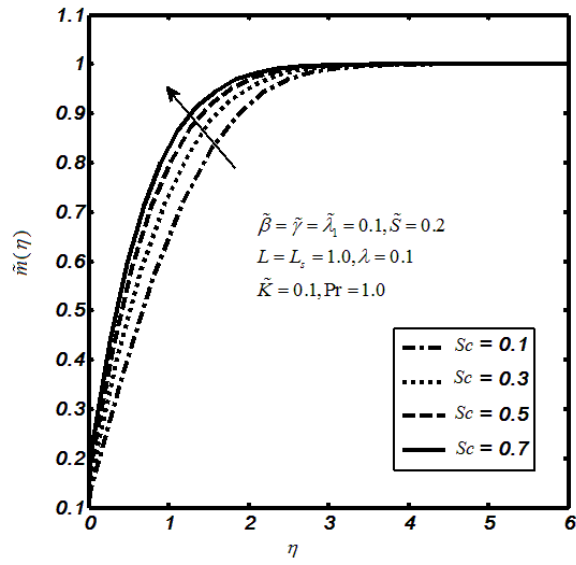


Fig. 3.8: Impacts of Sc on $\tilde{m}(\eta)$.

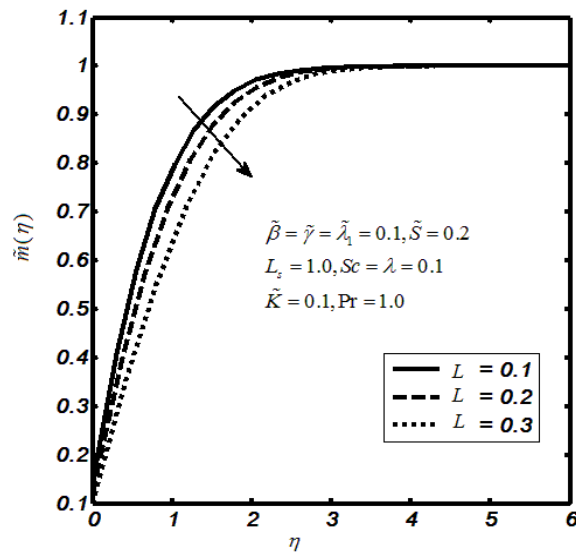


Fig. 3.9: Impacts of L on $\tilde{m}(\eta)$.

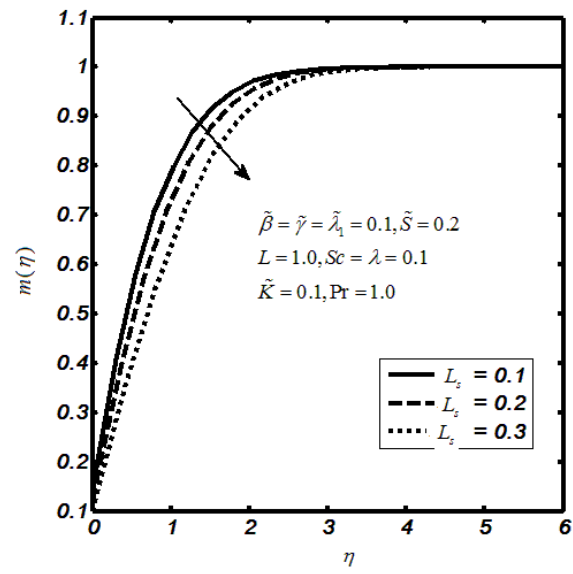


Fig. 3.10: Impacts of L_s on $\tilde{m}(\eta)$.

Table 3.1. The numerical approximations for the local skin friction $\frac{1}{2}\sqrt{\text{Re}_x}C_f$ when $\tilde{\gamma} = 0.2, \tilde{K} = 0.5$ and $\tilde{s} = 0.3$.

$\tilde{\beta}$	$\tilde{\lambda}_1$	Hayat et al. [83]	Current results
0.1	0.2	0.95743	0.9563
0.1	0.3	0.91987	0.9185
0.1	0.4	0.88641	0.8851
0.1	0.5	0.85635	0.8554
0.2	0.2	1.00000	1.000
0.2	0.3	0.96077	0.9600
0.2	0.4	0.92582	0.9251
0.2	0.5	0.89442	0.8941
0.3	0.2	1.0408	1.0406
0.3	0.3	1.0000	1.0000
0.3	0.4	0.96362	0.9630
0.3	0.5	0.93095	0.9301
0.4	0.2	1.0801	1.0801
0.4	0.3	1.0378	1.0362
0.4	0.4	1.0000	1.0000
0.4	0.5	0.96608	0.9653

Table 3.2. The numerical approximations for the local skin friction $\frac{1}{2}\sqrt{\text{Re}_x}C_f$ when $\tilde{\gamma} = 0.2, \tilde{K} = 0.5$ and $\tilde{s} = 0.3$.

$\tilde{\lambda}_1$	$\tilde{\beta}$	Abbasi et al. [84]	Hayat et al. [83]	Current results
0.0	0.2	1.09545	1.09545	1.0951
0.5	0.2	0.89443	0.89442	0.8943
0.7	0.2	0.84017	0.84016	0.8401
1.0	0.2	0.77460	0.77460	0.7745

0.4	0.0	0.84515	0.84515	0.8450
0.4	0.3	0.96362	0.96362	0.9635
0.4	0.6	1.06904	1.06904	1.0691
0.4	1.0	1.19523	1.19523	1.1953

3.5 Concluding remarks

In the Jeffery fluid model, we studied thermal relaxation and thermal stratification effects. The flow is discussed at a stagnation point and is invoked by the cylindrical surface. The Cattaneo-Christov theory is executed for energy equation. The concentration equation is modelled through heterogeneous- homogeneous chemical reactions. The flow describing coupled PDE's descend to ODE's by appropriate transformation. The obtained system is sorted out numerically via Runge-Kutta methodology with shooting approach. The outcomes are compared with exiting literature. The key points for shooting methodology are as follows:

- The decaying behaviour of velocity profile for Deborah number is noticed.
- The curvature parameter with increasing values enlarges fluid velocity profile.
- The decline trend for temperature profile is captured on exceeding thermal relaxation parameter.
- The temperature curves decay against parameter of thermal stratification.
- The Jeffery temperature declines on exceeding Prandtl number.
- The curvature parameter provides a reason for uplift in temperature profile.
- The Jeffery concentration increases when Schmidt number enlarges.
- The decline behaviour of concentration profile is observed towards parameter of homogeneous reaction.
- The decaying curves for the concentration are examined towards higher values of parameter of heterogeneous reaction.

- The coefficient of skin friction coefficient declines towards thermal relaxation parameter.
- Increase in Deborah number provides a reason for coefficient of skin friction to get inclined.

Chapter 4

MHD effects in a non-Newtonian flow model with homogeneous-heterogeneous reactions

The Jeffery fluid past a point of stagnation towards a cylindrical surface with the homogenous-heterogeneous reactions, magnetic field and heat generation effects are elaborated in this chapter. The heat transport process is debated by Cataneo-Christov heat flux concerned to thermal stratification. The consequential PDE's descend to ODE's by carrying out the set of similarity transformation. These equations are sorted out in a numerical procedure named as Runge-Kutta Fehlberg method with shooting approach. The effects of involved parameters are analysed by means of graphs. The obtain outcomes are validated with an existing published work.

4.1 Mathematical formulation

For better description of transfer of heat, the model of generalized Fourier's law is suggested as

$$\tilde{\lambda}^* [\bar{V} \cdot \nabla q - q \cdot \nabla \bar{V} + (\nabla \cdot \bar{V})q + \frac{\partial q}{\partial t}] + q = -\nabla T k, \quad (4.1)$$

where q is the heat flux, $\tilde{\lambda}^*$ is the thermal relaxation time, k is the thermal conductivity. Fourier's law is the simplified form of Eq. (4.1) by taking $\tilde{\lambda}^* = 0$. Now, for the steady incompressible fluid, the above equation reduces to the following.

$$q + \tilde{\lambda}^* [\bar{V} \cdot \nabla q - q \cdot \nabla \bar{V}] = -\nabla T k, \quad (4.2)$$

The energy equation can be deduced from Eq. (4.2).

Consider a two-dimensional flow of the Jeffery fluid through a stretched cylinder having velocity $u_w(x) = \frac{bx}{\tilde{l}}$. The velocity of free stream is considered as $u_e(x) = \frac{cx}{\tilde{l}}$, where \tilde{l} is the characteristic length and the flow is taken along the stagnation point. The coordinates in cylindrical form as \tilde{x} and \tilde{r} are assumed along the axial direction and normal to surface. For homogeneous-heterogeneous chemical reactions we have isothermal cubic autocatalytic reaction (homogenous) within the boundary layer but a first order single reaction (heterogeneous) on the catalyst and exhibited as:

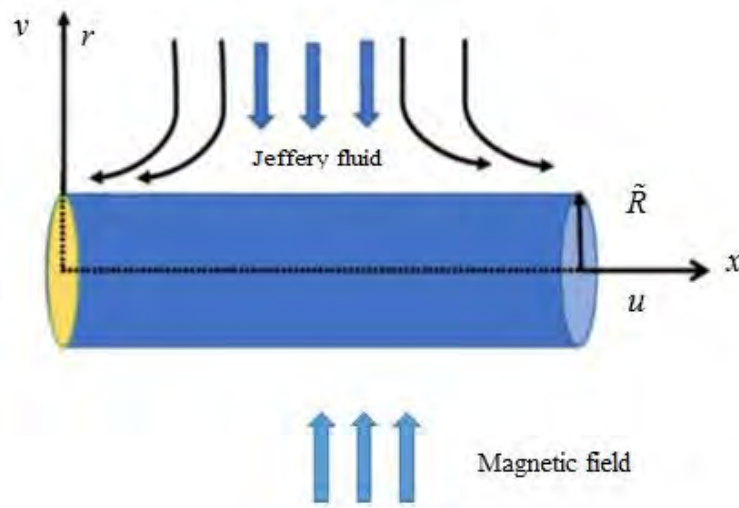


Fig. 4.1. Physical illustration of the problem.



where concentration of chemical species A and B are termed as \tilde{a} and \tilde{b} respectively, \tilde{l}_1 and \tilde{l}_s are constants. Now the flow equations are depicted as:

$$\frac{\partial}{\partial x}(ru) + \frac{\partial}{\partial r}(rv) = 0, \quad (4.5)$$

$$u \frac{\partial u}{\partial x} + v \frac{\partial u}{\partial r} = u_e(x) \frac{d}{dx} u_e(x) + \frac{\mu}{\rho(1+\tilde{\lambda}_1)} \left[\frac{1}{r} \frac{\partial u}{\partial r} + \frac{\partial^2 u}{\partial r^2} + \tilde{\lambda}_2 \left(\frac{\partial^2 u}{\partial r^2} \frac{\partial v}{\partial r} + \frac{\partial^2 u}{\partial r^2} \frac{v}{r} + \frac{\partial^3 u}{\partial r^3} v \right) \right. \\ \left. + \frac{\partial^2 u}{\partial r \partial x} \frac{u}{r} + \frac{\partial^3 u}{\partial r^2 \partial x} u + \frac{\partial^2 u}{\partial r \partial x} \frac{\partial u}{\partial r} \right] - \frac{\sigma B_\circ^2}{\rho} (u - u_e), \quad (4.6)$$

$$u \frac{\partial T}{\partial x} + v \frac{\partial T}{\partial r} + \tilde{\lambda}^* \left(u^2 \frac{\partial^2 T}{\partial x^2} + v^2 \frac{\partial^2 T}{\partial r^2} + 2uv \frac{\partial^2 T}{\partial x \partial r} + u \frac{\partial u}{\partial x} \frac{\partial T}{\partial x} + u \frac{\partial v}{\partial x} \frac{\partial T}{\partial r} + v \frac{\partial u}{\partial r} \frac{\partial T}{\partial x} \right. \\ \left. + v \frac{\partial v}{\partial r} \frac{\partial T}{\partial r} \right) = \alpha \left(\frac{\partial T}{\partial r} \frac{1}{r} + \frac{\partial^2 T}{\partial r^2} \right) + \frac{Q_\circ}{\rho c_p} (T - T_\infty), \quad (4.7)$$

$$\frac{\partial \tilde{a}}{\partial x} u + \frac{\partial \tilde{a}}{\partial r} v = \left(\frac{\partial^2 \tilde{a}}{\partial r^2} + \frac{1}{r} \frac{\partial \tilde{a}}{\partial r} \right) \tilde{D}_A - \tilde{l}_1 \tilde{a} \tilde{b}^2, \quad (4.8)$$

$$\frac{\partial \tilde{b}}{\partial x} u + \frac{\partial \tilde{b}}{\partial r} v = \left(\frac{\partial^2 \tilde{b}}{\partial r^2} + \frac{\partial \tilde{b}}{\partial r} \frac{1}{r} \right) \tilde{D}_B + \tilde{l}_1 \tilde{a} \tilde{b}^2, \quad (4.9)$$

where (u, v) are the components of velocity, ρ as fluid density, σ as electrical conductivity,

B_\circ as magnetic field coefficient, μ as viscosity of fluid, T as temperature of fluid, $\alpha = \frac{k}{\rho c_p}$

as thermal diffusivity, Q_\circ coefficient of heat generation, c_p the specific heat capacity, T_∞ the

ambient temperature, $\tilde{\lambda}_1$ as the ratio between relaxation and retardation, $\tilde{\lambda}_2$ as retardation time,

A and B are the chemical species with diffusion coefficients as \tilde{D}_A and \tilde{D}_B . The associated end

point conditions are as follows:

$$u = u_w(x) = \frac{bx}{\tilde{l}}, v = 0 \text{ at } r = \tilde{R}, u = u_e(x) = \frac{cx}{\tilde{l}} \text{ as } r \rightarrow \infty, \quad (4.10)$$

$$T = T_w(x) = T_\circ + \tilde{c} \left(\frac{x}{\tilde{l}} \right) \text{ at } r = \tilde{R}, T = T_\infty(x) = T_\circ + \tilde{d} \left(\frac{x}{\tilde{l}} \right) \text{ as } r \rightarrow \infty, \quad (4.11)$$

$$\tilde{D}_A \frac{\partial \tilde{a}}{\partial r} = \tilde{l}_s \tilde{a}, \tilde{D}_B \frac{\partial \tilde{b}}{\partial r} = -\tilde{l}_s \tilde{a} \text{ at } r = \tilde{R}, \tilde{a} \rightarrow \tilde{a}_\infty, \tilde{b} \rightarrow 0 \text{ as } r \rightarrow \infty, \quad (4.12)$$

where \tilde{c} and \tilde{d} are the dimensionless constants, \tilde{R} is the radius of cylinder. Implementing the similarity transformations as:

$$\begin{aligned} \eta &= \sqrt{\frac{b}{\tilde{l}v^*}} \left(\frac{r^2 - \tilde{R}^2}{2\tilde{R}} \right), \quad u = f'(\eta) \frac{bx}{\tilde{l}}, \quad v = -\frac{\tilde{R}}{r} \sqrt{\frac{bv^*}{\tilde{l}}} f(\eta), \\ \theta(\eta) &= \frac{T - T_\infty}{T_w - T_c}, \quad \tilde{m}(\eta) = \frac{\tilde{a}}{\tilde{a}_c}, \quad \tilde{n}(\eta) = \frac{\tilde{b}}{\tilde{a}_c}. \end{aligned} \quad (4.13)$$

Now by invoking Eq. (4.13) into Eq. (4.6) - (4.9), we get the following:

$$\begin{aligned} (1 + 2\tilde{K}\eta)f''' + (1 + \tilde{\lambda}_1)(f f'' - f'^2) + 2\tilde{K} f'' + \tilde{K} \tilde{\beta} (f'' f' - 3f f''') \\ + \tilde{\beta} (1 + 2\tilde{K}\eta)(f''^2 - f f^{(4)}) + (1 + \tilde{\lambda}_1)\lambda^2 - M^2 f' = 0, \end{aligned} \quad (4.14)$$

$$\begin{aligned} (1 + 2\tilde{K}\eta)\theta'' + 2\tilde{K}\theta' + \text{Pr} f\theta' - \text{Pr}(\tilde{S} + \theta)f' + \text{Pr} \tilde{\gamma} [(\tilde{S} + \theta)f'' f - \theta' f f'] \\ - (\tilde{S} + \theta)f'^2 - \theta'' f^2 + \theta \delta = 0, \end{aligned} \quad (4.15)$$

$$\frac{1}{Sc} [(1 + 2\tilde{K}\eta)\tilde{m}'' + 2\tilde{K}\tilde{m}'] + f\tilde{m}' - \tilde{m}\tilde{n}^2 L = 0, \quad (4.16)$$

$$\frac{\tilde{\delta}^*}{Sc} [\tilde{n}''(1 + 2\tilde{K}\eta) + 2\tilde{n}'\tilde{K}] + f\tilde{n}' + \tilde{m}\tilde{n}^2 L = 0, \quad (4.17)$$

and the transformed boundary conditions are.

$$f(0) = 0, f'(0) = 1, \theta(0) = 1 - \tilde{S}, \tilde{m}'(0) = L_s \tilde{m}(0), \tilde{\delta}^* \tilde{n}'(0) = -L_s \tilde{n}(0), \quad (4.18)$$

$$\tilde{f}'(\infty) = \tilde{A}, \tilde{\theta}(\infty) = 0, \tilde{m}(\infty) \rightarrow 1, \tilde{n}(\infty) \rightarrow 0,$$

where $\tilde{K} = \sqrt{\frac{v^* \tilde{l}}{b \tilde{R}^2}}$ as the parameter of curvature, $\tilde{\beta} = \frac{b \tilde{\lambda}_2}{\tilde{l}}$ as the Deborah number, $\text{Pr} = \frac{\mu c_p}{k}$ is the Prandtl number, $\tilde{\gamma} = \frac{b \tilde{\lambda}^*}{\tilde{l}}$ is the thermal relaxation parameter, $\delta = \frac{\tilde{l} Q_o}{b \rho c_p}$ the parameter of heat generation, $Sc = \frac{v^*}{\tilde{D}_A}$ the Schmidt number, $\tilde{\delta}^* = \frac{\tilde{D}_A}{\tilde{D}_B}$ the ratio of coefficient of mass diffusion, $L = \frac{\tilde{l}_1 \tilde{a}_o^2 \tilde{l}}{u_w}$ is the parameter of homogeneous reaction, $\lambda = \frac{c}{b}$ is the Velocity ratio parameter, $\tilde{S} = \frac{\tilde{d}}{\tilde{c}}$ the thermal stratification parameter, $L_s = \frac{\tilde{l}_s}{\tilde{D}_A} \sqrt{\frac{v^* \tilde{l}}{b}}$ the strength of heterogeneous reaction parameter.

By assuming \tilde{D}_A and \tilde{D}_B equal as $\tilde{\delta}^* = 1$. Therefore, $\tilde{m}(\eta) + \tilde{n}(\eta) = 1$, so from Eq. (4.16)- (4.17), we have

$$\frac{1}{Sc} [\tilde{m}'' (1 + 2\tilde{K}\eta) + 2\tilde{m}' \tilde{K}] + f \tilde{m}' - \tilde{m}(1 - \tilde{m})^2 L = 0, \quad (4.19)$$

subject to conditions at end point

$$\tilde{m}'(0) = \tilde{m}(0) L_s, \quad \tilde{m}(\infty) \rightarrow 1. \quad (4.20)$$

The involved engineering quantities are.

$$C_f = \frac{2\tau_w}{\rho u_w^2}, \quad Nu_x = \frac{x q_w}{k(T_w - T_o)} \quad (4.21)$$

$$\tau_w = \left[\frac{\mu}{1 + \tilde{\lambda}_1} \left(\frac{\partial u}{\partial r} \right) + \frac{\mu \tilde{\lambda}_2}{1 + \tilde{\lambda}_1} \left(v \frac{\partial^2 u}{\partial r^2} + u \frac{\partial^2 u}{\partial x \partial r} \right) \right]_{r=\tilde{R}}, \quad q_w = - \left(\frac{\partial T}{\partial r} \right)_{r=\tilde{R}} k,$$

where C_f and Nu_x are the coefficient of skin friction and local Nusselt number with τ_w and q_w as relation of wall stress shear and surface flux at $r = \tilde{R}$. The above expressions in dimensionless form are:

$$\begin{aligned} \frac{1}{2}\sqrt{\text{Re}_x} C_f &= \frac{1}{(1+\tilde{\lambda}_1)} [f''(0) - \tilde{\beta} f'''(0) f(0) - \tilde{\beta} \tilde{K} f''(0) f(0) + \tilde{\beta} f'(0) f''(0)], \\ \frac{Nu_x}{\sqrt{\text{Re}_x}} &= -\theta'(0), \end{aligned} \quad (4.22)$$

where $\text{Re}_x = \frac{\tilde{l} u_w}{\nu^*}$ is named as Reynolds number.

4.2 Computational algorithm

The basic mathematical laws involved in the field of fluid dynamics yields a system of coupled differential equations. Such equations are further converted into the coupled system of ordinary differential equations by dropping number of independent variables. The independent variables are dropped by means of set of similarity transformation (see Eq 4.13). The reduced system is solved numerically with the aid of shooting proficiency with fourth-fifth order Runge-Kutta Fehlberg technique. The system of governing equations Eq. (4.14) - (4.20) is extremely nonlinear coupled shape. For this purpose, necessary steps are executed. Firstly, we may write Eq. (4.14), (4.15) and Eq. (4.19) as follows:

$$\begin{aligned} (1+2\tilde{K}\eta) f''' + (1+\tilde{\lambda}_1)(f f'' - f'^2) + 2\tilde{K} f'' + \tilde{K} \tilde{\beta} (f'' f' - 3f'' f) + \tilde{\beta} (1+2\tilde{K}\eta) f''^2 \\ f^{(4)} = \frac{+(1+\tilde{\lambda}_1)\lambda^2 - M^2 f'}{\tilde{\beta} (1+2\tilde{K}\eta)}, \end{aligned} \quad (4.23)$$

$$\theta'' = \frac{\text{Pr}(\tilde{S} + \theta) f' - 2\tilde{K} \theta' - \text{Pr} f \theta' - \text{Pr} \tilde{\gamma} [(\tilde{S} + \theta) f'' f - \theta' f f' - (\tilde{S} + \theta) f'^2] - \delta \theta}{(1+2\tilde{K}\eta) - \tilde{\gamma} \text{Pr} f^2}, \quad (4.24)$$

$$\tilde{m}'' = \frac{Sc[L\tilde{m}(1-\tilde{m})^2 - f\tilde{m}'] - 2\tilde{K}\tilde{m}'}{(1+2\tilde{K}\eta)}, \quad (4.25)$$

Secondly, to reduce the above set of higher order differential equations into first order system of differential equations, by new variables as:

$$y_1 = f, y_2 = f', y_3 = f'', y_4 = f''', y_4' = f^{(4)}, \quad (4.26)$$

$$y_5 = \theta, y_6 = \theta', y_6' = \theta'', y_7 = \tilde{m}, y_8 = \tilde{m}', y_8' = m'',$$

Now, by applying Eq. (4.26) in Eq. (4.23) – (4.25), we obtained.

$$\begin{aligned} y_1' &= y_2 \\ y_2' &= y_3 \\ y_3' &= y_4 \\ y_4' &= f^{(4)} = \frac{(1+2\tilde{K}\eta)y_4 + (1+\tilde{\lambda}_1)(y_1y_3 - y_2^2) + 2\tilde{K}y_3 + \tilde{K}\tilde{\beta}(y_2y_3 - 3y_1y_3) + \tilde{\beta}(1+2\tilde{K}\eta)y_3^2 + (1+\tilde{\lambda}_1)\lambda^2 - M^2y_2}{\tilde{\beta}(1+2\tilde{K}\eta)} \\ y_5' &= y_6 \\ y_6' &= \frac{\text{Pr}(\tilde{S} + y_5)y_2 - 2\tilde{K}y_6 - \text{Pr}y_1y_6 - \text{Pr}\tilde{\gamma}[(\tilde{S} + y_5)y_1y_3 - y_1y_2y_6 - (\tilde{S} + y_5)(y_2^2)] - \delta y_5}{(1+2\tilde{K}\eta) - \text{Pr}\tilde{\gamma}y_1^2} \\ y_7' &= y_8 \\ y_8' &= \frac{Sc[Ly_7(1-y_7)^2 - y_1y_8] - 2\tilde{K}y_8}{(1+2\tilde{K}\eta)}, \end{aligned} \quad (4.27)$$

and the boundary conditions given in Eq. (4.18) and Eq. (4.20) are transformed as:

$$y_1(0) = 0, y_2(0) = 1, y_5(0) = 1 - \tilde{S}, y_8(0) = L_s y_7(0), \quad (4.28)$$

$$y_2(\infty) \rightarrow \lambda, y_5(\infty) \rightarrow 0, y_7(\infty) \rightarrow 1,$$

Here, $y_3(0) = u_1, y_4(0) = u_2, y_6(0) = u_3, y_8(0) = u_4$ are the initial guesses for the values of $f''(0), f'''(0), \theta'(0),$ and $m'(0),$.

We have done with the following procedure to pursue shooting methodology.

- Suggest the values of η_∞ that lies in between 5 and 10.
- Taking initial guess for $y_3(0), y_4(0), y_6(0)$ and $y_8(0)$ as $y_3(0) = y_4(0) = y_6(0) = y_8(0) = 1$.
- Numerical solution of Odes with the help of fourth-fifth order R-K technique is computed.
- The absolute variation in the given and calculated values of $y_2(\infty), y_5(\infty)$, and $y_7(\infty)$ (i.e., boundary residuals) are calculated.
- The obtained solutions will be convergent if this residual value is less than tolerance, which is assumed to be 10^{-5} .

4.3 Results and discussion

Jeffery fluid model towards cylindrical surface is considered in the present investigation. Here Jeffery stagnation point flow field is manifested with externally applied magnetic field. The energy equation dragged by way of Cattaneo-Christov improvement. Thermal boundary layer is carried out both for heat generation and temperature stratification effects. Further, the whole thermally stratified MHD Jeffery fluid flow field is conjectured/ designed for homogeneous and heterogeneous reactions. The obtained physical parameters are \tilde{K} (curvature parameter), M (magnetic field parameter), δ (heat generation parameter), \tilde{S} (temperature stratification parameter), L (homogeneous parameter), L_s (heterogeneous parameter) and Sc . The adopted values of rest of parameters while execution of computational algorithm is $\tilde{\beta} = 1, \tilde{\lambda}_1 = 0.5, Pr = 0.3$, and $\lambda = 1$. The influence of M and \tilde{K} on Jeffery velocity is inspected and depicted by way of *Figs. 4.2-4.3*. Moreover, the effects of M, δ and \tilde{S} upon Jeffery

temperature are examined and the output in this direction is provided with the help of *Figs. 4.4 - 4.6*. Further, the variations in Jeffery fluid concentration towards S_c, L and L_s are obtained and offered by way of *Figs. 4.7-4.9*. In detail, *Fig. 4.1* illustrates the flow model of Jeffery fluid. The effects of M on velocity is tested and provided in *Fig. 4.2*. The Jeffery velocity shows descending values for M . In actual when we iterate $M = (0.2, 0.3, 0.4, 0.5)$, the Lorentz force enhanced. It is resistive force therefore the Jeffery fluid face resistance and the velocity of Jeffery fluid declines. The impact of \tilde{K} on Jeffery fluid velocity is examined and the variation in this direction is concluded by means of *Fig. 4.3*. It is seen that the Jeffery fluid velocity show inclined curves towards higher values of \tilde{K} . When we iterate $\tilde{K} = (0.1, 0.2, 0.3, .4)$, the curvature radius subject to surface of cylinder decreases. Therefore, the surface area in contact between the cylinder and the fluid reduces. Hence, the Jeffery fluid particles face less resistance which helps to boost in fluid velocity. The Jeffery fluid temperature depends upon the variation of M, δ and \tilde{S} . In particular, the impact of M on Jeffery fluid temperature is examined and offered with the aid of *Fig. 4.4*. It is expected that if the Jeffery fluid velocity declines towards $M = (0.1, 0.2, 0.3, 0.4)$ than the Jeffery fluid temperature reduces. Because the temperature is second measure of average kinetic energy that contains average velocity variations. Therefore, for $M = (0.1, 0.2, 0.3, 0.4)$, the Lorentz force enhances, and the resistance faced by fluid particles increases and average kinetic energy reduces as a results temperature reduces. *Fig. 4.5* is plotted to offer the observation regarding the relation of heat generation with Jeffery fluid temperature. When we iterate $\delta = (0.1, 0.2, 0.3, 0.4)$, the Jeffery fluid temperature enhances which is quite expected. This factor is due to production of heat energy against the higher values of $\delta = (0.1, 0.2, 0.3, 0.4)$. It is important to note that sometimes we may have overshoot in the temperature profile, and it is monitored by introducing sink to avoid turbulence. The temperature stratification parameter

\tilde{S} appears on considering temperature stratification phenomena. The effect of \tilde{S} on Jeffery fluid temperature is examined and the ultimate variation in temperature is shared through *Fig. 4.6*. One can easily conclude from *Fig. 4.6* that the Jeffery fluid temperature reflects declined curves towards \tilde{S} . When we iterate $\tilde{S} = (0.0, 0.1, 0.2, 0.3)$, the potential difference between ambient region and the cylindrical surface reduced which cause the reduction in Jeffery fluid temperature. The impact of Sc, L and L_s on Jeffery fluid concentration are measured and shown with the help of *Fig. 4.7-4.9* respectively. In detail, the relation between Jeffery fluid concentration and Schmidt number Sc is illustrated in *Fig. 4.7*. It is noticed that when we iterate $Sc (= 0.1, 0.3, 0.5, 0.7)$, the Jeffery fluid concentration magnifies. Since the mass diffusivity has inverse relation with Sc so the higher values of $Sc (= 0.1, 0.2, 0.3)$ cause weaker rate of mass diffusion and as a result the Jeffery fluid concentration magnifies. The influence of both L and L_s on Jeffery fluid concentration is reported with the help of *Fig. 4.8* and *Fig. 4.9*, respectively. It is noticed that in a thermally stratified Jeffery flow field the higher values of both $L (= 0.1, 0.2, 0.3)$ and $L_s (= 0.1, 0.2, 0.3)$ brings reduction in Jeffery fluid concentration. The variations in the coefficient of local skin friction are evaluated for involved parameters ($\tilde{\lambda}_1$ and $\tilde{\beta}$). The developed values are provided with the aid of **Table 4.1** and **Table 4.2**. It is seen that we have an excellent match with Hayat et al. [83] in **Table 4.1** while the values of skin friction matches with both Abbasi et al. [84] and Hayat et al. [83] in **Table 4.2**.

4.4 Graphical representation

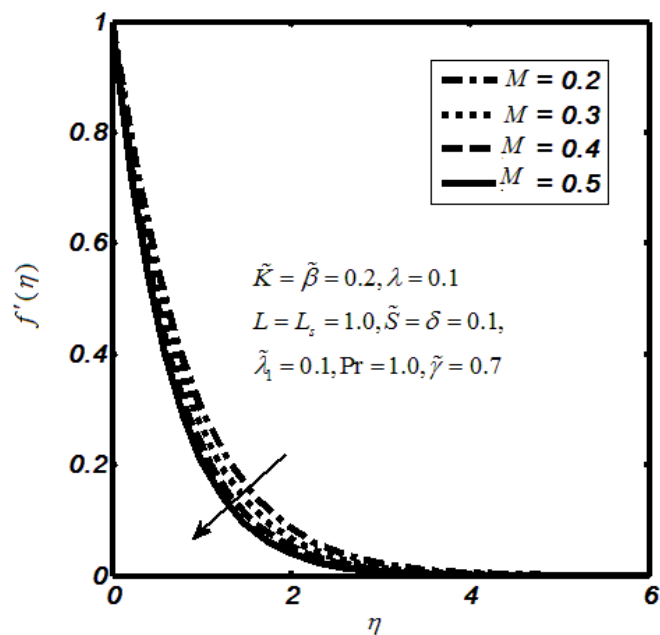


Fig. 4.2: Impacts of M upon $f'(\eta)$.

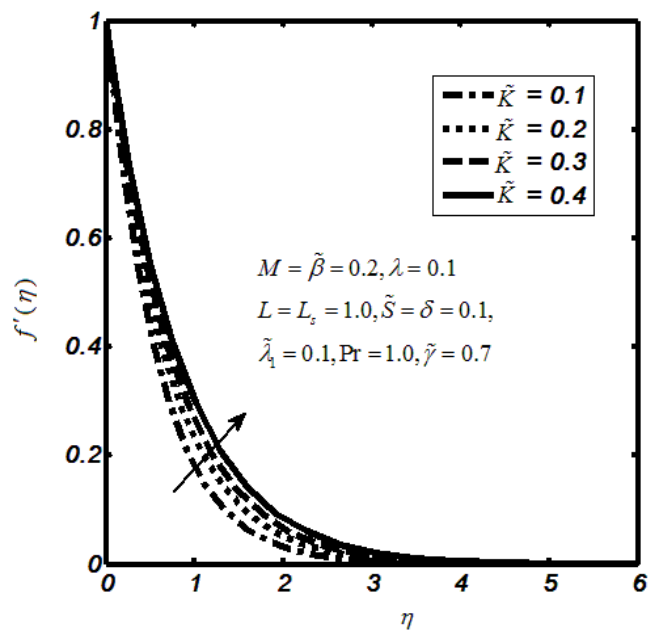


Fig. 4.3: Impacts of \tilde{K} upon $f'(\eta)$.

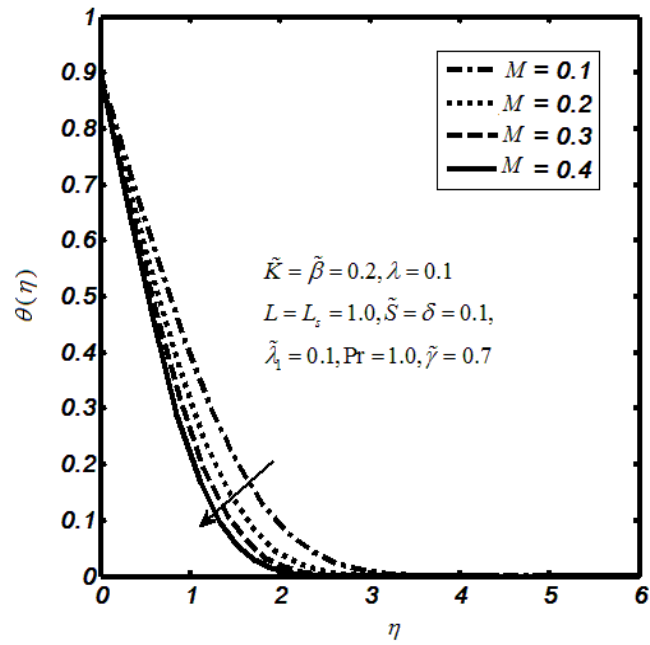


Fig. (4.4): The impact of M upon $\theta(\eta)$.

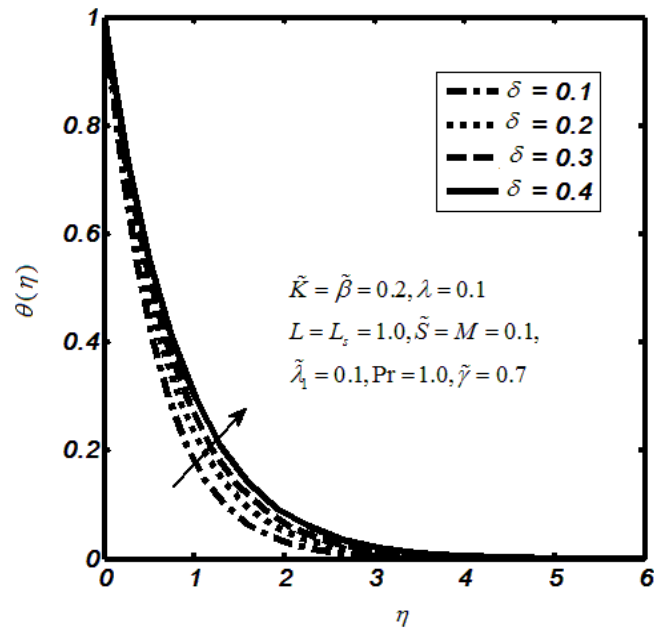


Fig. (4.5): Impacts of δ on $\theta(\eta)$.

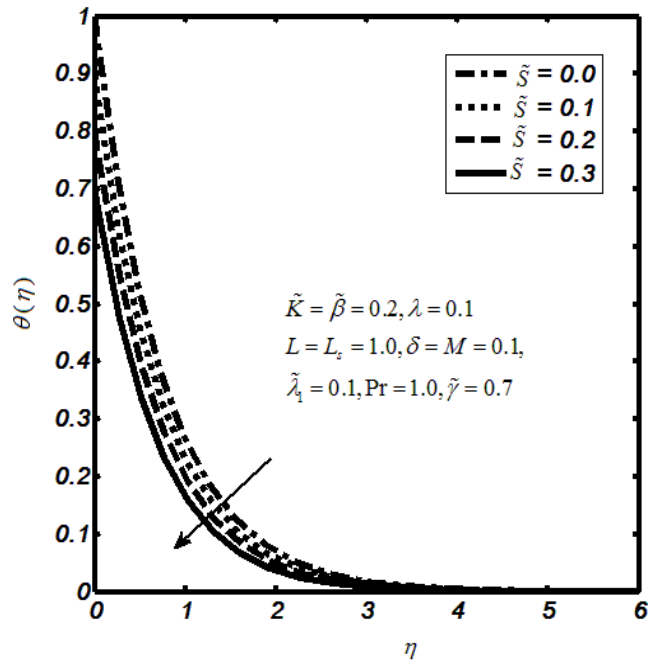


Fig. (4.6): Impacts of \tilde{S} upon $\theta(\eta)$.

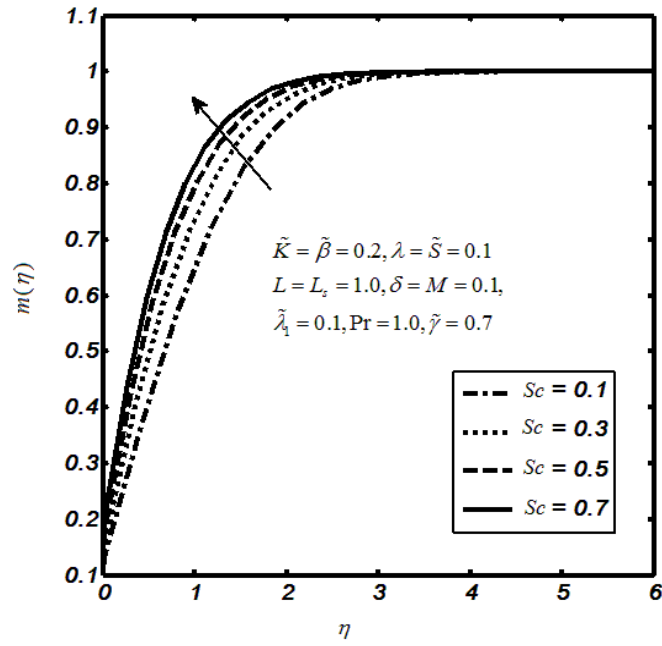


Fig. (4.7): Impacts of Sc upon $m(\eta)$.

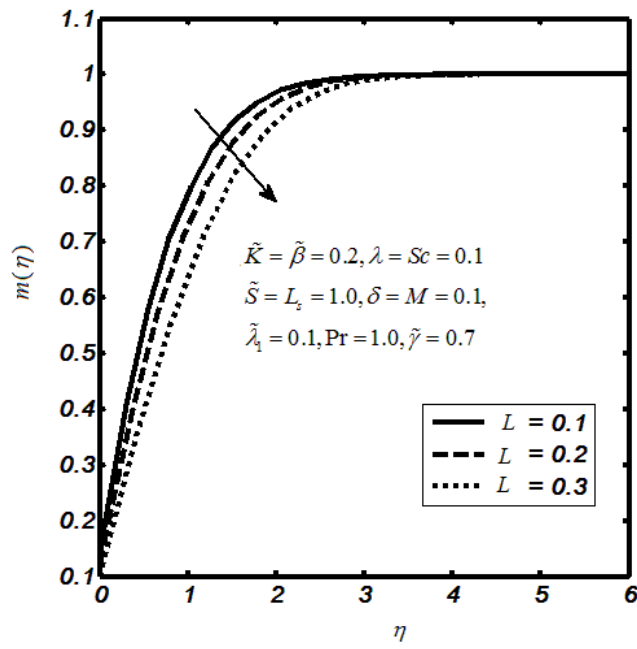


Fig. (4.8): Impacts of L on $m(\eta)$.

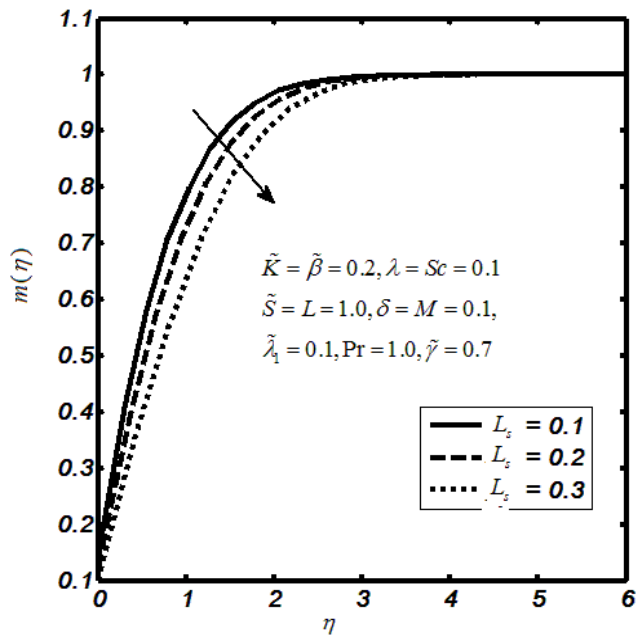


Fig. (4.9): Impacts of L_s on $m(\eta)$.

Table 4.1: Numerical approximations for coefficient of skin friction $\frac{-1}{2}\sqrt{\text{Re}_x}C_f$ when $M = 0.5, \tilde{K} = 0.3, \tilde{S} = 0.2$ and $\delta = 0.2$.

$\tilde{\beta}$	$\tilde{\lambda}_1$	Hayat et al. [83]	Current results
0.1	0.2	0.95743	0.9563
0.1	0.3	0.91987	0.9185
0.1	0.4	0.88641	0.8851
0.1	0.5	0.85635	0.8554
0.2	0.2	1.00000	1.0000
0.2	0.3	0.96077	0.9600
0.2	0.4	0.92582	0.9251
0.2	0.5	0.89442	0.8941
0.3	0.2	1.0408	1.0406
0.3	0.3	1.0000	1.0000
0.3	0.4	0.96362	0.9630
0.3	0.5	0.93095	0.9301
0.4	0.2	1.0801	1.0810
0.4	0.3	1.0378	1.0362
0.4	0.4	1.0000	1.0000
0.4	0.5	0.96608	0.9653

Table 4.2: The numerical approximations for the coefficient of local skin friction $\frac{-1}{2}\sqrt{\text{Re}_x}C_f$ when $\tilde{M} = 0.5, \tilde{K} = 0.3, \tilde{S} = 0.2$ and $\tilde{\delta} = 0.1$.

$\tilde{\lambda}_1$	$\tilde{\beta}$	Abbasi et al. [84]	Hayat et al. [83]	Current results
0.0	0.2	1.09545	1.09545	1.0951
0.5	0.2	0.89443	0.89442	0.8943
0.7	0.2	0.84017	0.84016	0.8401
1.0	0.2	0.77460	0.77460	0.7745
0.4	0.0	0.84515	0.84515	0.8450
0.4	0.3	0.96362	0.96362	0.9635
0.4	0.6	1.06904	1.06904	1.0691
0.4	1.0	1.19523	1.19523	1.1953

4.5 Concluding remarks

This chapter comprises of generalized Fourier's law in a thermally stratified Jeffery flow at a point of stagnation induced by the magnetic effects, generation of heat and heterogeneous-homogeneous reactions. The obtained flow equations are solved by using shooting scheme and the computed values of local skin friction coefficient are examined and compared with literature in Tables 4.1 and 4.2. The key outcomes are itemized as follows:

- The velocity of Jeffery fluid reflects declined curves towards magnetic field parameter.
- The upward trend is noticed for the fluid velocity curvature parameter.
- Jeffery fluid temperature shows an increasing behaviour towards heat generation parameter whereas opposite trend is observed for magnetic field parameter.
- In thermally stratified medium the Jeffery fluid concentration declines towards both heterogeneous and homogenous reaction parameters.
- The Jeffery fluid concentration is increasing for higher values of Schmidt number.

Chapter 5

On Cattaneo-Christov heat flux in a Newtonian flow field with MHD and velocity slip

Emphasize of this chapter is on magneto-hydrodynamics, heat generation/absorption and slip effects over a Newtonian flow field with homogeneous-heterogeneous chemical reactions induced by the rotating disk. The concerned steady state flow is examined in case when reactants and auto-catalyst possess equality in coefficients of diffusion. The Cattaneo-Christov approach is proposed to derive the energy equation and heat transfer phenomena. The consequential PDE's (Partial Differential Equations) descend to ODE's (Ordinary Differential Equations) by insinuating similarity transform. Further, these equations are sorted out by way of numerical scheme called Runge-Kutta Fehlberg method with shooting scheme. The influence of arising parameters towards fluid velocity, temperature and concentration is observed through graphs. Further, the numerical results for coefficient of friction and the rate of heat transfer are examined.

5.1 Mathematical formulation

Introducing the model of Cattaneo-Christov heat flux to imply heat transfer as:

$$[\bar{V} \cdot \nabla q - q \cdot \nabla \bar{V} + (\nabla \cdot \bar{V})q + \frac{\partial q}{\partial t}] \tilde{\lambda}^2 + q = -\nabla T k, \quad (5.1)$$

Consider q as flux of heat, $\tilde{\lambda}^*$ as relaxation of time of heat flux, k as thermal conductivity.

This Eq. (5.1) is simplified to the Fourier's law by taking $\tilde{\lambda}^* = 0$. Now, for the incompressible fluid, Eq. (5.1) reduces to the following form i.e.

$$[\bar{V} \cdot \nabla q - q \cdot \nabla \bar{V} + \frac{\partial q}{\partial t}] \tilde{\lambda}^* + q = -\nabla T k, \quad (5.2)$$

Consider viscous fluid over a rotating disk with constant angular velocity $\tilde{\Omega}$ where the flow is taken along the disk $z > 0$. The magnetic field is applied along z -axis. Also, the energy equation is equipped with heat generation-absorption. The velocity component u is along radial r -direction, v is along tangential ϕ -direction and w is along axial z -direction. Consider the homogeneous-heterogeneous model as:

$$A + 2B \rightarrow 3B, \text{ rate} = \tilde{l}_1 \tilde{a} \tilde{b}^2, \quad (5.3)$$

$$A \rightarrow B, \text{ rate} = \tilde{l}_s \tilde{a}, \quad (5.4)$$

The laws of momentum conservation and energy conservation are considered for fluid motion.

Thus, the flow describing equations are exhibited as:

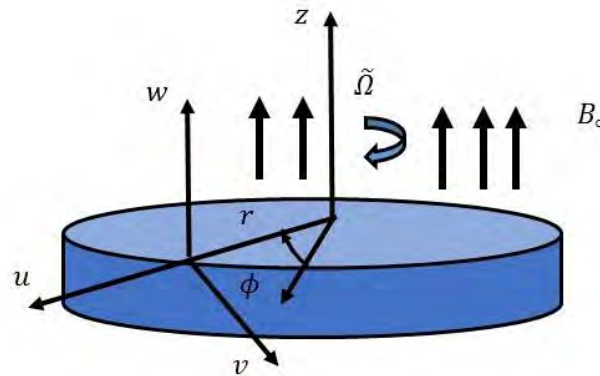


Fig. 5.1: Physical illustration for the flow problem.

$$\frac{\partial u}{\partial r} + \frac{\partial w}{\partial z} + \frac{u}{r} = 0, \quad (5.5)$$

$$\frac{\partial u}{\partial r} u - \frac{v^2}{r} + \frac{\partial u}{\partial z} w = \nu^* \left(\frac{\partial^2 u}{\partial r^2} + \frac{\partial^2 u}{\partial z^2} + \frac{\partial u}{\partial r} \frac{1}{r} - \frac{u}{r^2} \right) - \frac{\sigma B_0^2}{\rho} u, \quad (5.6)$$

$$\frac{\partial v}{\partial r} u + \frac{\partial v}{\partial z} w + \frac{uv}{r} = \nu^* \left(\frac{\partial^2 v}{\partial r^2} + \frac{\partial v}{\partial r} \frac{1}{r} - \frac{v}{r^2} + \frac{\partial^2 v}{\partial z^2} \right) - \frac{\sigma B_0^2}{\rho} v, \quad (5.7)$$

$$\frac{\partial w}{\partial r}u + \frac{\partial w}{\partial z}w = \nu^* \left(\frac{\partial^2 w}{\partial z^2} + \frac{\partial^2 w}{\partial r^2} + \frac{1}{r} \frac{\partial w}{\partial r} \right), \quad (5.8)$$

$$\begin{aligned} \frac{\partial T}{\partial r}u + \frac{\partial T}{\partial z}w = \alpha \left[\frac{\partial^2 T}{\partial z^2} + \frac{\partial^2 T}{\partial r^2} + \frac{1}{r} \frac{\partial T}{\partial r} \right] - \tilde{\lambda}^* \left(u^2 \frac{\partial^2 T}{\partial r^2} + w^2 \frac{\partial^2 T}{\partial z^2} + 2uw \frac{\partial^2 T}{\partial z \partial r} \right) \\ + \left(\frac{\partial u}{\partial r}u + \frac{\partial u}{\partial z}w \right) \frac{\partial T}{\partial r} + \left(\frac{\partial w}{\partial r}u + \frac{\partial w}{\partial z}w \right) \frac{\partial T}{\partial z} + (T - T_\infty) \frac{Q_\circ}{\rho c_p}, \end{aligned} \quad (5.9)$$

$$u \frac{\partial \tilde{a}}{\partial r} + w \frac{\partial \tilde{a}}{\partial z} = \tilde{D}_A \left(\frac{\partial^2 \tilde{a}}{\partial z^2} \right) - \tilde{l}_1 \tilde{a} \tilde{b}^2, \quad (5.10)$$

$$u \frac{\partial \tilde{b}}{\partial r} + w \frac{\partial \tilde{b}}{\partial z} = \tilde{D}_B \left(\frac{\partial^2 \tilde{b}}{\partial z^2} \right) + \tilde{l}_1 \tilde{a} \tilde{b}^2, \quad (5.11)$$

Consider $\nu^* = \frac{\mu}{\rho}$ as kinematic viscosity with μ, ρ as dynamical viscosity and density of the

fluid and $\sigma, B_\circ, Q_\circ, c_p, \tilde{D}_A, \tilde{D}_B, \alpha = \frac{k}{\rho c_p}$, represents the electrical conductivity, applied

magnetic field coefficient, heat generation coefficient, specific heat capacity at constant pressure, diffusion coefficients for chemical species A and B , thermal diffusivity respectively.

The corresponding end point conditions are.

$$u = \tilde{L} \frac{\partial u}{\partial z}, v = r \tilde{\Omega} + \tilde{L} \frac{\partial v}{\partial z}, w = 0, T = T_w, \tilde{D}_A \frac{\partial \tilde{a}}{\partial z} = \tilde{l}_s \tilde{a}, \tilde{D}_B \frac{\partial \tilde{b}}{\partial z} = -k_s \tilde{a} \text{ at } z = 0, \quad (5.12)$$

$$u \rightarrow 0, v \rightarrow 0, T \rightarrow T_\infty, \tilde{a} \rightarrow \tilde{a}_\circ, \tilde{b} \rightarrow 0 \text{ as } z \rightarrow \infty$$

where \tilde{L} is the velocity slip coefficient. Consider the following admissible similarity transformations:

$$\begin{aligned} \xi = \sqrt{\frac{2\tilde{\Omega}}{\nu^*}} z, u = \frac{dF(\xi)}{d\xi} \tilde{\Omega} r, v = G(\xi) r \tilde{\Omega}, w = -\sqrt{2\tilde{\Omega} \nu^*} F(\xi), \\ \theta(\xi) = \frac{T - T_\infty}{T_w - T_\infty}, g(\xi) = \frac{\tilde{a}(z)}{\tilde{a}_\circ}, h(\xi) = \frac{b(z)}{\tilde{a}_\circ}, \end{aligned} \quad (5.13)$$

Using the transformations given in Eq. (5.13), Eq. (5.5) identically satisfied and Eq. (5.6)-

(5.11) becomes:

$$2\frac{d^3F}{d\xi^3} - \left(\frac{dF}{d\xi}\right)^2 + 2F\frac{d^2F}{d\xi^2} + G^2 - M^2\frac{dF}{d\xi} = 0, \quad (5.14)$$

$$2\frac{d^2G}{d\xi^2} - 2F\frac{dG}{d\xi} - 2G\frac{dF}{d\xi} - M^2G = 0, \quad (5.15)$$

$$\frac{d^2\theta}{d\xi^2} + \text{Pr}(2F\text{Re}\frac{d\theta}{d\xi} - 4\tilde{\gamma}\text{Re}(F^2\frac{d^2\theta}{d\xi^2} + F\frac{dF}{d\xi}\frac{d\theta}{d\xi})) + \delta\theta = 0, \quad (5.16)$$

$$\frac{1}{Sc}\frac{d^2g}{d\xi^2} + F\frac{dg}{d\xi} - Lgh^2 = 0, \quad (5.17)$$

$$\frac{\tilde{\delta}^*}{Sc}\frac{d^2h}{d\xi^2} + F\frac{dh}{d\xi} + Lgh^2 = 0, \quad (5.18)$$

where $M^2 = \frac{\sigma B_o^2}{\tilde{\Omega}\rho}$, $\text{Pr} = \frac{\nu^*}{\alpha}$, $L = \frac{\tilde{l}_1 a_o^2}{2\tilde{\Omega}}$, $\delta = \frac{Q_o}{2\tilde{\Omega}\rho c_p}$, $Sc = \frac{\nu^*}{\tilde{D}_A}$, $\tilde{\gamma} = \tilde{\lambda}^*\tilde{\Omega}$ are the magnetic

field parameter, Prandtl number, homogeneous reaction parameter, heat generation parameter,

Schmidt number and thermal relaxation parameter. The boundary conditions in Eq. (5.12)

becomes:

$$F(\xi) = 0, \frac{dF(\xi)}{d\xi} = \frac{d^2F(\xi)}{d\xi^2}\alpha^*, G(\xi) = \alpha^*\frac{dG(\xi)}{d\xi} + 1, \theta(\xi) = 1, \frac{dg(\xi)}{d\xi} = L_s g(\xi),$$

$$\tilde{\delta}^*\frac{dh(\xi)}{d\xi} = -L_s g(\xi) \text{ as } \xi = 0,$$

$$\frac{dF(\xi)}{d\xi} \rightarrow 0, G(\xi) \rightarrow 0, \theta(\xi) \rightarrow 0, g(\xi) \rightarrow 1, h(\xi) \rightarrow 0 \text{ as } \xi \rightarrow \infty, \quad (5.19)$$

where $L_s = \frac{\tilde{l}_s}{\tilde{D}_A}\sqrt{\frac{\nu^*}{2\tilde{\Omega}}}$ is heterogeneous reaction parameter and $\alpha^* = \tilde{L}\sqrt{\frac{2\tilde{\Omega}}{\nu^*}}$ is the velocity

slip parameter. By assuming \tilde{D}_A and \tilde{D}_B equal that is $\delta^* = 1$. Therefore, $h(\xi) + g(\xi) = 1$. Hence,

from Eq. (5.17)-(5.18), we have

$$\frac{1}{Sc}\frac{d^2g}{d\xi^2} + F\frac{dg}{d\xi} - Lg(1-g)^2 = 0, \quad (5.20)$$

with end point conditions

$$\frac{dg(0)}{d\xi} = L_s g(0) \text{ and } g(\infty) \rightarrow 1, \quad (5.21)$$

for physical model, the non-dimensional form of local coefficient of skin friction and Nusselt number are computed as:

$$\text{Re}_r^{1/2} C_F = \frac{d^2 F(0)}{d\xi^2}, \text{Re}_r^{1/2} C_G = \frac{dG(0)}{d\xi}, \quad (5.22)$$

$$\text{Re}_r^{-1/2} Nu = -\frac{d\theta(0)}{d\xi},$$

where $\text{Re}_r = \frac{2\tilde{\Omega}r^2}{\nu^*}$ as local Reynold number.

5.2 Computational algorithm

The system of governing *Eq.* (5.14)-(5.16) and (5.20) with boundary conditions *Eq.* (5.19)-(5.21) are highly nonlinear coupled ordinary differential equations. The shooting algorithm associated by Runge-Kutta fourth-fifth order integration methodology is utilized to compute the solution of this system along with boundary conditions. Therefore, this system is assembled into a set of first order ODE as initial value problems that can be sorted out by using Runge-Kutta Fehlberg method. Thus, we may write *Eq.* (5.14)-(5.16) and (5.20) as:

$$\frac{d^3 F}{d\xi^3} = -\frac{1}{2} \left(2F \frac{d^2 F}{d\xi^2} - M^2 \frac{dF}{d\xi} - \left(\frac{dF}{d\xi} \right)^2 + G^2 \right), \quad (5.23)$$

$$\frac{d^2 G}{d\xi^2} = -(2F \frac{dG}{d\xi} - 2 \frac{dF}{d\xi} G - M^2 G), \quad (5.24)$$

$$\frac{d^2 \theta}{d\xi^2} = -\frac{\text{Pr}(2\text{Re} \frac{d\theta}{d\xi} F - 4\tilde{\gamma}\text{Re} \frac{dF}{d\xi} \frac{d\theta}{d\xi} F + \delta\theta)}{(1 - 4\tilde{\gamma}\text{Pr}\text{Re}F^2)}, \quad (5.25)$$

$$\frac{d^2g}{d\xi^2} = -Sc(F \frac{dg}{d\xi} - Kg(1-g)^2), \quad (5.26)$$

To reduce Eq. (5.23) – (5.26) into system of first order ODE's, consider new set of variables as:

$$\begin{aligned} y_1 = F(\xi), y_2 = y_1' = \frac{dF}{d\xi}, y_3 = y_2' = \frac{d^2F}{d\xi^2}, y_4 = G(\xi), y_5 = y_4' = \frac{dG}{d\xi}, y_6 = \theta(\xi), \\ y_7 = y_6' = \frac{d\theta}{d\xi}, y_8 = g(\xi), y_9 = y_8' = \frac{dg}{d\xi}, \end{aligned} \quad (5.27)$$

where prime denotes derivative w.r.t ξ . By inserting Eq. (5.27) into Eq. (5.23) - (5.26), we obtain the following.

$$\begin{aligned} y_1' &= y_2 \\ y_2' &= y_3 \\ y_3' &= -\frac{1}{2}(2y_1y_3 - y_2^2 + y_4^2 - M^2y_2) \\ y_4' &= y_5 \\ y_5' &= -\frac{1}{2}(2y_1y_5 - 2y_2y_4 - M^2y_4) \\ y_6' &= y_7 \\ y_7' &= -\frac{\text{Pr}(2 \text{Re } y_1y_7 - 4\tilde{\gamma} \text{Re } y_1y_2y_7 + \delta y_6)}{(1 - 4\tilde{\gamma} \text{Pr Re } y_1^2)} \\ y_8' &= y_9 \\ y_9' &= -Sc(y_1y_9 - Ky_8(1 - y_8)^2), \end{aligned} \quad (5.28)$$

with transformed boundary conditions:

$$\begin{aligned} y_1(\xi) = 0, y_2(\xi) = \alpha y_3(\xi), y_4(\xi) = 1 + \alpha y_5(\xi), y_6(\xi) = 1, \\ y_9(\xi) = K_s y_8(\xi), \text{ at } \xi = 0, \end{aligned} \quad (5.29)$$

$$y_2(\xi) \rightarrow 0, y_4(\xi) \rightarrow 0, y_6(\xi) \rightarrow 0, y_8(\xi) \rightarrow 1 \text{ at } \xi \rightarrow \infty$$

Consider the initial guesses for $\frac{d^2F(0)}{d\xi^2}, \frac{dG(0)}{d\xi}, \frac{dT(0)}{d\xi}, \frac{dg(0)}{d\xi}$. Shooting method is

implemented to solve the above system and the key points are as follows:

- Suggest the values of ξ_∞ that lies in between 5 and 10.

- Assume that $y_3(0) = y_5(0) = y_7(0) = y_9(0) = 1$.
- Then we found the solution of Odes with the help of four-fifth order R-K methodology.
- Lastly, the absolute variations in provided and newly computed values of $y_1(\infty), y_3(\infty), y_5(\infty), y_7(\infty)$ and $y_9(\infty)$ that is residuals at boundary are computed. The solution converges if its residual values are less than given tolerance value, which is supposed to be 10^{-5} .
- If the values found in previous point are greater than permitted error, then the values of $y_3(0), y_5(0), y_7(0)$ and $y_9(0)$ will be redefined by Newton's method.

5.3 Results and discussion

The rotating disk viscous fluid model is discussed in this chapter. Further, the fluid flow is manifested by the externally applied magnetic field with slip effects. Energy equation is presumed by the Cattaneo-Christov heat flux model. Thermal boundary layer is executed by the heat generation/absorption. In this work, the chemical reaction named homogeneous-heterogeneous is considered. Also, the conservation laws for energy and momentum are used to describe the flow field that can be shown in the form of coupled partial differential equations. Later, these equations are further reformed into coupled ordinary differential equations. Similarity transformation is carried out to minimize the number of independent variables. This reduced system is sorted out numerically by way of shooting algorithm with Runge-Kutta methodology. The engineering parameters are M (magnetic field parameter), α^* (velocity slip), $\delta > 0$ (parameter of heat generation), $\delta < 0$ (parameter of heat absorption), Sc , L and L_s . Here, impacts of M on viscous fluid velocity is investigated and provided by means of *Fig. 5.2* and *Fig. 5.4*. The results of velocity field upon velocity slip parameter are indicated

through *Fig. 5.3* and *Fig. 5.5*. The influences of $\delta < 0$, $\delta > 0$, Pr on viscous temperature are portrait and the results are delineated in *Figs. 5.6 - 5.8*. The fluctuation in viscous fluid concentration against L , L_s and Sc are depicted in *Figs. 5.9-5.11*.

Now in detail *Fig. 5.2* presents the impact of M on velocity $F'(\xi)$. It testifies that velocity profile reflects deteriorate towards M that is $M = 0.1, 0.3, 0.5$. Because of increase in M causes the enhancement of Lorentz's force which is a sort of resisting force that opposes fluid particles to move in a free manner and as a result, velocity of fluid declines. *Fig. 5.3* depicts the impact of α^* on $F'(\xi)$ when $\alpha^* = 0.1, 0.3, 0.5$ and reflect a decline trend because Lorentz force occurs due to enhancement in M which resist the flow and as a result we obtain decreasing curves of $F'(\xi)$. The impacts of α^* upon $G(\xi)$ is shown in *Fig. 5.5* and captured as decaying curves.

The temperature of viscous fluid relies upon the variation of $\delta < 0, \delta > 0$ and Pr . In particular, the impacts of $\delta < 0$ on temperature of viscous fluid are inspected and the outcomes are portrait (see *Fig. 5.6*). On maximizing $\delta < 0$ i.e., $\delta = -0.3, -0.2, -0.1$ declines the viscous fluid temperature. Because, in case of heat absorption, the heat energy is lost and hence fluid temperature profile declines. It is necessary to notify that an incrementing behavior is captured in the flow path. This behavior can be overhauled through intake of sink factor as delineated in *Fig. 5.7*. This reports an inclining trend of viscous fluid temperature when heat generation enlarges (i.e., $\delta = 0.3, 0.5, 0.7$). The reason behind is the heat energy evolved towards the flow path for enhancing values of $\delta > 0$. Temperature profile increases at any point inside the boundary layer whenever heat generation parameter attains the higher values. Also, the thickness of thermal boundary layer indicates significant enhancement corresponding to the higher values of heat generation parameter. *Fig. 5.8* shows the impact of viscous fluid temperature for Pr . This depicts the fluid temperature that decreases after increasing

$Pr (= 0.3, 0.5, 0.7)$. Physically, the ratio of thermal to momentum diffusivity is termed as Prandtl number. The thickness of thermal boundary layer decreases due to higher values of Pr as it yields small amount of thermal diffusivity. Hence, decline in heat transfer rate occurs. Also, the inverse relation between Pr and thermal conductivity declines the thermal layer thickness because large values of Pr provides less energy diffusion. Therefore, fluid temperature decreases. *Fig. 5.9* shows the variation in fluid temperature towards $\tilde{\gamma}$. The impacts of fluid temperature due to iterative values of $\tilde{\gamma} = (0.3, 0.5, 0.7)$ is presented. The temperature profile decreases for $\tilde{\gamma}$. *Fig. 5.10* depicts the fluctuation in viscous fluid concentration towards homogeneous reaction parameter L . The increasing values of $L (= 0.3, 0.5, 0.7)$ causes decline in concentration trend. As the enhancement in homogeneous reaction parameter causes reduction in fluid concentration profile because of consumption of reactions. Also, it yields fluid viscosity that provides a reason for decline in fluid concentration trend. The variations in viscous fluid concentration towards heterogeneous reaction parameter L_s is delineated in *Fig. 5.11*. The diffusion rate reduces due to higher values of L_s i.e., $L_s = 0.3, 0.5, 0.7$ which enhances the concentration because diffusion rate decreases as the reaction rate increase. Therefore, concentration trend of chemical species towards L_s decreases. *Fig. 5.12* is offered to show the link between Schmidt number and viscous fluid concentration. On iterating the values of Sc i.e., $Sc (= 0.5, 1.0, 1.5)$, one can see that the viscous fluid concentration reflects the inclined trend in curves. Physically, the ratio between viscous diffusion to molecular diffusion is termed as Schmidt number. The enhancement in Schmidt number exhibit small molecular diffusivity. The inclination in momentum diffusivity rate enhances the concentration trend. The numerical approximations for Nusselt number and the coefficient of skin friction are shown by **Table 5.1** and **Table 5.2**.

5.4 Graphical representation

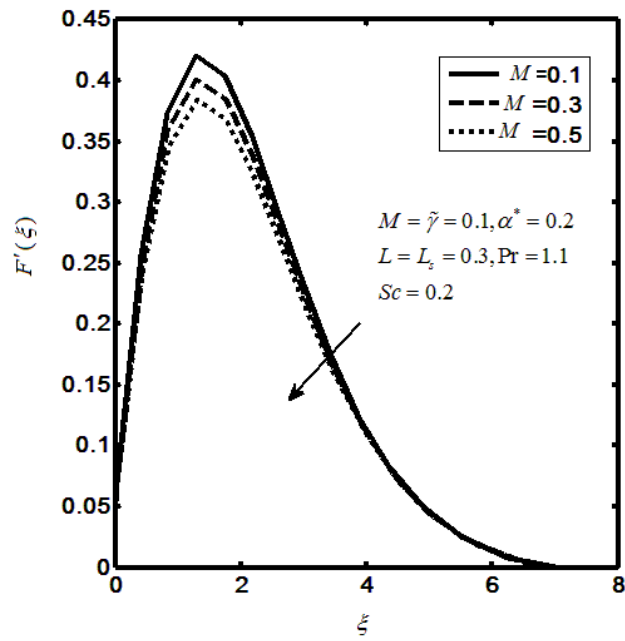


Fig. (5.2): Impacts of M upon $F'(\xi)$.

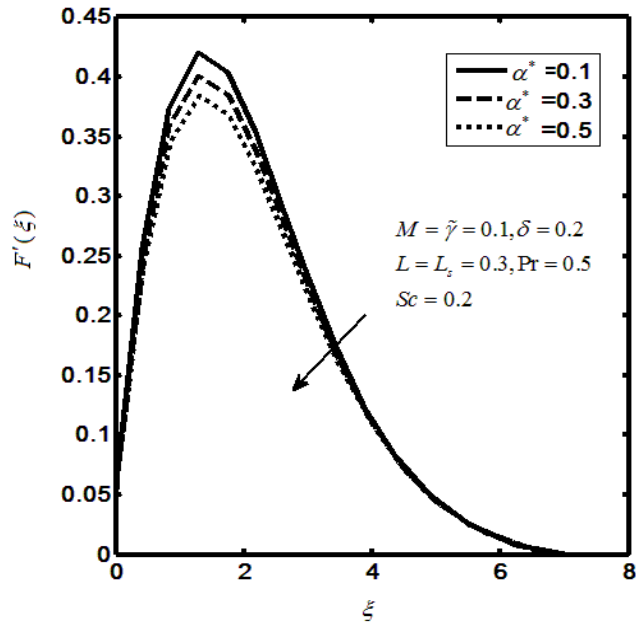


Fig. (5.3): Impacts of α^* upon $F'(\xi)$.

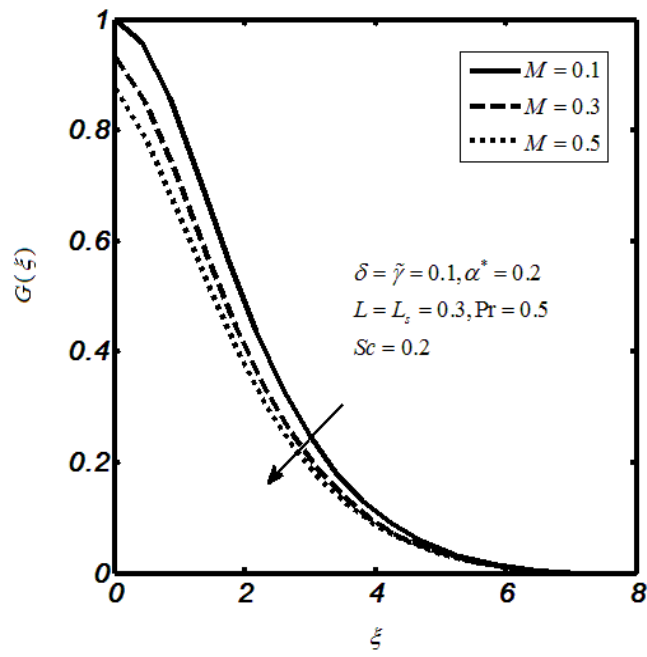


Fig. 5.4: Impacts of M on $G(\xi)$.

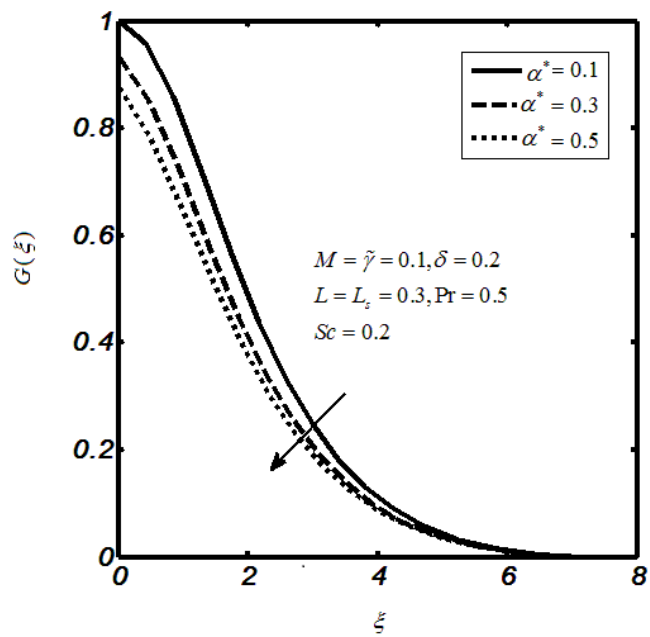


Fig. (5.5): Impacts of α^* upon $G(\xi)$.

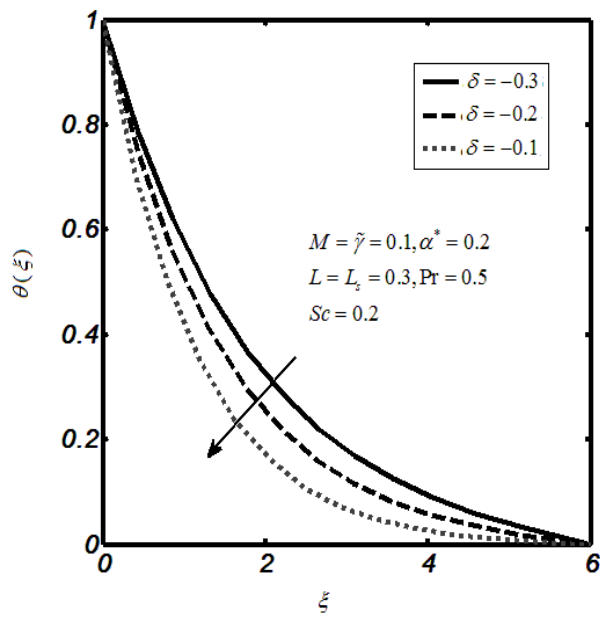


Fig. (5.6): Impacts of $\delta < 0$ upon $\theta(\xi)$.

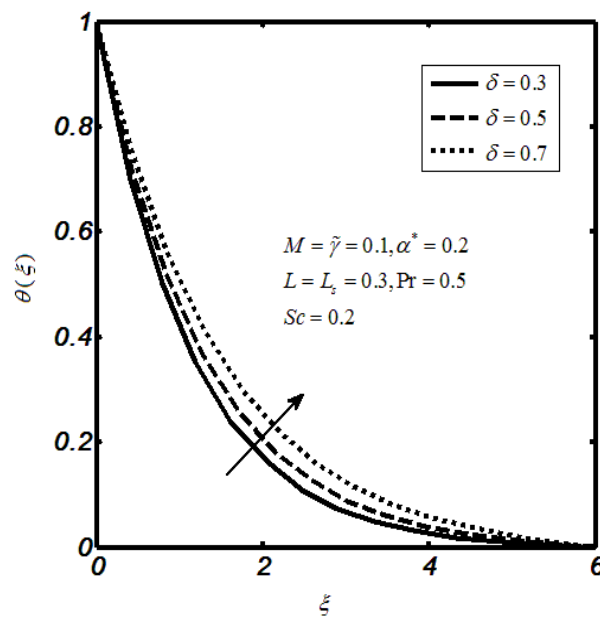


Fig. (5.7): Impacts of $\delta > 0$ upon $\theta(\xi)$.

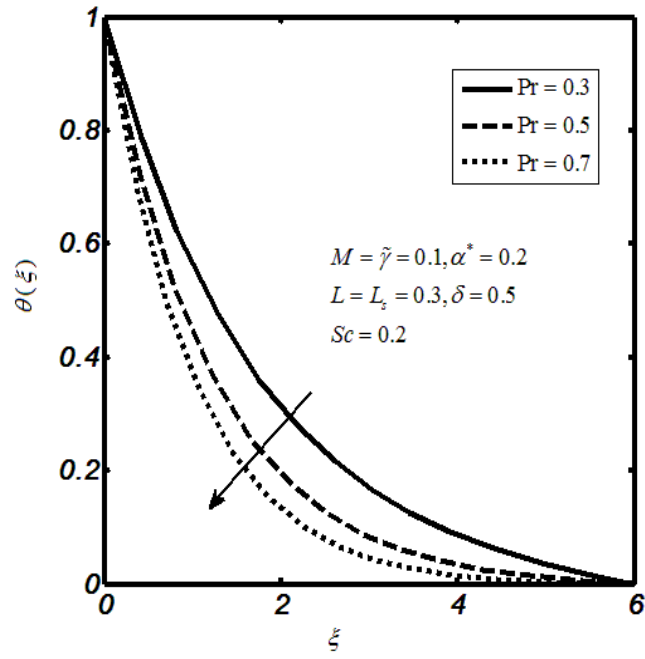


Fig. (5.8): Impacts of Pr upon $\theta(\xi)$.

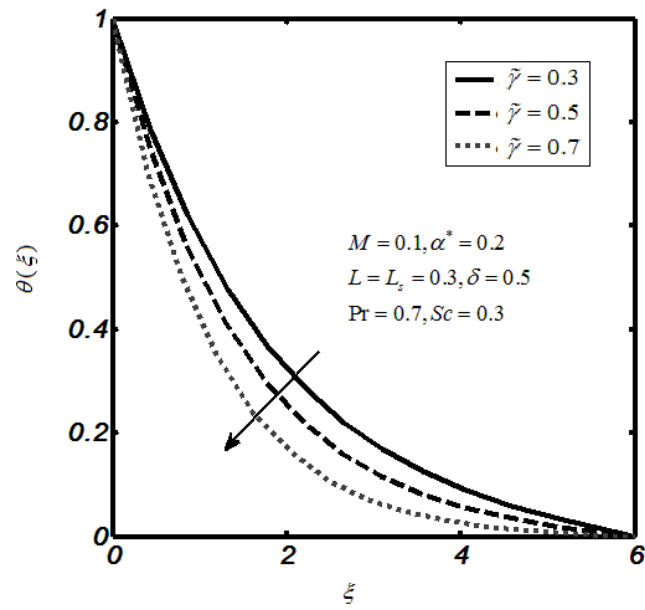


Fig. (5.9): Impacts of $\tilde{\gamma}$ upon $\theta(\xi)$.

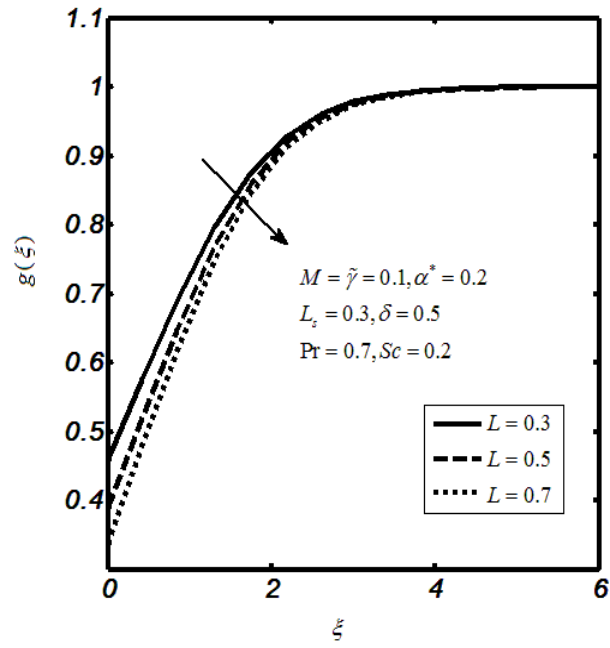


Fig. (5.10): Impacts of L on $g(\xi)$.

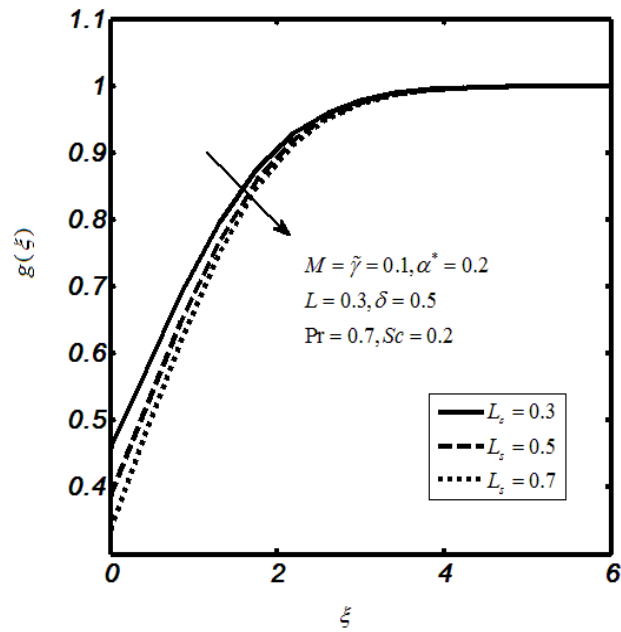


Fig. (5.11): Impacts of L_s upon $g(\xi)$.

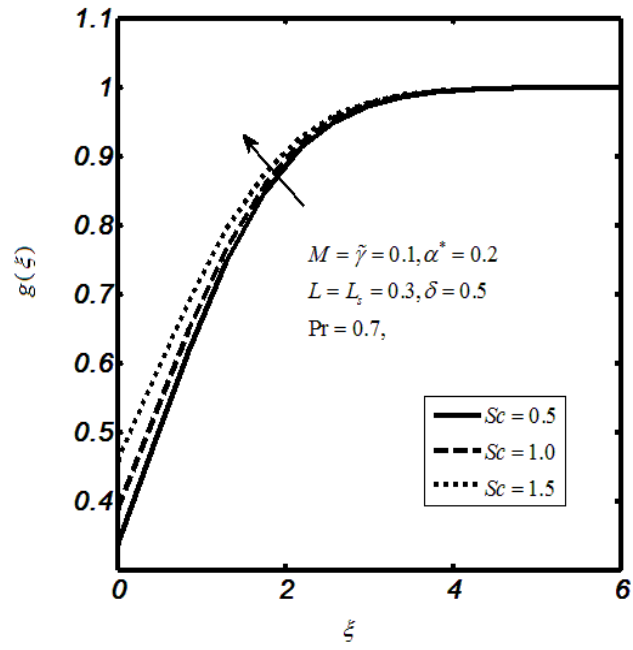


Fig. (5.12): Impacts of Sc upon $g(\xi)$.

Table 5.1: Numerical values of skin friction coefficient $F''(0)$ and $G'(0)$ for various values of M and α^* when $Pr = 1.1$.

M	α^*	$F''(0)$	$G'(0)$
0.0	0.25	0.25953	-0.41678
0.2	0.25	0.19118	-0.50954
0.4	0.25	0.14606	-0.59952
0.6	0.25	0.11670	-0.68036
0.8	0.25	0.09676	-0.75154

Table 5.2: Numerical approximations for local Nusselt number upon variations in $\alpha^*, M, Pr, \delta, Sc$ where $\lambda = 0.5$ and $Sc = 1.2$.

M	α^*	δ	Pr	Sc	$Re_r^{-1/2} Nu$
0.1	0.4	0.1	1.0	1.0	0.158252
0.2	0.4	0.1	1.0	1.0	0.135111
0.3		0.1	1.0	1.0	0.084889
0.5	0.2	0.1	1.0	1.0	0.175103
0.2	0.5	0.1	1.0	1.0	0.138543
0.2	0.8	0.1	1.0	1.0	0.109233
0.2	0.4	0.1	1.0	1.0	0.156255
0.2	0.4	0.1	1.0	1.0	0.149729
0.2	0.4	0.1	1.0	1.0	0.143689
0.2	0.4	0.1	1.0	1.0	0.148478
0.2	0.4	0.1	1.0	1.0	0.153036
0.2	0.4	0.1	1.0	1.0	0.155802

5.5 Concluding remarks

Our major concern in this chapter is to describe the magneto-hydrodynamics, heat generation/absorption and slip effects in a viscous fluid with homogeneous-heterogeneous chemical reactions when the flow field occurs due to disk rotation. The Cattaneo-Chritov approach is considered to extract energy equation. The resulting PDE's descend to ODE's by similarity transformation and the Runge-Kutta Fehlberg method with shooting scheme is implemented to compute numerical solutions. The effects of involved physical parameters are studied through graphs and tables. The key aspects are mentioned as:

- The decaying behaviour of viscous fluid velocity trend towards magnetic field parameter.
- The heat absorption parameter causes decrease in temperature whereas inverse trend is observed for parameter of heat generation.
- The temperature of viscous fluid shows decline curves upon Prandtl number.
- The decreasing behaviour of fluid concentration is noticed against homogeneous reaction parameter.
- The concentration of fluid declines towards parameter of heterogeneous reaction.
- The fluid concentration profile increases towards Schmidt number.

Chapter 6

On thermal radiation and joule heating in a mixed convective nanofluid flow

A Newtonian nanofluid flow field is demonstrated in this chapter with thermal radiation and heat generation/absorption. Further, in this study mixed convection, magnetic field, stagnation point, temperature stratification, Joule heating, concentration stratification and chemical reaction are included. The flow field is caused by the inclined stretching cylinder. The mathematical model is developed in the form of coupled partial differential framework and is descended to coupled ordinary differential framework by means of admissible similarity transformation. The temperature towards higher values of heat absorption/generation and thermal radiation is studied and analysed in detail. Further, the guesstimates for local Nusselt number as well as the skin friction coefficient are presented.

6.1 Mathematical formulation

The equations of motion for the Newtonian flow field are modelled mathematically. The motion of fluid is examined over an inclined and stretched cylinder with $u = a^* x$ as stretching velocity and $u_e = a' x$ as free stream velocities. For convenience, the axial direction of cylinder is taken to be parallel to x -axis. In the meanwhile, the perpendicular axis to the x -axis is supposed to be taken as r -axis (radial direction) with \tilde{R} as the radius of cylinder. By applying the laws of conservation, we get the following flow describing equations as:

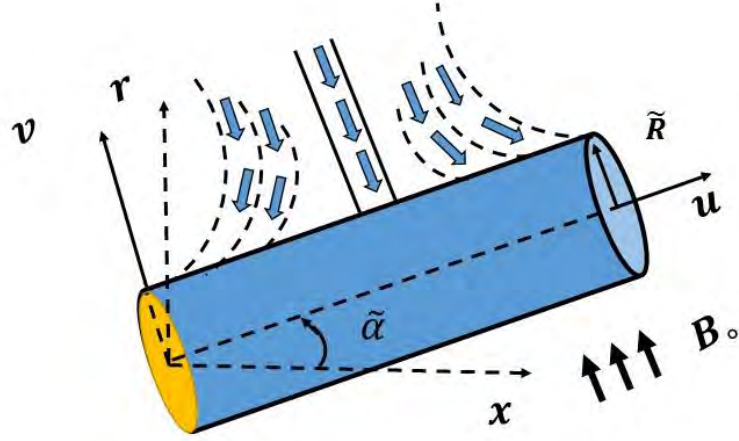


Fig. 6.1: Physical illustration of the model.

$$\frac{\partial(ru)}{\partial x} + \frac{\partial(rv)}{\partial r} = 0, \quad (6.1)$$

$$\begin{aligned} \frac{\partial u}{\partial x} u + \frac{\partial u}{\partial r} v = v^* \left(\frac{\partial^2 u}{\partial r^2} + \frac{1}{r} \frac{\partial u}{\partial r} \right) + u_e \frac{\partial u_e}{\partial x} - \frac{\sigma B_0^2}{\rho} (u - u_e) + (\bar{T} - \bar{T}_\infty) g \beta_T \cos \tilde{\alpha} \\ + (\bar{C} - \bar{C}_\infty) g \beta_c \cos \tilde{\alpha}, \end{aligned} \quad (6.2)$$

$$\begin{aligned} \frac{\partial \bar{T}}{\partial x} u + \frac{\partial \bar{T}}{\partial r} v = \frac{\partial}{\partial r} \left(r \frac{\partial \bar{T}}{\partial r} \right) \frac{\alpha}{r} + \tau \left(\frac{D_T}{\bar{T}_\infty} \left(\frac{\partial \bar{T}}{\partial r} \right)^2 + D_B \frac{\partial \bar{T}}{\partial r} \frac{\partial \bar{C}}{\partial r} \right) - \frac{1}{\rho c_p r} \frac{\partial}{\partial r} (r q_r) \\ + \frac{Q_0}{c_p \rho} (\bar{T} - \bar{T}_\infty) + \frac{\sigma B_0^2 u^2}{\rho c_p}, \end{aligned} \quad (6.3)$$

$$\frac{\partial \bar{C}}{\partial x} u + \frac{\partial \bar{C}}{\partial r} v = \left(\frac{\partial \bar{C}}{\partial r} \frac{1}{r} + \frac{\partial^2 \bar{C}}{\partial r^2} \right) D_B + \frac{D_T}{\bar{T}_\infty} \left(\frac{\partial \bar{T}}{\partial r} \frac{1}{r} + \frac{\partial^2 \bar{T}}{\partial r^2} \right) - K_c (\bar{C} - \bar{C}_\infty), \quad (6.4)$$

By using the Roseland radiative heat flux that is $q_r = -\left(\frac{4}{3}\right) \frac{\sigma^*}{k^*} \frac{\partial \bar{T}^4}{\partial r}$, where σ^* the coefficient

of Stefan Boltzmann and k^* the absorption coefficient. We can modify Eq. (6.4) as:

$$\begin{aligned} \frac{\partial \bar{T}}{\partial x} u + \frac{\partial \bar{T}}{\partial r} v = \frac{\partial}{\partial r} \left(\frac{\partial \bar{T}}{\partial r} r \right) \frac{\alpha}{r} + \tau \left(\frac{D_T}{\bar{T}_\infty} \left(\frac{\partial \bar{T}}{\partial r} \right)^2 + \frac{\partial \bar{T}}{\partial r} \frac{\partial \bar{C}}{\partial r} D_B \right) \\ + \frac{1}{\rho c_p r} \left(\frac{4}{3} \right) \frac{\sigma^*}{k^*} \frac{\partial}{\partial r} \left(r \frac{\partial \bar{T}^4}{\partial r} \right) + \frac{Q_0}{c_p \rho} (\bar{T} - \bar{T}_\infty) + \frac{\sigma B_0^2 u^2}{\rho c_p}, \end{aligned} \quad (6.5)$$

with end point conditions:

$$\begin{aligned}
u = U(x) &= a^* x, v = 0, \bar{T}(x, r) = \bar{T}_w(x) = \frac{b x}{\tilde{l}} + \bar{T}_0, \\
\bar{C}(x, r) &= \bar{C}_w(x) = \frac{d x}{\tilde{l}} + \bar{C}_0 \text{ at } r = \tilde{R}, \\
u \rightarrow u_e &= a' x, \bar{T}(x, r) \rightarrow \bar{T}_\infty(x) = \frac{c x}{\tilde{l}} + \bar{T}_0, \\
\bar{C}(x, r) &\rightarrow \bar{C}_\infty(x) = \frac{e x}{\tilde{l}} + \bar{C}_0 \text{ as } r \rightarrow \infty,
\end{aligned} \tag{6.6}$$

since the mathematical problem described in Eq. (6.4) - (6.5) with end point conditions shown in Eq. (6.6) are highly nonlinear therefore the exact solution seems to be unworkable. Thus, we need an equivalent system of ordinary differential equations in order to find the numerical solutions. It can be attained by using the set of similarity transformations given as:

$$\begin{aligned}
u = \frac{U_0 x}{\tilde{l}} F'(\eta), v = -F(\eta) \frac{\tilde{R}}{r} \sqrt{\frac{U_0 v^*}{\tilde{l}}}, \eta = \left(\frac{U_0}{v^* \tilde{l}} \right)^{\frac{1}{2}} \frac{r^2 - \tilde{R}^2}{2\tilde{R}}, \psi = \left(\frac{U_0 v^* x^2}{\tilde{l}} \right)^{\frac{1}{2}} \tilde{R} F(\eta), \\
C(\eta) = \frac{\bar{C} - \bar{C}_\infty}{\bar{C}_w - \bar{C}_0}, T(\eta) = \frac{\bar{T} - \bar{T}_\infty}{\bar{T}_w - \bar{T}_0},
\end{aligned} \tag{6.7}$$

the velocity relation towards stream functions is expressed as:

$$u = \frac{1}{r} \left(\frac{\partial \psi}{\partial r} \right), \quad v = -\frac{1}{r} \left(\frac{\partial \psi}{\partial x} \right), \tag{6.8}$$

Eq. (6.1) satisfies after using Eq. (6.7) -(6.8), whereas Eq. (6.2) - (6.5) gives.

$$\begin{aligned}
(1 + 2\tilde{K}\eta) \frac{d^3 F(\eta)}{d\eta^3} + 2 \frac{d^2 F(\eta)}{d\eta^2} \tilde{K} + \frac{d^2 F(\eta)}{d\eta^2} F(\eta) - \left(\frac{dF(\eta)}{d\eta} \right)^2 \\
-M^2 \left(\frac{dF(\eta)}{d\eta} - \lambda \right) + \lambda^2 + \lambda_m (T(\eta) + NC(\eta)) \cos \tilde{\alpha} = 0,
\end{aligned} \tag{6.9}$$

$$\begin{aligned}
(1 + 2\tilde{K}\eta) \left(1 + \frac{4}{3} R_r \right) \frac{d^2 T(\eta)}{d\eta^2} + 2\tilde{K} \left(1 + \frac{4}{3} R_r \right) \frac{dT(\eta)}{d\eta} + \text{Pr } N_b (1 + 2\tilde{K}\eta) \left(\frac{dT(\eta)}{d\eta} \frac{dC(\eta)}{d\eta} \right) \\
+ \text{Pr} \left(F(\eta) \frac{dT(\eta)}{d\eta} - \frac{dF(\eta)}{d\eta} \tilde{S} + \delta T(\eta) - \frac{dF(\eta)}{d\eta} T(\eta) + EcM^2 F^2(\eta) \right) \\
+ \text{Pr } N_b (1 + 2\tilde{K}\eta) \left(\frac{N_t}{N_b} \left(\frac{dT(\eta)}{d\eta} \right)^2 \right) = 0,
\end{aligned} \tag{6.10}$$

$$(1+2\tilde{K}\eta)\left(\frac{d^2C(\eta)}{d\eta^2}+\frac{N_t}{N_b}\frac{d^2T(\eta)}{d\eta^2}\right)+\text{Pr}Le\left(F(\eta)\frac{dC(\eta)}{d\eta}-\frac{dF(\eta)}{d\eta}C(\eta)-\frac{dF(\eta)}{d\eta}\delta_2\right) \\ +2\tilde{K}\left(\frac{dC(\eta)}{d\eta}+\frac{N_t}{N_b}\frac{dT(\eta)}{d\eta}\right)-\gamma C(\eta)=0, \quad (6.11)$$

with transformed boundary conditions:

$$\frac{dF(\eta)}{d\eta}=1, F(\eta)=0, T(\eta)=1-\tilde{S}, C(\eta)=1-\delta_2, \text{ at } \eta=0, \quad (6.12) \\ \frac{dF(\eta)}{d\eta}\rightarrow\lambda, T(\eta)\rightarrow 0, C(\eta)\rightarrow 0, \text{ when } \eta\rightarrow\infty.$$

The involved engineering parameters are defined as:

$$\tilde{K}=\frac{1}{\tilde{R}}\sqrt{\frac{v^*}{a^*}}, a^*=\frac{U_0}{\tilde{l}}, M=\sqrt{\frac{\sigma B_0^2}{\rho a^*}}, \lambda=\frac{a'}{a^*}, \lambda_m=\frac{Gr}{\text{Re}_x^2}, N=\frac{Gr^*}{Gr}, R_T=\frac{4\sigma^*T_\infty^3}{k^*k}, \quad (6.13) \\ \text{Pr}=\frac{v^*}{\alpha}, N_b=(C_w-C_\infty)\frac{\tau D_B}{v^*}, N_t=(T_w-T_\infty)\frac{\tau D_T}{T_\infty v^*}, \tilde{S}=\frac{c}{b}, Q=\frac{\tilde{l}Q_0}{U_0\rho c_p}, Le=\frac{\alpha}{D_B}, \\ \delta_2=\frac{e}{d}, \gamma=\frac{K_0\tilde{l}}{U_0}, Gr=\frac{g\beta_T(T_w-T_0)x^3}{v^{*2}}, Gr^*=\frac{g\beta_C(C_w-C_0)x^3}{v^{*2}}, Ec=\frac{U_0x}{c_p(T_w-T_\infty)\tilde{l}},$$

where $\tilde{K}, M, \lambda, \lambda_m, N, R_T, \text{Pr}, N_b, N_t, \tilde{S}, \delta, Le, \delta_2, \gamma$ and Ec are named as parameter of curvature, parameter of magnetic field, parameter of velocity ratio, parameter of mixed convection, parameter of buoyancy force, parameter of thermal radiation, Prandtl's number, parameter of Brownian motion, parameter of thermophoresis, parameter of thermal stratification, parameter of heat generation, Lewis's number, parameter of concentration stratification, parameter of chemical reaction and Eckert number. The coefficient of skin friction at the surface of cylinder is shown by.

$$C_f=\frac{2\tau_w}{\rho U^2}, \tau_w=\mu\left(\frac{\partial u}{\partial r}\right)_{r=\tilde{R}}, \quad (6.14)$$

in dimensionless practice, it is written as:

$$0.5C_f\sqrt{\text{Re}_x}=F''(0), \quad (6.15)$$

The expression for both the local Nusselt and the local Sherwood number is:

$$\begin{aligned}
Nu_x &= \frac{q_w x}{(T_w - T_0)k}, q_w = -\left(\frac{\partial T}{\partial r}\right)_{r=\tilde{R}} k + (q_r)_{r=\tilde{R}}, \\
Sh &= \frac{x j_w}{D(C_w - C_0)}, j_w = -D\left(\frac{\partial C}{\partial r}\right)_{r=\tilde{R}},
\end{aligned} \tag{6.16}$$

the dimensionless form of these expression is pre-arranged as:

$$\begin{aligned}
\frac{Nu_x}{\sqrt{Re_x}} &= -\left(1 + \frac{4}{3}R_d\right)T'(\eta), \quad \text{as } \eta \rightarrow 0, \\
\frac{Sh_x}{\sqrt{Re_x}} &= -C'(\eta), \quad \text{as } \eta \rightarrow 0.
\end{aligned} \tag{6.17}$$

with $Re_x = \frac{u x^2}{\nu l}$ be the local Reynold's number.

6.2 Computational algorithm

The governing Eq. (6.9)-(6.11) with conditions at the boundary Eq. (6.12) are coupled nonlinear system. The algorithm of shooting method with integration scheme named as fourth order Runge-Kutta methodology is suggested to acquire solutions. For this purpose, we consider the steps as follows. First, we may write Eq. (6.9) - (6.11) as:

$$\frac{d^3 F(\eta)}{d\eta^3} = -\frac{1}{(1+2\tilde{K}\eta)} \left(\begin{aligned} &2\tilde{K} \frac{d^2 F(\eta)}{d\eta^2} - \left(\frac{dF(\eta)}{d\eta}\right)^2 + \frac{d^2 F(\eta)}{d\eta^2} F(\eta) \\ &-\left(\frac{dF(\eta)}{d\eta} - \lambda\right)M^2 + \lambda^2 + \lambda_m (T(\eta) + NC(\eta)) \cos \tilde{\alpha} \end{aligned} \right), \tag{6.18}$$

$$\frac{d^2 T(\eta)}{d\eta^2} = -\frac{1}{(1+2\tilde{K}\eta)\left(1 + \frac{4}{3}R_T\right)} \left(\begin{aligned} &2\tilde{K} \left(1 + \frac{4}{3}R_T\right) \frac{dT(\eta)}{d\eta} + Pr N_b (1+2\tilde{K}\eta) \left(\frac{dT(\eta)}{d\eta} \frac{dC(\eta)}{d\eta}\right) \\ &+ Pr \left(F(\eta) \frac{dT(\eta)}{d\eta} - \frac{dF(\eta)}{d\eta} \tilde{S} + \delta T(\eta) - \frac{dF(\eta)}{d\eta} T(\eta) \right) \\ &+ Ec M^2 F(\eta)^2 \\ &+ Pr N_b (1+2\tilde{K}\eta) \left(\frac{N_t}{N_b} \left(\frac{dT(\eta)}{d\eta}\right)^2\right) \end{aligned} \right), \tag{6.19}$$

$$\left(\frac{d^2 C(\eta)}{d\eta^2} + \frac{N_t}{N_b} \frac{d^2 T(\eta)}{d\eta^2} \right) = - \frac{1}{(1+2\tilde{K}\eta)} \left(\text{Pr Le} \left(F(\eta) \frac{dC(\eta)}{d\eta} - \frac{dF(\eta)}{d\eta} C(\eta) - \frac{dF(\eta)}{d\eta} \delta_2 \right) + 2\tilde{K} \left(\frac{dC(\eta)}{d\eta} + \frac{N_t}{N_b} \frac{dT(\eta)}{d\eta} \right) - \gamma C(\eta) \right), \quad (6.20)$$

Define the following:

$$\begin{aligned} y_1 &= F(\eta), y_2 = y_1' = \frac{dF(\eta)}{d\eta}, y_3 = y_2' = \frac{d^2 F(\eta)}{d\eta^2}, y_4 = T(\eta), y_5 = y_4' = \frac{dT(\eta)}{d\eta}, \\ y_6 &= C(\eta), y_7 = y_6' = \frac{dC}{d\eta}, \end{aligned} \quad (6.21)$$

by inserting the above Eq. (6.21) into Eq. (6.18)-(6.20), we get the set of first order ODE's as:

$$\begin{aligned} y_1' &= y_2 \\ y_2' &= y_3 \\ y_3' &= -\frac{1}{(1+2\tilde{K}\eta)} (2\tilde{K}y_3 + y_1 y_3 - y_2^2 - M^2(y_2 - \lambda) + \lambda^2 + \lambda_m(y_4 + N y_6) - \cos \tilde{\alpha}) \\ y_4' &= y_5 \\ y_5' &= -\frac{1}{(1+2\tilde{K}\eta)} (2\tilde{K}(1 + \frac{4}{3} R_T) y_5 + \text{Pr } N_b (1+2\tilde{K}\eta) y_5 y_7 + \text{Pr } N_b (1+2\tilde{K}\eta) (\frac{N_t}{N_b} y_5^2)) \\ y_6' &= y_7 \\ y_7' &= -\frac{1}{(1+2\tilde{K}\eta)} (\text{Pr Le}(y_1 y_7 - y_2 y_6 - \delta_2 y_2) + 2\tilde{K}(y_7 + \frac{N_t}{N_b} y_5) - \gamma y_6), \end{aligned} \quad (6.22)$$

along with the end point conditions,

$$y_1(0) = 0, y_2(0) = 1, y_4(0) = 1 - \tilde{S}, y_6(0) = 1 - \delta_2, \quad (6.23)$$

$$y_2 \rightarrow \lambda, y_4 \rightarrow 0, y_6 \rightarrow 0 \text{ as } \eta \rightarrow \infty$$

Here we considered the initial guesses for the values of $\frac{d^2 F(0)}{d\eta^2}, \frac{dT(0)}{d\eta}, \frac{dC(0)}{d\eta}$,

- Firstly, choose the value of $\eta_\infty = 6$.
- Then we suppose the initial guesses for $y_3(0), y_5(0)$ and $y_7(0)$ as,

$$y_3(0) = y_5(0) = y_7(0) = 1.$$
- Solve ODE's (Ordinary Differential Equations) with by four-fifth order R-K theory.

- The absolute variations in the provided and approximated values for $y_1(\infty), y_3(\infty), y_5(\infty)$ and $y_7(\infty)$ that is residuals at boundary are calculated. Thus, the solution converges if its end point residuals are less than tolerance (i.e., 10^{-5}).
- If the values found in previous point are greater than permitted error, then the initial guesses for $y_3(0), y_5(0)$ and $y_7(0)$ will be modified by applying Newton's method.

6.3 Results and discussion

This chapter narrates the specifications of Newtonian nano-fluid model towards inclined cylindrical surface. The conservation law of momentum is considered to describe the flow field in the shape of coupled PDE's. These equations are then purified into coupled ODE's by reducing the number of independent variables through similarity transformation technique. The numerical findings are interpreted by the shooting scheme with Runge-Kutta Fehlberg method.

The involved physical parameters are $\tilde{K}, M, \lambda_m, R_T, Pr, N_t, N_b, \delta^-, \delta^+, \gamma$. The influences of \tilde{K}, M and λ_m on velocity of Newtonian fluid are explored and shown by way of *Figs. 6.2 - 6.4*. Further, the impacts of $R_T, Pr, N_t, N_b, \delta^-, \delta^+, \gamma$ and λ_m on a temperature of Newtonian fluid are delineated in *Figs. 6.5 - 6.12*. Also, the variation in Newtonian fluid concentration towards N_t, N_b, γ and λ_m are presented in the form of *Figs. 6.13 - 6.16*. Now in detail, *Fig. 6.2* depicts the impact of \tilde{K} on velocity of Newtonian fluid. It is witnessed that the velocity of fluid shows the inclining behaviour towards \tilde{K} when $\tilde{K} = 0.1, 0.2, 0.3$. This is because the curvature radius subject to surface area of cylinder diminish. Therefore, the particles of Newtonian fluid in contact with the surface area of cylinder reduces. The lesser the resistance faced by the Newtonian fluid particles; the greater will be the average Newtonian fluid velocity. *Fig. 6.3* shows the fluctuation in Newtonian fluid velocity corresponding to M . This picture testifies that the fluid velocity has declining nature towards M when we iterate

$M = 0.1, 0.2, 0.3$. Since, the increasing values of M causes increase in Lorentz force. This force reasons resistance with the fluid particles to move in a free manner therefore average velocity of Newtonian fluid decreases. The salient features of λ_m upon $F'(\eta)$ is portrayed in Fig. 6.4. Here we witness that $F'(\eta)$ amplifies towards large values of λ_m . Infact by enhancing the values of λ_m that is $\lambda_m = 0.1, 0.3, 0.5$, the buoyancy forces enhance due to gravity which magnifies the fluid velocity.

The Newtonian fluid temperature relies upon $R_T, Pr, N_t, N_b, \delta^-, \delta^+, \gamma$ and λ_m . More specifically, the dimensionless fluid temperature fluctuates for various values of R_T i.e., $R_T = 0.0, 0.3, 0.6$ and is expressed by Fig. 6.5. This indicates that fluid temperature enhances when enlarging parameter of thermal radiation. Physically, more heat is produced to the working fluid that causes temperature to be increased. The impacts of Pr on temperature of fluid is inspected and displayed by means of Fig. 6.6. It is evident that temperature profile rises towards higher values of Pr i.e., $Pr = 0.1, 0.2, 0.3$. The effects of temperature profile for N_t are discussed in Fig. 6.7. Here, we claim that the growing values of N_t i.e., $N_t = 0.1, 0.3, 0.7$ causes enhancement in the Newtonian fluid temperature. The strength of N_t produces the thermophoresis force due to temperature gradient that causes the boundary layer to become thicker and thus temperature enhances. Fig. 6.8 indicate the impacts of N_b that presents the picture of temperature profile inclined towards large values of N_b i.e., $N_b = 0.1, 0.3, 0.7$. This is because the strength of N_b causes uplift in thermal conduction of base fluid. Therefore, the boundary layer becomes thicker and temperature increases. It is seen from the profile of temperature distribution that Fig. 6.9 delineates the variation in temperature towards δ^+ . When we iterate $\delta^+ = 0.0, 0.3, 0.6$, the nanoparticle temperature testifies to be increasing. This is

because bulk amount of energy is produced on enlarging heat generation parameter and hence temperature shoots up. It is important to note that sometimes we introduce sink factor to control the overshoot in the temperature profile. It is witnessed from *Fig. 6.10* that nanofluid temperature towards δ^- decreases. This phenomenon happens because of the lowest values of the heat absorption parameter i.e., $\delta^- = -0.1, -0.3, -0.6$, that produces lesser amount of heat. Therefore, decline in temperature is witnessed. *Fig. 6.11* shows the variation in fluid temperature towards γ . For various values of γ i.e., $\gamma = 0.0, 0.1, 0.5$, the temperature gives decline trend. The salient features of λ_m upon $T(\eta)$ is portrayed in *Fig. 6.12*. Here we witness that $F'(\eta)$ diminish towards large values of λ_m . Physically, by enhancing the values of λ_m that is $\lambda_m = 0.1, 0.3, 0.5$, the buoyancy force enhances due to gravity which magnifies the rate of heat transfer. *Figs. 6.13 – 6.14* indicates that on enlarging N_t and N_b i.e. $N_t = 0.1, 0.3, 0.5$ and $N_b = 0.0, 0.1, 0.5$, the thickness of the concentration boundary layer increases for N_t whereas enlarging in N_b causes decline in the concentration boundary layer. In view of the physical aspect, one can justify these factors because in a nanofluid system, Brownian motion occurs due to collision of the nanoparticles with base fluid. It happens because Brownian diffusion is manifested with heat conduction. The enhancement in cylindrical surface area for heat transfer is caused by the nanoparticles. A nanofluid is such a system where the freely moving nanoparticles enhances the kinetic energy. As the diffusion of the nanoparticles is extremely influenced by the Brownian motion. Moreover, the nanoparticles are supposed to be dispersed from the hot surface towards the ambient fluid due to thermophoresis phenomena. Since, the nanometre sized particles produce resistance through the heated surface. Therefore, the thermophoresis force allows nanoparticles to incorporate heat from the surface to the fluid in motion. Thus, the concentration boundary layer becomes thicker towards N_t and hence

nanoparticle concentration increases whereas the opposite trend is witnessed for N_b . *Fig. 6.15* shows the variation in nanoparticle concentration towards γ . For various values of γ i.e., $\gamma = 0.1, 0.3, 0.5$, the nanoparticle concentration shows declining trend.

Fig. 6.16 shows the decaying behaviour of concentration profile towards λ_m . Physically, buoyancy forces exert as a compatible pressure gradient. Therefore, stronger buoyancy forces help to move in a vertical direction and as a result concentration declines. **Table 6.1** and **Table 6.2** shows the numerical values of the skin friction coefficient and local Nusselt number.

6.4 Graphical representation

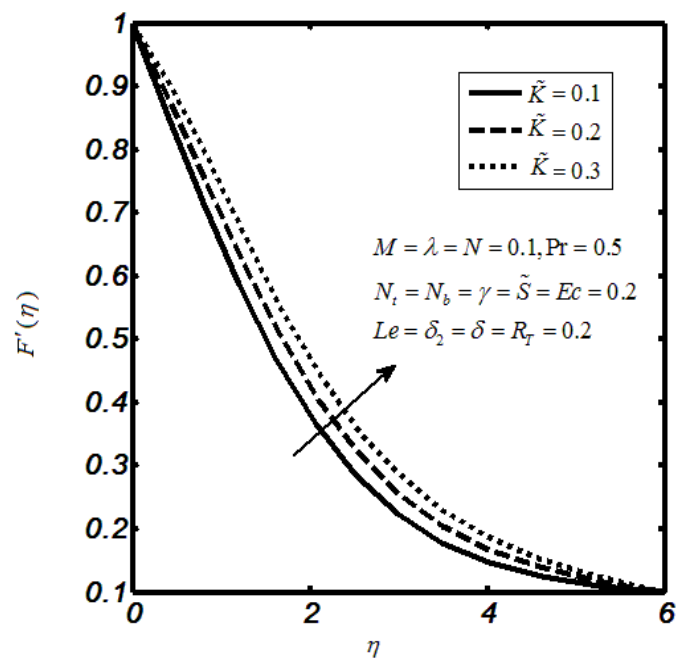


Fig. (6.2): Impacts of \tilde{K} upon $F'(\eta)$.

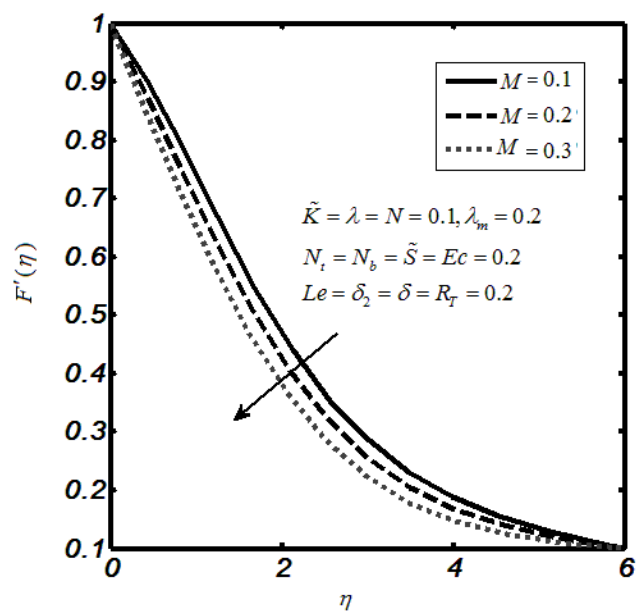


Fig. (6.3): Impacts of M upon $F'(\eta)$.

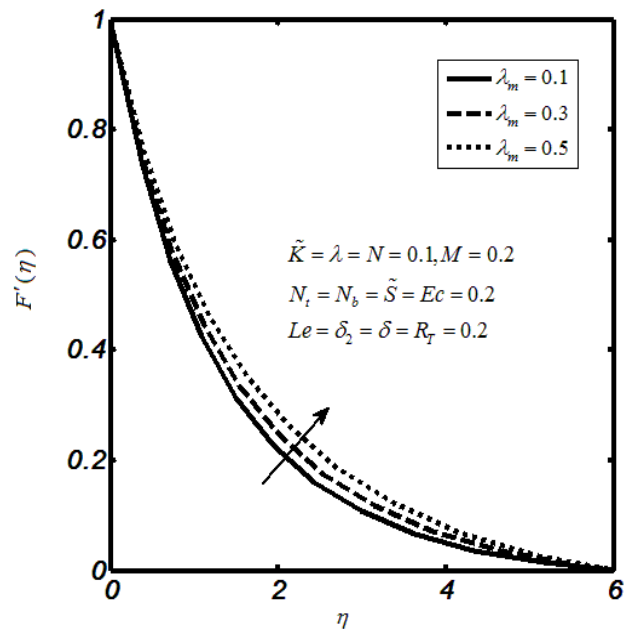


Fig. (6.4): Impacts of λ_m on $F'(\eta)$.

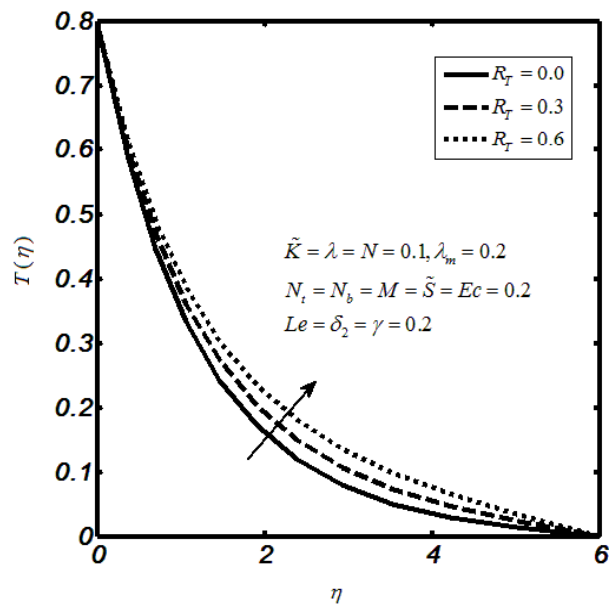


Fig. (6.5): Impacts of R_T on $T(\eta)$.

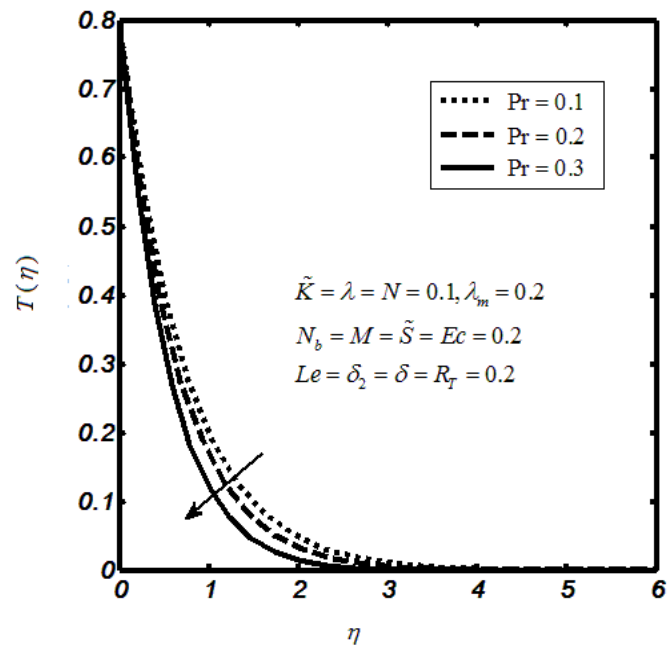


Fig. 6.6: Impacts of Pr on $T(\eta)$.

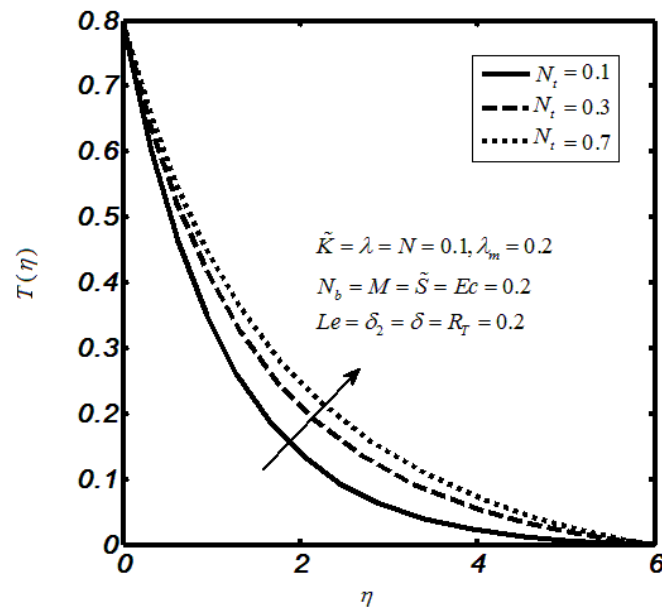


Fig. 6.7: Influence of N_t on $T(\eta)$.

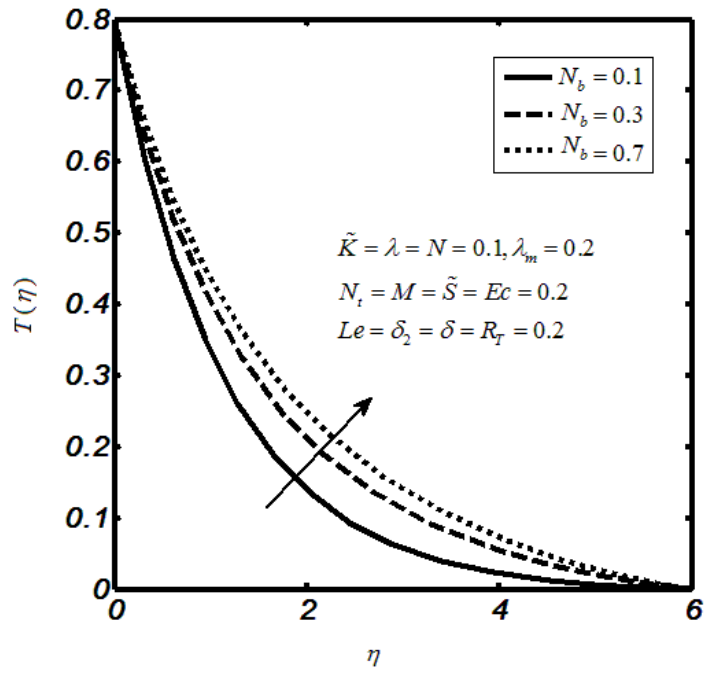


Fig. 6.8: Influence of N_b on $T(\eta)$.

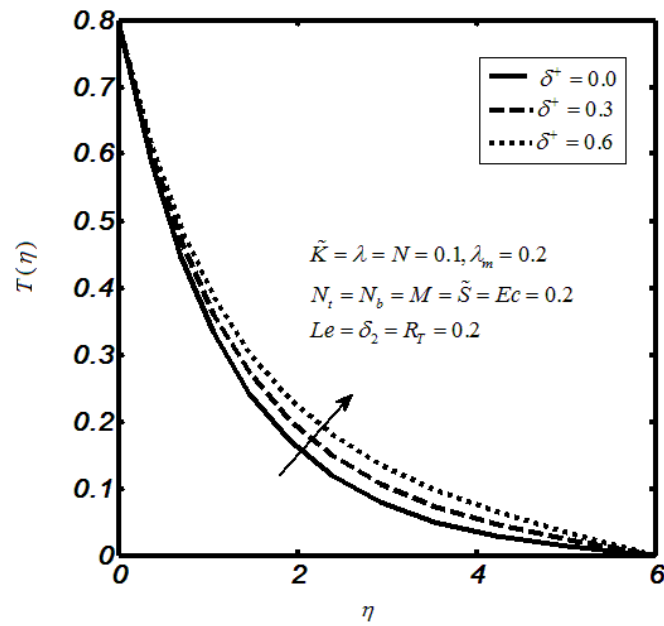


Fig. 6.9: Influence of δ^+ on $T(\eta)$.

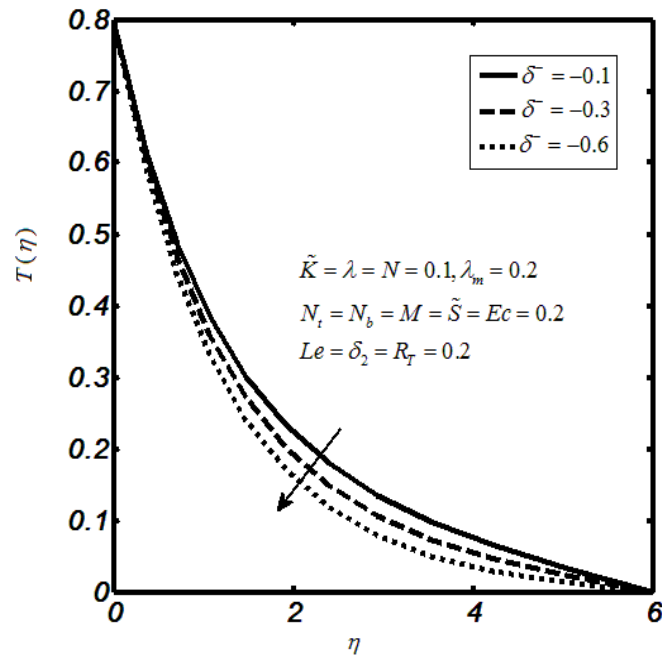


Fig. 6.10: Influence of δ^- on $T(\eta)$.

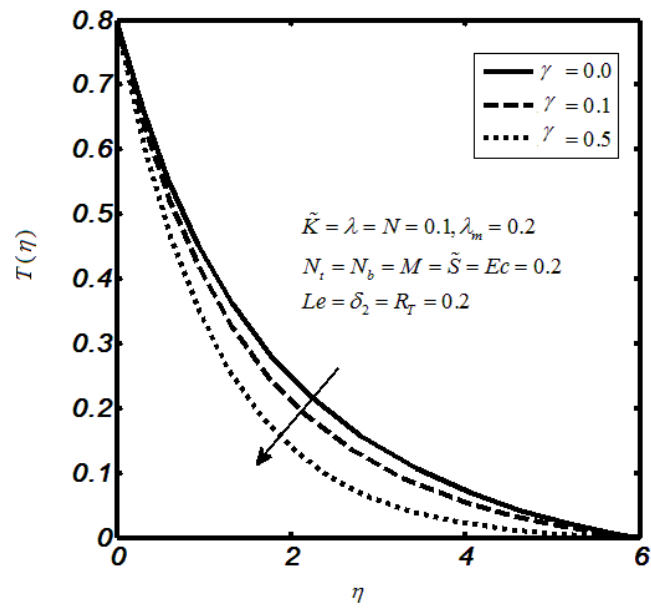


Fig. 6.11: Influence of γ on $T(\eta)$.

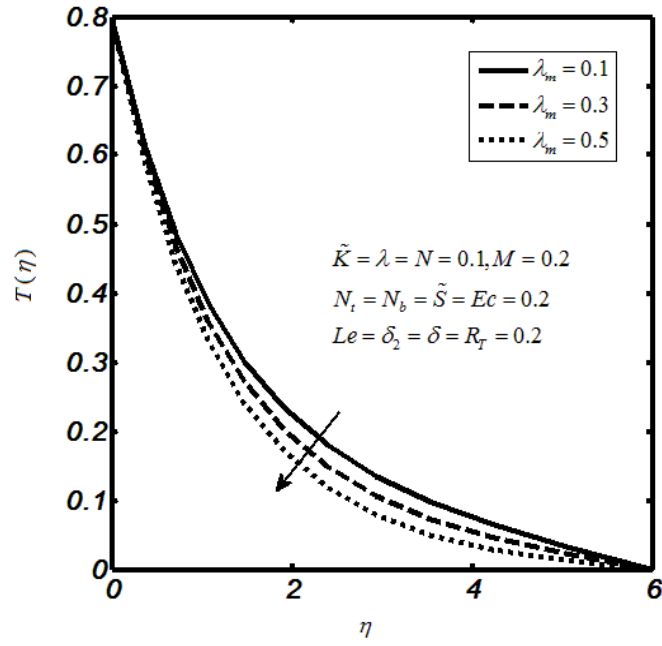


Fig. 6.12: Influence of λ_m on $T(\eta)$.

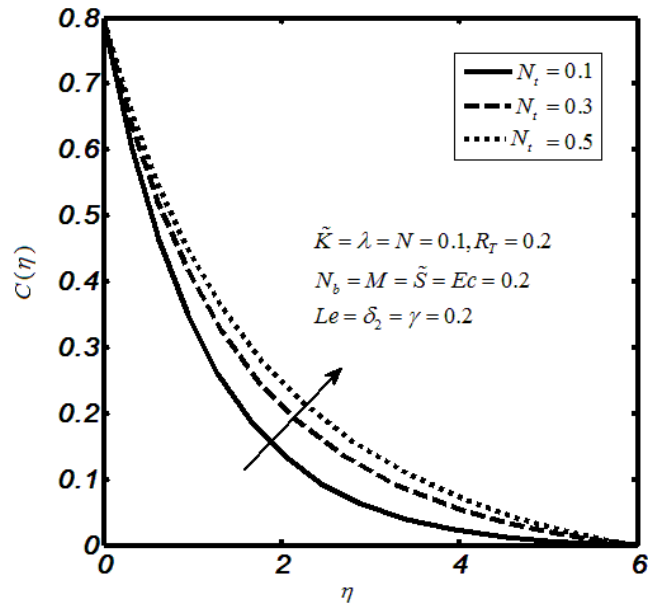


Fig. 6.13: Influence of N_t on $C(\eta)$.

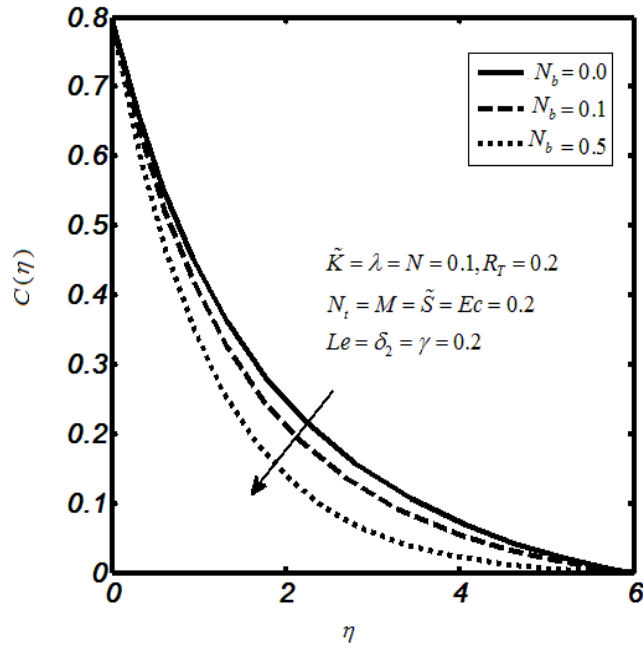


Fig. 6.14: Influence of N_b on $C(\eta)$.

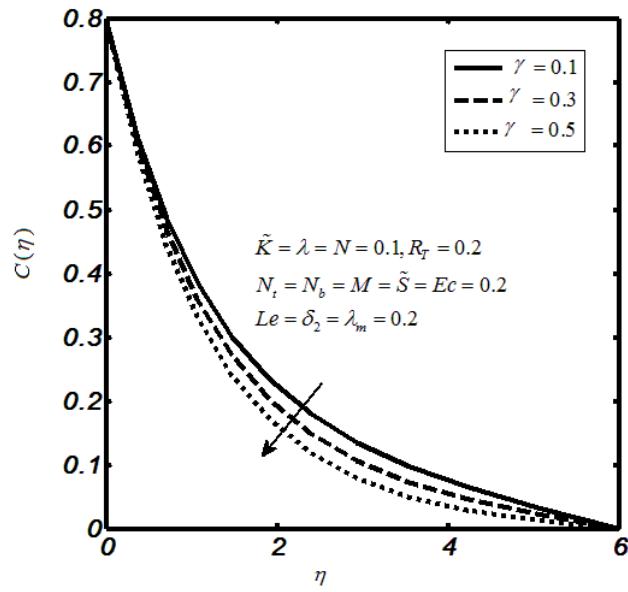


Fig. 6.15: Impacts of γ on $C(\eta)$.

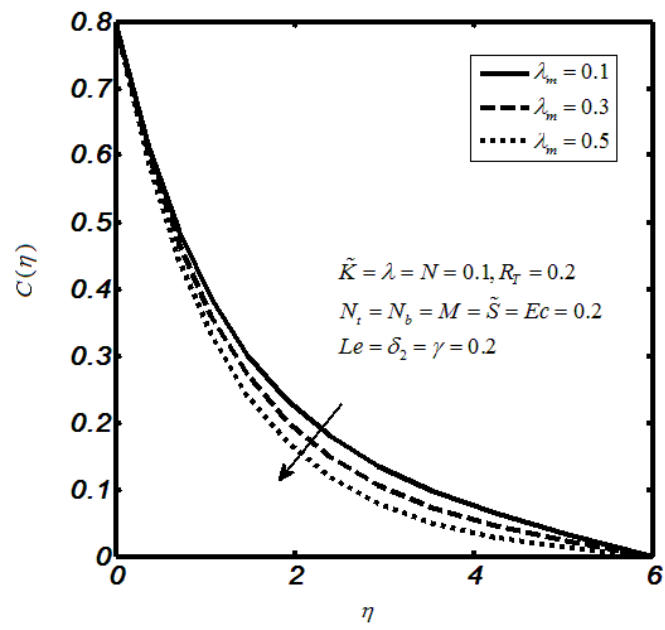


Fig. 6.16: Influence of λ_m on $C(\eta)$.

Table 6.1: Numerical approximations for coefficient of skin friction when $\lambda = 0.2, \lambda_m = 0.5, N_b = 0.1$ and $N_t = 0.1$.

M	Pr	\tilde{K}	Le	$0.5C_f\sqrt{\text{Re}_x} = F''(0),$
0	3	0.3	0.001	-1.053800
0.3	3	0.3	0.001	-1.090060
0.6	3	0.3	0.001	-1.194930
0.8	3	0.3	0.001	-1.298290
0.3	2	0.3	0.001	-1.012570
0.3	3	0.3	0.001	-1.090060
0.3	3.5	0.3	0.001	-1.125350
0.3	4	0.3	0.001	-1.158450
0.3	3	0.7	0.001	-1.090060
0.3	3	1.3	0.001	-0.490977
0.3	3	0.3	0.001	0.598867
0.3	3	0.7	0.001	1.827620
0.3	3	1.3	0.001	-1.090210
0.3	3	1.7	0.001	-1.059190
0.3	3	0.3	0.0	-1.024390
0.3	3	0.3	0.2	-1.007155

Table 6.2: Numerical approximations for Nusselt number towards various values of Pr, N_t and N_b when $\tilde{K} = 0.3, \lambda = 0.2, \lambda_m = 0.5, M = \delta = 0.1$.

Pr	N_t	N_b	$\frac{Nu_x}{\sqrt{\text{Re}_x}}$
1.0	0.2	0.3	0.31492
1.0	0.2	0.3	0.2141
1.0	0.2	0.3	0.2765
1.0	0.2	0.3	0.3166
3.0	0.3	0.3	0.3234
3.0	0.3	0.3	0.2902

3.0	0.3	0.3	0.2861
3.0	0.3	0.3	0.2397
5.0	0.5	0.3	0.2921
5.0	0.5	0.3	0.3327
5.0	0.5	0.3	0.2690

6.5 Concluding remarks

This chapter comprises Newtonian nanofluid manifested with thermal radiation and heat absorption/generation. The governing equations descend to ordinary differential system through similarity transformations. The numerical results are deduced by way of Runge-Kutta Fehlberg technique with shooting algorithm. The numerical findings for coefficient of friction and the heat transfer rate are examined. The key findings are mentioned below.

- The flow velocity shows an inclined trend towards curvature parameter.
- The fluid velocity decreases upon variation in parameter of magnetic field.
- The varying values of parameter of thermal radiation enhances the temperature profile.
- The Newtonian fluid temperature declines towards Prandtl number.
- The fluid temperature depicts the uplifting trend by maximizing the values of parameter of thermophoresis and Brownian motion.
- Heat generation provides a source for higher temperature profile whereas heat absorption gives reason for lesser temperature.
- The Newtonian fluid concentration shows an uplift towards thermophoresis parameter whereas opposite trend is observed for parameter of Brownian motion.
- The fluid concentration declines for higher values of concentration parameter.

Summary

This chapter is dedicated to summarizing whole thesis. Focus of the chapter 1 is on study of heat and mass transfer in a Carreau steady two-dimensional viscosity model over a moving wedge with infinite shear rate viscosity. The results for the shear thinning as well as shear thickening are reported. Symmetry transformation is applied which reduces modelled partial differential equations to the coupled system of ordinary differential equations. This system is sorted out in a numerical way by means of Runge-Kutta methodology associated by shooting algorithm. The reduction in the temperature of Carreau fluid is noticed due to large values of viscosity ratio parameter in case of shear thickening and, reverse trend is examined for the shear thinning case. Further, the concentration in Carreau fluid declines against wedge angle parameter for shear thickening and thinning.

In chapter 2 the effects of heat absorption/generation and chemical reaction are included in chapter 1; an extension of Chapter 1. For this purpose, the mathematical model is designed in terms of coupled partial differential equations and then solved numerically by Runge-Kutta Fehlberg technique chartered with shooting scheme. To investigate the impacts of physical parameter upon temperature and concentration, graphs are plotted. The temperature behaviour is examined for heat generation/absorption parameter. Further, the Carreau fluid concentration is inspected for chemical reaction parameter.

The Chapter 3 includes the results for Jeffery fluid with thermal stratification effects at a stagnation point. The thermal energy characteristics are studied through the generalized Fourier's law of heat flux. The flow is magnified by the stretching cylinder. The homogeneous-heterogeneous reactions are considered in this chapter. The concerned mathematical problem is developed by laws of conservation of momentum, mass and energy which provides a system of coupled partial differential equations. The order of these equations is reduced by way of similarity transformation. Later, the set of reduced coupled equations are computed

numerically by implementing Runge-Kutta Fehlberg technique with shooting algorithm. The curves for temperature and velocity of fluid are plotted for involved engineering parameters. The numerical values for the coefficient of skin friction are examined, and the obtained outcomes are compared with existing literature.

The Chapter 4 is the extension of Chapter 3 after including the effects of magnetic field and heat generation. The consequential PDE's descend to ODE's by carrying out the set of similarity transformations. These equations are solved numerically by shooting technique along with Runge-Kutta Fehlberg method. The effects of involved parameters are analysed and debated by means of graphs. The obtain outcomes are validated with the published work.

The Chapter 5 emphasizes on magneto-hydrodynamics, heat generation/absorption and slip effects over a Newtonian flow field with homogeneous-heterogeneous chemical reactions induced by the rotating disk. The Cattaneo-Christov approach is proposed to derive the energy equation and heat transfer phenomena. The equations are solved by numerical technique called Runge-Kutta Fehlberg method with shooting scheme. The influence of arising parameters towards fluid velocity, temperature and concentration is elaborated in graphs. Further, the numerical results for the skin friction coefficient and the rate of heat transfer are examined.

In Chapter 6, a Newtonian nanofluid flow field is demonstrated. The effects used in this chapter includes thermal radiation, heat generation/absorption., mixed convection, magnetic field, stagnation point, temperature stratification, Joule heating, concentration stratification and chemical reaction. The flow field is caused by the inclined stretching cylinder. The mathematical model is developed in the form of coupled partial differential framework and is descended to a system of coupled ordinary differential equations by means of admissible similarity transformation. The numerical findings are presented by Runge-Kutta Fehlberg method along with shooting scheme. The impacts of physical parameters upon fluid velocity,

temperature and concentration are discussed through graphs. Further, the guesstimates for local Nusselt number as well as the skin friction coefficient are presented.

Future work

This thesis focuses on studying the methods that can enhance or reduce heat transfer rate for which different fluid models reflects by including number of physical parameters. This study can be extended:

- for various non-Newtonian fluid models like Maxwell, Williamson, Eyring-Powell etc.
- to debate under the influence of nonlinear thermal radiation, thermal stratification, joule heating.
- by taking the convective boundary condition.
- to various geometries like, exponentially stretching sheet, vertical cylinder, rotating wedge, rotating cones in addition with porosity and convectively heated effects.
- to find the numerical solutions through FEM (Finite Element Method) for complex geometries.

References

- [1] K. N. Mehta and K. N. Rao, (1994), Buoyancy-induced flow of non-Newtonian fluids in a porous medium past a vertical flat plate with nonuniform surface heat flux, *International Journal of Engineering Science*, 32(2), 297-302.
- [2] J. P. Pascal and H. Pascal, (1995). On some non-linear shear flows of non-Newtonian fluids. *International Journal of Non-linear Mechanics*, 30(4), 487-500.
- [3] A. Kaye, (1962). *Non-Newtonian Flow in Incompressible Fluids*. College of Aeronautics Cranfield.
- [4] I. Machac, B. Siska and R. Teichman, (2002). Fall of non-spherical particles in a Carreau model liquid. *Chemical Engineering and Processing: Process Intensification*, 41(7), 577-584.
- [5] G. C. Georgiou, (2003). The time-dependent, compressible Poiseuille and extrudate-swell flows of a Carreau fluid with slip at the wall. *Journal of Non-Newtonian Fluid Mechanics*, 109(2-3), 93-114.
- [6] I. Machac, B. Siska, and R. Teichman, (2002). Fall of non-spherical particles in a Carreau model liquid. *Chemical Engineering and Processing: Process Intensification*, 41(7), 577-584.
- [7] H. I. Andersson, O. R. Hansen and B. Holmedal, (1994). Diffusion of a chemically reactive species from a stretching sheet. *International Journal of Heat and Mass Transfer*, 37(4), 659-664.
- [8] J. Argyris, I. S. Doltsinis, H. Friz and J. Urban, (1994). Physical and computational aspects of chemically reacting hypersonic flows. *Computer Methods in Applied Mechanics and Engineering*, 111(1-2), 1-35.
- [9] V. P. Motulevich, (1996). Impact of chemical reactions upon heat transfer. *Journal of Hazardous Materials*, 46(2-3), 225-229.
- [10] J. A. M. Kuipers and W. P. M. van Swaaij, (1998). Computational fluid dynamics applied to chemical reaction engineering. In *Advances in Chemical Engineering* (Vol. 24, pp. 227-328). Academic Press.
- [11] D. Pal, (1999). Effect of chemical reaction on the dispersion of a solute in a porous medium. *Applied Mathematical Modelling*, 23(7), 557-566.

- [12] E. Samson, J. Marchand and J. J. Beaudoin, (2000). Modeling the influence of chemical reactions on the mechanisms of ionic transport in porous materials: an overview. *Cement and Concrete Research*, 30(12), 1895-1902.
- [13] L. K. Hjertager, B. H. Hjertager and T. Solberg, (2001). CFD modeling of fast chemical reactions in turbulent liquid flows. In *Computer Aided Chemical Engineering* (Vol. 9, pp. 159-164). Elsevier.
- [14] G. Bisio, M. Cartesegna and G. Rubatto, (2002). Thermodynamic analysis of fluids with the possible presence of chemical reactions. *Energy Conversion and Management*, 43(13), 1619-1637.
- [15] R. Kandasamy, K. Periasamy and K. S. Prabhu, (2005). Effects of chemical reaction, heat and mass transfer along a wedge with heat source and concentration in the presence of suction or injection. *International Journal of Heat and Mass Transfer*, 48(7), 1388-1394.
- [16] A. Raptis and C. Perdakis, (2006). Viscous flow over a non-linearly stretching sheet in the presence of a chemical reaction and magnetic field. *International Journal of Non-Linear Mechanics*, 41(4), 527-529.
- [17] M. Bhuvaneswari, S. Sivasankaran and M. Ferdows, (2009). Lie group analysis of natural convection heat and mass transfer in an inclined surface with chemical reaction. *Nonlinear Analysis: Hybrid Systems*, 3(4), 536-542.
- [18] C. H. Chen, (2009). Magneto-hydrodynamic mixed convection of a power-law fluid past a stretching surface in the presence of thermal radiation and internal heat generation/absorption. *International Journal of Non-Linear Mechanics*, 44(6), 596-603.
- [19] C. Y. Cheng, (2009). Natural convection boundary layer on a horizontal elliptical cylinder with constant heat flux and internal heat generation. *International Communications in Heat and Mass Transfer*, 36(10), 1025-1029.
- [20] P. M. Patil and S. Roy, (2010). Unsteady mixed convection flow from a moving vertical plate in a parallel free stream: Influence of heat generation or absorption. *International Journal of Heat and Mass Transfer*, 53(21-22), 4749-4756.
- [21] A. Mahdy, (2010). Effect of chemical reaction and heat generation or absorption on double-diffusive convection from a vertical truncated cone in porous media with

- variable viscosity. *International Communications in Heat and Mass Transfer*, 37(5), 548-554.
- [22] F. M. Hady, F. S. Ibrahim, S. M Abdel-Gaied and M. R. Eid, (2011). Effect of heat generation/absorption on natural convective boundary-layer flow from a vertical cone embedded in a porous medium filled with a non-Newtonian nanofluid. *International Communications in heat and mass transfer*, 38(10), 1414-1420.
- [23] R. A. Van Gorder and K. Vajravelu, (2011). Convective heat transfer in a conducting fluid over a permeable stretching surface with suction and internal heat generation/absorption. *Applied Mathematics and Computation*, 217(12), 5810-5821.
- [24] K. U. Rehman, M. Y. Malik, T. Salahuddin and M. Naseer, (2016). Dual stratified mixed convection flow of Eyring-Powell fluid over an inclined stretching cylinder with heat generation/absorption effect. *AIP Advances*, 6(7), 075112.
- [25] M. A. Mahmoud, (2011). Slip velocity effect on a non-Newtonian power-law fluid over a moving permeable surface with heat generation. *Mathematical and Computer Modelling*, 54(5-6), 1228-1237.
- [26] M. Rajarathinam and N. Nithyadevi, (2017). Heat transfer enhancement of Cu-water nanofluid in an inclined porous cavity with internal heat generation. *Thermal Science and Engineering Progress*, 4, 35-44.
- [27] D. Angirasa and G. P. Peterson, (1997). Natural convection heat transfer from an isothermal vertical surface to a fluid saturated thermally stratified porous medium. *International Journal of Heat and Mass Transfer*, 40(18), 4329-4335.
- [28] A. J. Chamkha, (1997). MHD-free convection from a vertical plate embedded in a thermally stratified porous medium with Hall effects. *Applied Mathematical Modelling*, 21(10), 603-609.
- [29] S. A. Devi and R. Kandasamy, (2001). Thermal stratification effects on laminar boundary-layer flow over a wedge with suction or injection. *Mechanics Research Communications*, 28(3), 349-354.
- [30] A. Bouhdjar and A. Harhad, (2002). Numerical analysis of transient mixed convection flow in storage tank: influence of fluid properties and aspect ratios on stratification. *Renewable Energy*, 25(4), 555-567.
- [31] B. Fabiano, R. J. A. Kersten, G. Opschoor and R. Pastorino, (2002). Theoretical and experimental investigation into the explosive boiling potential of thermally stratified

- liquid–liquid systems. *Journal of Hazardous Materials*, 93(1), 107-121. X and Y found the useful results to purify seawater through solar energy.
- [32] B. Straughan, (2010). Porous convection with Cattaneo heat flux. *International Journal of Heat and Mass Transfer*, 53(13-14), 2808-2812.
- [33] B. Straughan, (2010). Acoustic waves in a Cattaneo–Christov gas, *Physics Letters A*, 374(26), 2667-2669.
- [34] H. Al-Qahtani and B. S. Yilbas, (2010). The closed form solutions for Cattaneo and stress equations due to step input pulse heating. *Physica B: Condensed Matter*, 405(18), 3869-3874.
- [35] V. Tibullo and V. Zampoli, (2011). A uniqueness result for the Cattaneo–Christov heat conduction model applied to incompressible fluids. *Mechanics Research Communications*, 38(1), 77-79.
- [36] S. Han, L. Zheng, C. Li and X. Zhang, (2014). Coupled flow and heat transfer in viscoelastic fluid with Cattaneo–Christov heat flux model. *Applied Mathematics Letters*, 38, 87-93.
- [37] S. A. M. Haddad, (2014). Thermal instability in Brinkman porous media with Cattaneo–Christov heat flux. *International Journal of Heat and Mass Transfer*, 68, 659-668.
- [38] I. S. Shivakumara, M. Ravisha, C. O. Ng and V. L. Varun, (2015). A thermal non-equilibrium model with Cattaneo effect for convection in a Brinkman porous layer. *International Journal of Non-Linear Mechanics*, 71, 39-47.
- [39] T. Hayat, K. Muhammad, M. Farooq and A. Alsaedi, (2016). Squeezed flow subject to Cattaneo–Christov heat flux and rotating frame. *Journal of Molecular Liquids*, 220, 216-222.
- [40] T. Hayat, M. I. Khan, M. Farooq, T. Yasmeen and A. Alsaedi, (2016). Stagnation point flow with Cattaneo-Christov heat flux and homogeneous-heterogeneous reactions. *Journal of Molecular Liquids*, 220, 49-55.
- [41] D. Biskamp, (1995). Scaling properties in MHD turbulence. *Chaos, Solitons & Fractals*, 5(10), 1779-1793.
- [42] J. F. Hawley and J. M. Stone, (1995). MOCCT: A numerical technique for astrophysical MHD. *Computer Physics Communications*, 89(1-3), 127-148.


- [43] M. Ishikawa, Y. Inui, J. Umoto and K. Yoshikawa, (1995). Preliminary analysis of MHD—Brayton cycle applied to fusion reactors (CFAR). *Fusion Engineering and Design*, 29, 57-63.
- [44] I. A. Evtushenko, I. R. Kirillov and C. B. Reed, (1995). MHD-flow in slotted channels with conducting walls. *Fusion Engineering and Design*, 27, 627-633.
- [45] Y. Inui, M. Ishikawa and J. Umoto, (1995). New conceptual design method of non-equilibrium disk MHD generator. *Energy Conversion and Management*, 36(2), 109-119.
- [46] A. Y. Ying and A. A. Gaizer, (1995). The effects of imperfect insulator coatings on MHD and heat transfer in rectangular ducts. *Fusion engineering and design*, 27, 634-641.
- [47] J. P. Goedbloed and A. Lifschitz, (1995). Comment on “Symmetry analysis of the nonlinear MHD equations” by Wu. *Physics Letters A*, 198(5-6), 467-468.
- [48] T. Q. Hua and J. S. Walker, (1995). MHD flow in rectangular ducts with inclined non-uniform transverse magnetic field. *Fusion Engineering and Design*, 27, 703-710.
- [49] A. S. Kumar, B. Gupta, and D. P. Tewari, (1998). Electrothermal instabilities in MHD boundary layers. *Energy Conversion and Management*, 39(1-2), 95-103.
- [50] H. V. Ersoy, (1999). MHD flow of an Oldroyd-B fluid between eccentric rotating disks. *International Journal of Engineering Science*, 37(15), 1973-1984.
- [51] A., Sugiyama, M. Hashiride, R. Morimoto, Y. Nagai and R. Aogaki, (2004). Application of vertical micro-disk MHD electrode to the analysis of heterogeneous magneto-convection. *Electrochimica Acta*, 49(28), 5115-5124.
- [52] D. O. Gomez, P. D. Mininni and P. Dmitruk, (2005). MHD simulations and astrophysical applications. *Advances in Space Research*, 35(5), 899-907.
- [53] X. Liu, T. Kiyoshi and M. Takeda, (2006). Simulation of a seawater MHD power generation system. *Cryogenics*, 46(5), 362-366.

- [54] G. Herdrich, M. Auweter-Kurtz, M. Fertig, A. Nawaz and D. Petkow, (2006). MHD flow control for plasma technology applications. *Vacuum*, 80(11-12), 1167-1173.
- [55] J. M. Stone and T. A. Gardiner, (2007). Recent progress in astrophysical MHD. *Computer Physics Communications*, 177(1-2), 257-259.
- [56] V. Dolejs and I. Machac, (1995). Pressure drop during the flow of a Newtonian fluid through a fixed bed of particles. *Chemical Engineering and Processing: Process Intensification*, 34(1), 1-8.
- [57] B. C. Bell and K. S. Surana, (1995). p-Version least squares finite element formulation for two-dimensional incompressible Newtonian and non-Newtonian non-isothermal fluid flow. *Computers & Structures*, 54(1), 83-96.
- [58] L. C. Musson and K. S. Surana, (1995). p-Version least squares finite element formulation for three-dimensional, isothermal, Newtonian fluid flow. *Computers & Structures*, 57(1), 107-124.
- [59] R. Kröger and H. J. Rath, (1995). Velocity and elongation rate distributions in stretched polymeric and Newtonian liquid bridges. *Journal of Non-newtonian Fluid Mechanics*, 57(2-3), 137-153.
- [60] E. Degand and K. Walters, (1995). On the motion of a sphere falling through an elastic liquid contained in a tightly-fitting cylindrical container. *Journal of Non-Newtonian Fluid Mechanics*, 57(1), 103-115.
- [61] P. Z. Bar-Yoseph and Y. Kryzhanovski, (1996). Axisymmetric vortex breakdown for generalized Newtonian fluid contained between rotating spheres. *Journal of Non-Newtonian Fluid Mechanics*, 66(2-3), 145-168.
- [62] J. M. Nouri and J. H. Whitelaw, (1997). Flow of Newtonian and non-Newtonian fluids in an eccentric annulus with rotation of the inner cylinder. *International Journal of Heat and Fluid Flow*, 18(2), 236-246.
- [63] R. E. Khayat, A. Luciani and L. A. Utracki, (1997). Boundary-element analysis of planar drop deformation in confined flow. Part 1. Newtonian fluids. *Engineering Analysis with Boundary Elements*, 19(4), 279-289.
- [64] V. Dolejs, P. Dolecek and B. Siska, (1998). Drag and fall velocity of a spherical particle in generalized Newtonian and viscoplastic fluids. *Chemical Engineering and Processing: Process Intensification*, 37(2), 189-195.
- [65] E. Comparini and P. Mannucci, (1998). Flow of a Bingham fluid in contact with a Newtonian fluid. *Journal of Mathematical Analysis and Applications*, 227(2), 359-381.

- [66] Y. Xuan and W. Roetzel, (2000). Conceptions for heat transfer correlation of nanofluids. *International Journal of Heat and Mass Transfer*, 43(19), 3701-3707.
- [67] Y. Xuan and Q. Li, (2000). Heat transfer enhancement of nanofluids. *International Journal of Heat and Fluid Flow*, 21(1), 58-64.
- [68] S. K. Das, N. Putra and W. Roetzel, (2003). Pool boiling characteristics of nanofluids. *International Journal of Heat and Mass Transfer*, 46(5), 851-862.
- [69] S. K. Das, N. Putra and W. Roetzel, (2003). Pool boiling of nano-fluids on horizontal narrow tubes. *International Journal of Multiphase Flow*, 29(8), 1237-1247.
- [70] D. Wen and Y. Ding, (2004). Experimental investigation into convective heat transfer of nanofluids at the entrance region under laminar flow conditions. *International Journal of Heat and Mass Transfer*, 47(24), 5181-5188.
- [71] H. Kikura, J. Matsushita, M. Matsuzaki, Y. Kobayashi and M. Aritomi, (2004). Thermal behaviour and particle size evaluation of primary clusters in a water-based magnetic fluid. *Science and Technology of Advanced Materials*, 5(5-6), 703-707.
- [72] H. Rafii-Tabar, (2004). Computational modelling of thermo-mechanical and transport properties of carbon nanotubes. *Physics Reports*, 390(4-5), 235-452.
- [73] K. Tanaka, T. Wakayasu, A. Kubono and R. Akiyama, (2004). Electro-rheological behavior of suspension composed of titanium dioxide nano-particles. *Sensors and Actuators A: Physical*, 112(2-3), 376-380.
- [74] C. D. Buioca, S. Noaghi, V. Iusan, M. Buioca and A. Stanci, (2004). Nano-and microparticles characterisation using Brownian diffusion measurements. *Journal of Magnetism and Magnetic Materials*, 272, E1063-E1065.
- [75] P. C. Fannin, (2004). Characterisation of magnetic fluids. *Journal of Alloys and Compounds*, 369(1-2), 43-51.
- [76] C. C. Wang, (2005). Mixed convection boundary layer flow on inclined wavy plates including the magnetic field effect. *International Journal of Thermal Sciences*, 44(6), 577-586.
- [77] J. F. Vinuesa and J. V. G. de Arellano, (2005). Introducing effective reaction rates to account for the inefficient mixing of the convective boundary layer. *Atmospheric Environment*, 39(3), 445-461.
- [78] J. Orfi and N. Galanis, (2005). Mixed convection with heat and mass transfer in horizontal tubes. *International Communications in Heat and Mass Transfer*, 32(3-4), 511-519.

- [79] E. Magyari and E. H. Aly, (2006). Mechanical and thermal characteristics of a mixed convection boundary-layer flow in a saturated porous medium. *International Journal of Heat and Mass Transfer*, 49(21-22), 3855-3865.
- [80] L. Deswita, R. Nazar, A. Ishak, R. Ahmad and I. Pop, (2010). Similarity solutions for mixed convection boundary layer flow over a permeable horizontal flat plate. *Applied Mathematics and Computation*, 217(6), 2619-2630.
- [81] A. Ishak, R. Nazar and I. Pop, (2010). MHD mixed convection boundary layer flow towards a stretching vertical surface with constant wall temperature. *International Journal of Heat and Mass Transfer*, 53(23-24), 5330-5334.
- [82] D. Pal, (2010). Mixed convection heat transfer in the boundary layers on an exponentially stretching surface with magnetic field. *Applied Mathematics and Computation*, 217(6), 2356-2369.
- [83] T. Hayat, S. Qayyum, M. Imtiaz and A. Alsaedi, (2016). Impact of Cattaneo-Christov heat flux in Jeffrey fluid flow with homogeneous-heterogeneous reactions. *PloS One*, 11(2).
- [84] F. M. Abbasi, S. A. Shehzad, T. Hayat, A. Alsaedi and M. A. Obid, (2015). Influence of heat and mass flux conditions in hydromagnetic flow of Jeffrey nanofluid. *AIP Advances*, 5(3), 037111.
- [85] A. Aziz, A. Alsaedi, T. Muhammad and T. Hayat, (2018). Numerical study for heat generation/absorption in flow of nanofluid by a rotating disk. *Results in Physics*, 8, 785-792.
- [86] M. Khan and H. Sardar, (2018). On steady two-dimensional Carreau fluid flow over a wedge in the presence of infinite shear rate viscosity. *Results in Physics*, 8, 516-523.

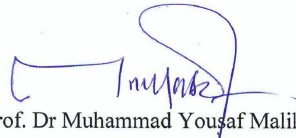
Turnitin Originality Report

A Computational Approach for the Thermal Aspects in Boundary Layer Flows by  Usman Ali .

From DRSM (DRSM L)

- Processed on 06-Apr-2021 07:59 PKT
- ID: 1551531219
- Word Count: 21087

Attested
(Supervisor)



Prof. Dr Muhammad Yousof Malik

Similarity Index

16%

Similarity by Source

Internet Sources:

8%

Publications:

13%

Student Papers:

3%

sources:

- 1 1% match (publications)
[Khalil Ur Rehman, M. Y. Malik, Qasem M. Al-Mdallal, Mostafa Zahri. "On both magnetized and non-magnetized dual stratified medium via stream lines topologies: A generalized formulation", Scientific Reports, 2019](#)
- 2 1% match (Internet from 19-Mar-2019)
<https://www.nrcresearchpress.com/doi/full/10.1139/cjp-2017-0222>
- 3 1% match (Internet from 18-Jul-2020)
<https://www.science.gov/topicpages/c/convection+stagnation+point+flow.html>
- 4 1% match (publications)
[M. Khan, M. Azam, A.S. Alshomrani. "Unsteady slip flow of Carreau nanofluid over a wedge with nonlinear radiation and new mass flux condition", Results in Physics, 2017](#)
- 5 < 1% match (publications)
["Advances in Fluid Dynamics", Springer Science and Business Media LLC, 2021](#)
- 6 < 1% match ()
<http://eprints.utm.my/id/eprint/74841/>
- 7 < 1% match (publications)
[Imad Khan, Khalil Ur Rehman, M.Y. Malik, Shafquatullah. "A computational analysis on homogeneous-heterogeneous mechanism in Carreau fluid flow", Results in Physics, 2018](#)
- 8 < 1% match (Internet from 09-Jun-2020)
<https://aip.scitation.org/doi/10.1063/1.5095546>
- 9 < 1% match (publications)
[M. Gholinia, Kh. Hosseinzadeh, H. Mehrzadi, D.D. Ganji, A.A. Ranjbar. "Investigation of MHD Eyring-Powell fluid flow over a rotating disk under effect of homogeneous-heterogeneous reactions", Case Studies in Thermal Engineering, 2019](#)
- 10 < 1% match (publications)
[Jing Li, Liancun Zheng, Lin Liu. "MHD viscoelastic flow and heat transfer over a vertical stretching sheet with Cattaneo-Christov heat flux effects", Journal of Molecular Liquids, 2016](#)
- 11 < 1% match (publications)
["Applications of Fluid Dynamics", Springer Science and Business Media LLC, 2018](#)
- 12 < 1% match (publications)